Studies on Some Vanadium Chelates with Polydentate Ligands

THESIS SUBMITTED FOR THE

DEGREE OF DOCTOR OF PHILOSOPHY (SCIENCE)

OF

JADAVPUR UNIVERSITY

BY

Mitali Majumder

DEPARTMENT OF CHEMISTRY
JADAVPUR UNIVERSITY
KOLKATA – 700 032, INDIA

যাদবপুর বিশ্ববিদ্যালয়
কলকাতা-৭০০০৩২, ভারত

*JADAVPUR UNIVERSITY
KOLKATA-700 032, INDIA

FACULTY OF SCIENCE: DEPARTMENT OF CHEMISTRY : INORGANIC CHEMISTRY SECTION

CERTIFICATE FROM THE SUPERVISOR

This is to certify that the thesis entitled **"Studies on Some Vanadium Chelates with Polydentate Ligands**" submitted by **Mitali Majumder** who got her name registered on 16.02.2018 for the award of Ph.D. (Science) degree of Jadavpur University, is absolutely based upon her own work under my supervision and neither this thesis nor any part of it has been submitted for any degree/diploma or any other academic award anywhere before.

Date: 12th July 2023

Kajal Krishna Rajak

(Prof. Kajal Krishna Rajak)
Signature of Supervisor date with office seal

Dr Kajal Krishna Rajak
Professor of Chemistry
Jadavpur University
Kolkata-700032

দূরভাষ: ২৪১৪-৬৬৬৬/৬১৯৪/৬৬৪৩/৬৪৯৫/৬৪৪৩ প্রসারণ: ২৪৬৯ Website:www.jadavpur.edu . Phone:2414-6666/6194/6643/6495/6443 Extn.2469
দূরবার্তা: (৯১)-০৩৩-২৪১৪-৬৪১৪/৬২১০/২৪১৩-৭১২১ E-mail : hod@chemistry.jdvu.ac.in Fax: (91)-033-2414-6414/6210/2413-7121

To
My Family

Preface

PREFACE

The work related to this thesis **'Studies on Some Vanadium Chelates with Polydentate Ligands'** commenced on the month of January, 2018.

The thesis is subdivided into five chapters enlarging methods, strategy, experimental findings and analysis of the reaction behavior of some vanadium (IV/V) complexes.

Chapter I contains summary of the work presented in this thesis with brief description of the physical methods and equipment employed.

Chapter II describes synthesis and characterization of three oxidovanadium (IV/V) complexes coordinated with a tridentate ligand (ONO binding mode) and also two different co-ligands. Experimental analysis of photophysical properties of these complexes along with a detailed DFT and TDDFT calculations are provided in this chapter. One of the complexes shows Catechol oxidase (the reaction mechanism was established by ^{1}H NMR titration) and the bromoperoxidase activity is investigated with the synthesized vanadium complexes.

Chapter III contains synthesis and characterization of three mononuclear oxidovanadium (IV/V) complexes having dibenzofuran based novel Schiff base ligand. The ligand binds with the complex through ONO binding sites. Experimental analysis of photophysical properties of these complexes along with a detailed DFT and TDDFT calculations are provided in this chapter.

Chapter IV contains some catalytic and biological activities of the synthesized complexes described in chapter III. The complexes show bromoperoxidase activity was well interpreted by GC-MS. The synthesized complexes show a noticeable intercalating as well as groove binding interaction with DNA molecule and also show interaction with BSA molecule. The interaction of biomolecules with the synthesized complexes were interpreted by UV-VIS, Fluorescence, CD, Viscometry, FT-IR and also molecular Docking etc.

Chapter V describes synthesis and characterization of two mononuclear oxidovanadium (IV) complexes having coumarin and naphthalene based two different Schiff base ligands. One of the

complexes show bromoperoxidase activity (phenol red to bromophenol blue) at a definite pH (pH=5.8). Both the complexes show binding interaction with DNA molecule was established by UV-VIS, Fluorescence and Viscometry method. The interaction of protein molecule (BSA) with the complexes were interpreted by UV-Vis spectroscopy, fluorescence spectroscopy and also FT-IR spectroscopy.

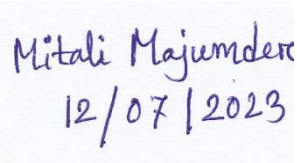

(Mitali Majumder)

Department of Chemistry
Jadavpur University
Kolkata -700032, India.

Acknowledgement

ACKNOWLEDGEMENT

I would like to extend my deep thanks to my supervisor, Prof. Kajal Krishna Rajak; I owe a debt of gratitude for his infinite patience, immense support and valuable guidance during the course of my research. Thank you Sir for sharing your wisdom and teaching me about chemistry; this thesis would not have been possible without your assistance.

No thanks can be enough to acknowledge the encouragement and support of my parents Ms. Provati Majumder and Mr. Chitta Majumder whose support has made this long journey a joy ride for me. Your inspirations play a vital role behind my all success. Special obligations to Maa, without your support this journey may not be possible by any chance.

I gratefully acknowledge the help and cooperation from my lab senior Tapashi Di and Niladri da. I also record my sense of appreciation to my labmates Amit Maity, Debopom Sinha, Supriya Debnath, Roumi Patra, Uday Shee, Sneha Ray and Biswajit Khutiya for their continuous help and valuable suggestions and the nice time we shared together.

I also acknowledge the help from Sarat Da, Soumitra Da, Mihir Da, and Rakesh in many ways. I would like to thank all the scholars of Prof. Subrata Konar and Prof. Kausikisankar Pramanik.

Words fail me to express my thanks to my brother Dr. Tapas Majumder, my husband Shubhagata Roy and my father-in-law Sunil Chandra Roy for their encouragement and understanding. My special regards to my daughter (Shrijoni Roy), she is the power house of my new life.

It is my pleasant duty to thank present Head Prof. Subrata Konar for providing the departmental and laboratory facilities and to all faculty and non-teaching staff of this department for their helpful attitude and constant encouragement. I would like to mention specially Prof.

Samaresh Bhattacharya, and Prof. Kausikisankar Pramanik, for the unbelievable cooperation and help they have rendered.

I would like to thank everybody who was important to the successful insight of thesis, as well as expressing my apology that I could not mention personally one by one.

Financial assistance received from State Government fellowship is gratefully acknowledged.

Last but not the least I would gratefully acknowledge, Jadavpur University for infrastructural facilities.

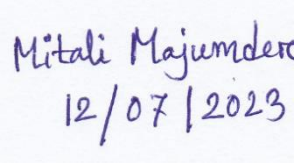

(Mitali Majumder)
June, 2023
Department of Chemistry
Jadavpur University
Kolkata-700032, India.

CONTENTS

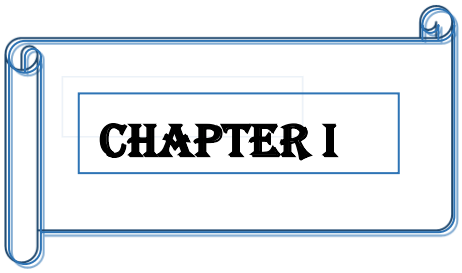
CHAPTER I

INTRODUCTION

ABSTRACT

The systems of chemical compounds consisting of this thesis are briefly introduced in this chapter following a preamble on chemistry of a transition metal, **vanadium**. The methods and equipment used in the work of this thesis are comprehensively summarized.

I.1 PREAMBLE

I.1.1 Chemistry of Vanadium

Vanadium (Z = 23), a transitional element listed in fourth row and Group VB in the periodic table is a hard, steel-gray metal with two naturally occurring isotopes, ^{50}V and ^{51}V. Vanadium takes its name from the Scandinavian goddess Vanadis and was discovered in 1801 by Andrés Manuel del Rio. It was rediscovered by Nils Gabriel Sefstrom (Swedish Chemist) in 1831[1]. Roscoe first characterized vanadium pentoxide, V_2O_5 in 1967 and later it becomes an important commercial oxidation catalyst as in the conversion of naphthalene to phthalic anhydride and of Sulphur dioxide to Sulphur trioxide. Vanadium can exist in a variety of oxidation states: −1, 0, +2, +3, +4, and +5. The states +2 to +5 can be sustained in aqueous solution. Interestingly, the most stable oxidation states +3, +4 and +5 both in vivo and in vitro[2]. The coordination numbers in the range 3 to 8 are observable, 5 and 6 occurring frequently[3-5].

Vanadium, as a plentiful element is widely spread and distributed with an average amount of 159 g/t and 0.14 mg kg−1 in earth crust. About 80% of the world produced V is being used in steel industry as additive. As one of the important raw materials, it has become an integral part of iron–steel industries and different manufacturing unit such as automobiles, shipyard, fertilizers, etc[6]. Vanadium compounds (pentoxide and certain vanadates) are used as catalysts in the contact process for manufacturing sulfuric acid; as oxidation catalysts in the syntheses of phthalic and maleic anhydrides; in the manufacture of polyamides such as nylon; and in the oxidation of such organic substances as ethanol to acetaldehyde, sugar to oxalic acid, and anthracene to anthraquinone.

The chemistry of vanadium has sparked renewed interest since the discovery of vanadium in many organisms[7-8] such as ascidians and Amanita mushrooms as a primary component in many enzymes[9]such as vanadium nitrogenase(V-Nase)[10-12] and haloperoxidases(VHPO)[13-15]. Vanadium bromoperoxidase (VHPO) catalyses the oxidative bromination of organic compounds[16] (hydrocarbons and alcohols, organic sulfide etc.) in presence of bromide ions[17] and hydrogen peroxide under physiological conditions. Irrespective of their origin they all show a high degree of amino acid homology with oxovanadium moiety in their active centers. The peroxidative bromination is an important path for the biosynthesis of many natural brominated organic

compounds[18]. Such importance of the VHPO reactions permits active research in developing new and newer vanadium based complexes capable of mimicking VHPO activity.

Metal complexes such as cisplatin and carboplatin are metal based drugs, which are widely used in cancer chemotherapy and also obtained a great success in the clinical treatment of human malignancies. That has stimulated research in the area of inorganic antitumor agents [19]. Due to severe toxicity and low selectivity of such DNA-targeting drugs, researchers had wanted to develop novel metallo drug by using transition metal complexes containing improved organic ligands [20-21]. Recently, there is a great interest on the binding of transition metal complexes with DNA because of their utility as DNA structural probes, DNA foot printing, sequence-specific cleavage agent and potential anticancer drug [22].

As vanadium is a bioessential element and also responsible for numerous bioactivities in living organism, [23-28] interaction of vanadium complexes with DNA has recently concerned much attention . [29-33] Vanadium(IV/V) complexes are oxophilic in nature and form a variety of oxido species such as VO2+, VO3+, and cis-VO2+; with these vanadium species there exists a growing interest toward therapeutic aspects in cancer treatment. Vanadium complexes (vanadocene dichloride, $Cp_2V^{IV}Cl_2$) were first studied for their anticancer activity in the treatment of Ehrlich ascites tumor in the 1983[34-36]. Later on Metvan, $[V^{IV}O(4,7\text{-}Me_2phen)_2(SO_4)]$ (4,7-Me_2phen = 4,7-dimethyl-1,10-phenanthroline), was reported to be a promising anticancer drug against various cancer cell lines, including cisplatin-resistant testicular and ovarian cancer[37]. Thus, the DNA-binding, DNA photocleavage activity of oxometal complexes based on vanadium and multifunctional ligands has been of recent interest [38-41].

In biological fluids, serum albumin contributes 52% of the total protein composition in the circulatory system. Due to importance in physiological and pharmacological functions it is advantageous to study serum albumin, as the limited number of binding sites with high specificity plays a pivotal role in the transportation and delivery of different endogenous and exogenous species[42]. Bovine serum albumin (BSA), having a 76% sequence homology for human serum albumins (HSA), has been broadly studied, as it is the most abundant model protein of blood plasma[43-44]. From literature reports, it has been observed that vanadium complexes showing higher DNA and protein binding ability exhibited better cytotoxicity, and so the assessment of this ability is an important aspect prior to anticancer studies [45-47].

There have been reports of vanadium complexes with a variety of biological activities, including antibacterial [48-50] anti-inflammatory [51], and anticancer [52-54] activity. Vanadium(IV/V) complexes' ability to imitate the effects of insulin, which was even confirmed in phase IIa clinical studies on humans for the treatment of type 2 diabetes mellitus, is another significant finding [55]. In addition, vanadium compounds are viewed as a new class of drugs that have the potential to exhibit significant anticancer effects and are also effective against parasitic diseases[56]. The realisation that vanadium is involved in life-related events has also sparked renewed research into the coordination chemistry of the metal in various ligand and geometrical environments.

The use of fossil fuels contributes to a number of natural disasters, including climate change, the greenhouse effect, and global warming. Utilising renewable energy in this situation is a different option. It has been claimed that vanadium-based oxides, sulphides, and their composites have provided super capacitors with a promising energy storage capacity. For energy storage applications, compounds with vanadium assistance thrive thanks to their stability, energy density, and extended cycle life [57-59].

On the other hand, cutting-edge research has been optimized to achieve improved performance of compounds assisted by vanadium that are commercially viable. Due to its low cost, layered structure, increased energy density, multivalent oxidation states, increased surface area, and ability to design a variety of nanostructures like nanowires, nanorods, nanoflakes, nanobelts, nanostrips, nanoparticles, nanospheres, nanoribbons, nanofibers, nanocuboids, nanoporous, nanoflowers, etc., vanadium oxide is offering significantly better performance than the other transition metal oxides in this context[60].

The main focus of this thesis has been on the synthesis and analysis of different oxidovanadium (IV/V) complexes containing tridentate O, N, O coordinating ligands. The details theoretical investigations of all the structural, photophysical, catalytic, and biological activities are also studied throughout our research.

I.1.2. Schiff Bases ligands

Schiff bases ligands are formed by condensation between a primary amine and carbonyl compound contain azomethine group (-CH=N-). Both aldehyde and ketone form Schiff bases but formation with aldehyde are more favourable than ketone. The lone pair of nitrogen in azomethine group readily coordinates with metal centre. Other than nitrogen if there is another donor centre in the

Schiff base act as multidentate ligand. Schiff base ligands are used in recent times because of their reactivity and flexibility towards the metal centre in the complex. There are lots of different Schiff base ligands are prepared easily nowadays.

I.1.3. Catechol Oxidase

Catechol oxidase is an enzyme of the oxidoreductase class that catalyzes the reaction between catechol and oxygen to yield benzoquinone and water. The resulting highly reactive o-quinones auto-polymerize to form brown polyphenolic catechol melanins, a process thought to protect the damaged tissues of plants from pathogens or insects. The active site of catechol oxidase contains an antiferromagnetically coupled (EPR silent) dicopper(II) center [61]. Moreover, some monometallic complexes of copper(II) [62] and some other metal ions, such as Mn(II/III/IV) [63-64], Fe(III) [65], Co(III) [66], Ni(II) [67] and Zn(II) [68], are also found to show catecholase activity. The catecholase activity of vanadium(V) was first reported by Chakravarty *et al.* [69] about a decade ago.

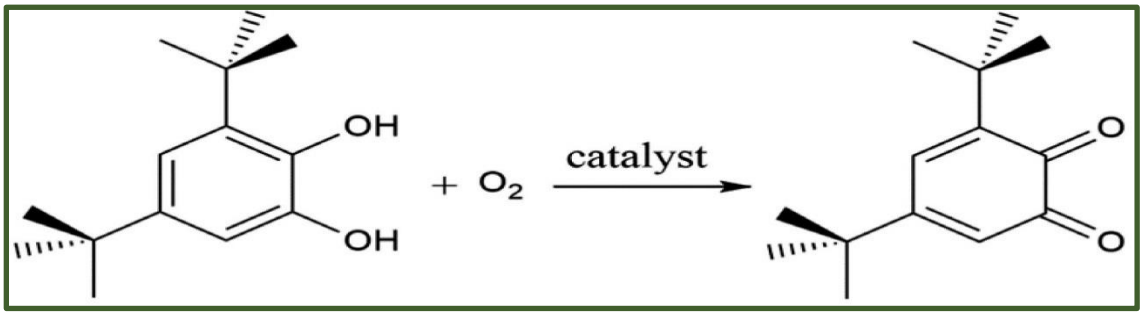

I.1.4. Bromoperoxidase

Bromide peroxidase (*bromoperoxidase*, *haloperoxidase (ambiguous)*, *eosinophil peroxidase*) is a family of enzymes with systematic name *bromide: hydrogen-peroxide oxidoreductase*. These enzymes catalyzes the following chemical reaction [70-71]

$$HBr + H_2O_2 \rightarrow HOBr + H_20$$

The HOBr is a potent brominating agent. The many organobromine compounds observed in marine environments are the products of reaction with this oxidized form of bromine.

Bromo peroxidases of red and brown marine algae (*Rhodophyta* and *Phaeophyta*) contain **vanadate** (vanadium bromoperoxidase). **Vanadium bromoperoxidases** are a kind of enzymes called haloperoxidases. Its primary function is to remove hydrogen peroxide which is produced during photosynthesis from in or around the cell. By producing hypobromous acid (HOBr) a secondary reaction with dissolved organic matter, what results is the bromination of organic compounds that are associated with the defense of the organism. Vanadium bromoperoxidases have been found in bacteria, fungi, marine macro algae (seaweeds), and marine microalgae (diatoms) which produce brominated organic compounds[72]. These enzymes produce the bulk of natural organobromine compounds in the world.

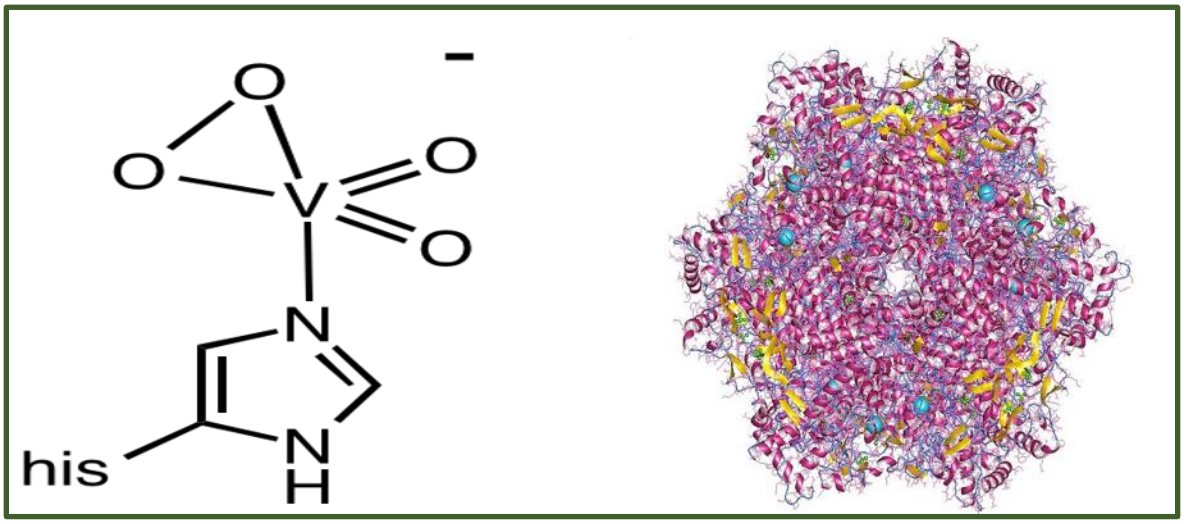

Active site of the enzyme vanadium bromoperoxidase, which produces most of the earth's **organobromine compounds**.

I.1.5. Deoxyribonucleic Acid (DNA)

DNA is a critical therapeutic target that is responsible for, and the focus of, a wide variety of intracellular interactions[73]. Each of the complementary strands of DNA are stabilized by hydrogen bonding between adenine and thymine (A–T) and guanine and cytosine (G–C) nucleic acids[74]. In B-DNA, the most common DNA form, the strands are held in the anti-parallel double helix by stacking interactions between parallel oriented bases[75] . The formation of this helix results in the presence of a major and minor groove which provide sites for the binding of small

molecules[76]. The major and minor groove differ significantly in size, shape, hydration, electrostatic potential and position of hydrogen bonding sites[77-78].

Most of the vital biochemical reactions in active cells like DNA replication, accurate transcription, processing, repair, specific package, and DNA rearrangement accurately represent a desired result of constant interaction between the functional molecules of nucleic acids and specific proteins [79]. The Interaction between specific protein and nucleic acids was carefully observed for the first time in an empirical study of DNA–protein complex crystallography in 1984 [80]. The varied structural complexity and polymorphic nature of DNA presents a number of potential intermolecular interactions, including irreversible covalent binding, reversible groove association or intercalation.[81]

Metal complex-DNA interactions showcase the influence that the coordination geometry of the metal and the disposition of the ligands have on the binding activity. For example, square planar complexes permit deeper insertion of an intercalator compared to octahedral or tetrahedral geometries.

Covalent binding is a common method of DNA interaction for anticancer drugs. Cisplatin is the most clinically successful DNA covalent binder, although it reacts with a diverse range of other biomolecules.[82-83]

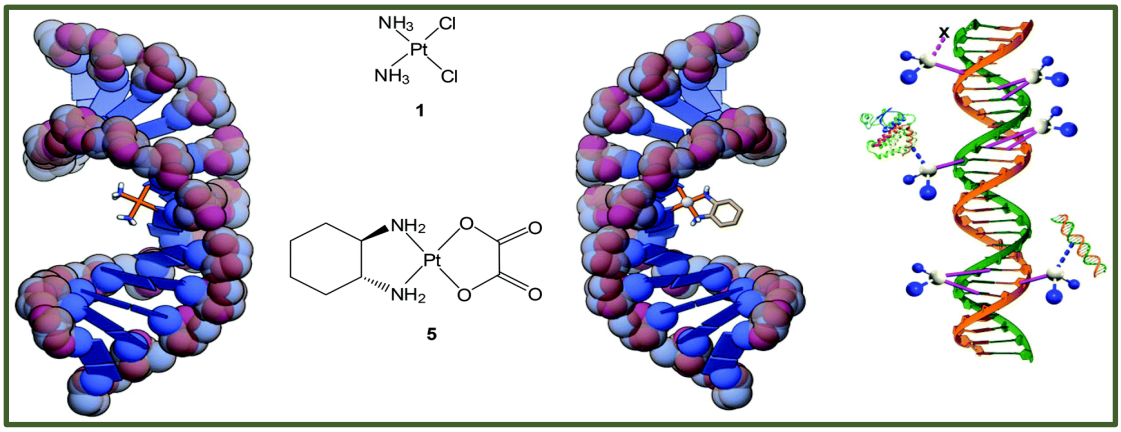

I.1.5. Bovine Serum Albumin(BSA)

Bovine serum refers to the liquid component of cow blood that remains after the blood cells have been removed by clotting or centrifugation. It is a commonly used supplement in cell culture and biotechnology applications due to its high content of nutrients, growth factors, and hormones. It is

used to support the growth and viability of cells in culture, and is particularly important for the growth of cells that are difficult to culture. However, the use of bovine serum is controversial due to concerns about the transmission of infectious agents and the ethical implications of using animal-derived products in research. As a result, alternative supplements such as synthetic media and plant-derived serum substitutes are being developed and used in some applications. Bovine serum albumin (BSA) is a widely studied protein that is commonly used as a model protein for investigating protein interactions with various molecules, including metal complexes. Metal complexes can interact with BSA through different mechanisms, such as coordination bonding, electrostatic interactions, and hydrogen bonding. These interactions can affect the conformational stability and biological activity of the protein.

BSA has 80% similarity with HSA (Human Serum Albumin) in structure with a major difference in the number of tryptophans, while HSA has only one tryptophan, BSA has two. BSA is usually selected for protein binding studies because of i) its abundance ii) low cost iii) ease of purification iv) stability v) medical and ligand binding properties [84-85].

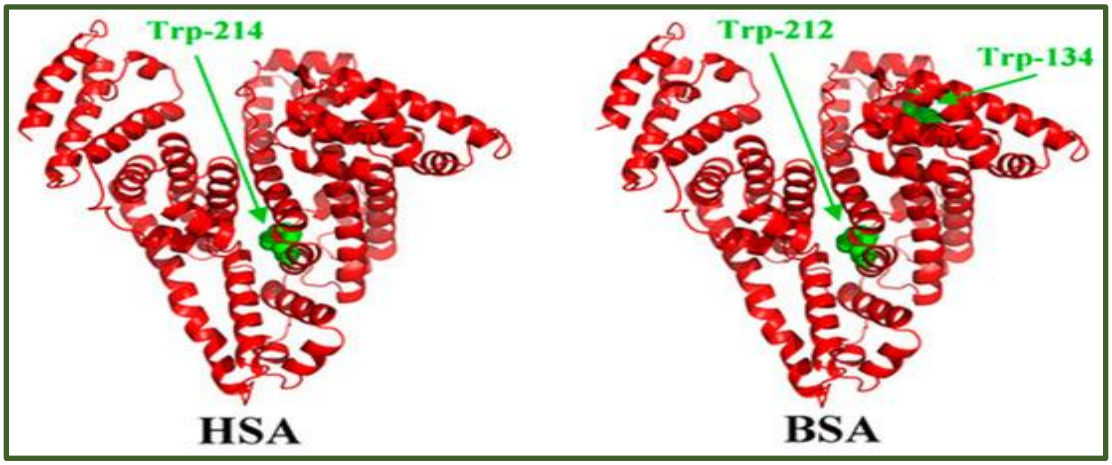

I.2 SUMMARY OF THE PRESENT WORK

The present work has been concentrated to search for some novel vanadium complexes with (**IV/V**) oxidation state, with different polydentate Schiff base ligands and investigate their important properties like structural, photophysical, electrochemical properties. Particularly in the ocean, vanadium is used by some life forms as an active center of enzymes, such as the vanadium bromoperoxidase of some ocean algae. Due to such kind of behavior, bromoperoxidase activity is also investigated with the synthesized vanadium complexes. As vanadium is an essential element

and also, vanadium and vanadium compounds inside the cells can interact with different proteins and act as inhibitor or activator (analog) and influence different signaling pathways. Some biological activity of the synthesized vanadium complexes also represented in this work. The work described in this thesis is divided into four parts: **Chapter II**, **III, IV** and **V**.

I.2.1. Chapter II

This chapter describes the preparation of three mononuclear vanadium (IV/V) complexes with a tridentate Schiff base ligand, H_2L_1 and some co-ligands (8-Hydroxyquinoline and 1,10-phenanthroline). The complexes obtained from the reaction of H_2L_1 and $[V^{IV}O(acac)_2]$ in presence if methanol affording the complex 1 and the other two complexes are obtained by the reaction of co-ligands with complex 1. The synthesized complexes were well characterized by different spectroscopic methods. The experimental results are inter-related with the theoretical results by using Density Functional Theory (DFT) method. It is being noted that the choice of such ligands helps to achieve our goal in the context of synthesis of such mononuclear Vanadium(IV/V) complexes with interesting catalytic properties (catechol oxidase and bromoperoxidase).

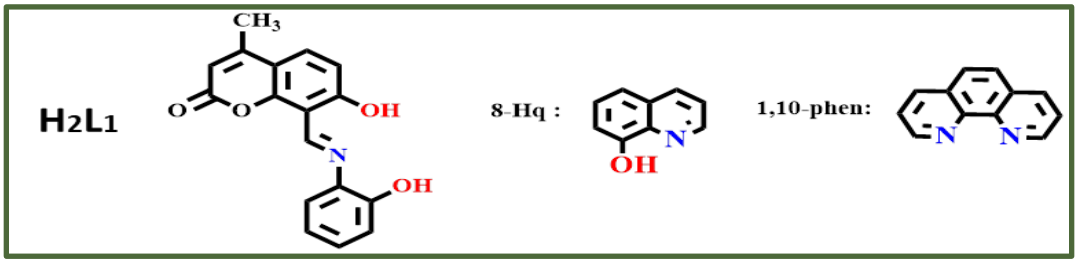

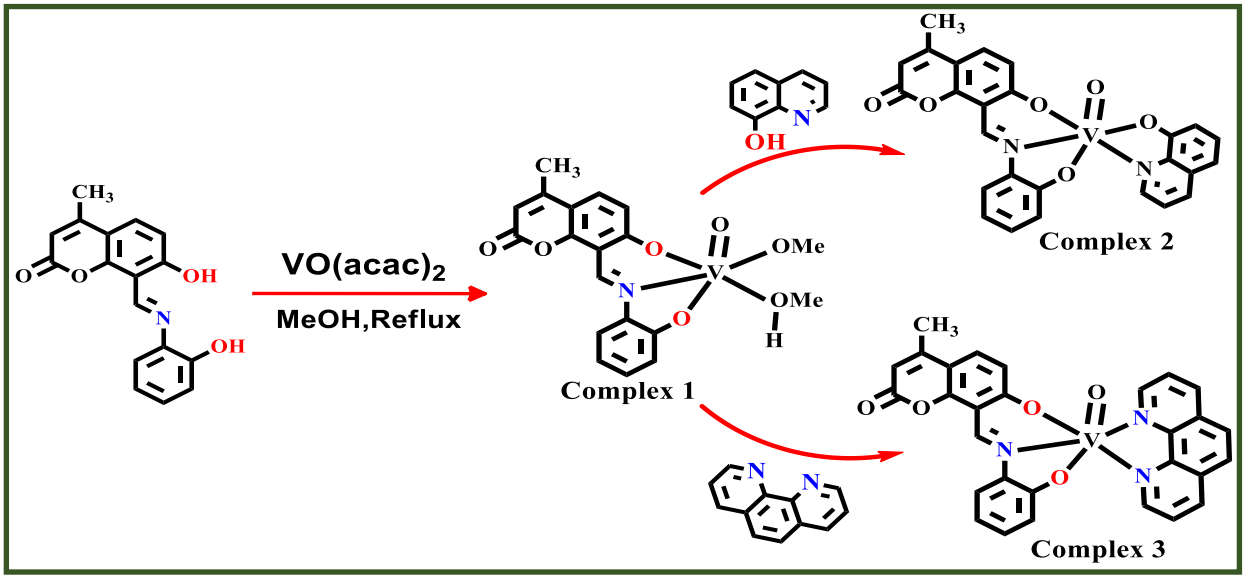

I.2.2. Chapter III

In presence of *ONO*- coordinating Schiff base ligand successful synthesis of three mononuclear oxidovanadium (IV/V) complexes were done. The complexes obtained from the reaction of H_2L_1 and $[V^{IV}O(acac)_2]$ in presence if methanol affording the complex 1 and the other two complexes are obtained by the reaction of co-ligands with complex 1. All the ligands and complexes were characterized by several spectroscopic techniques. The detailed study with DFT was performed for both ligands and complexes.

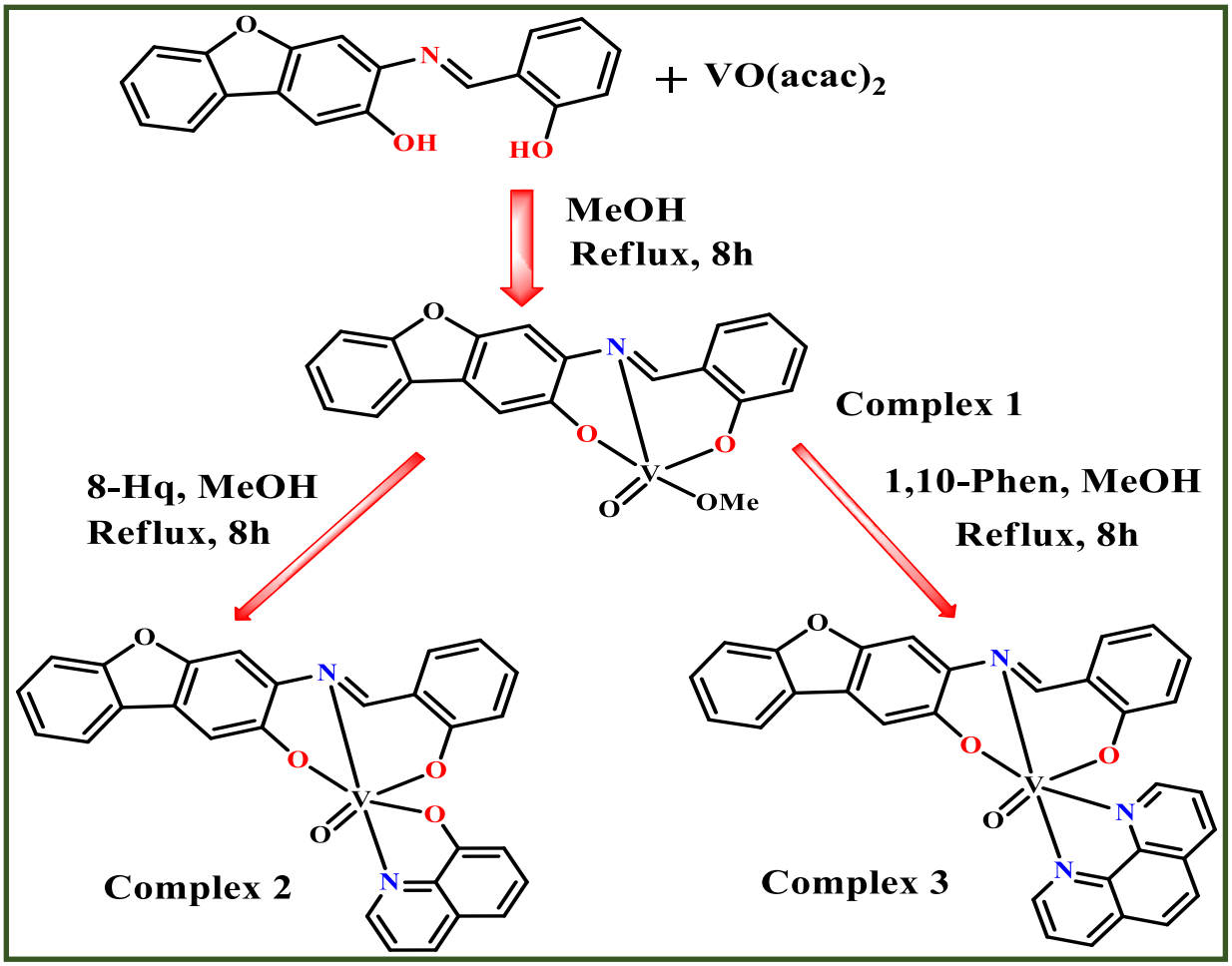

I.2.3. Chapter IV

In this chapter illustrate the catalytic and biological activities of the synthesized vanadium (IV/V) complexes which is the extended work of chapter 3. The mononuclear oxidovanadium complexes shows bromoperoxidase activity with salicylaldehyde having a good yield of the bromo derivated

salicylaldehyde products and characterised by GC-MS. The synthesized vanadium complexes shows intercaleting interaction as well as groove binding with DNA molecules and interaction with protein molecule (BSA) are characterised by spectroscopical techniques and doacking method.

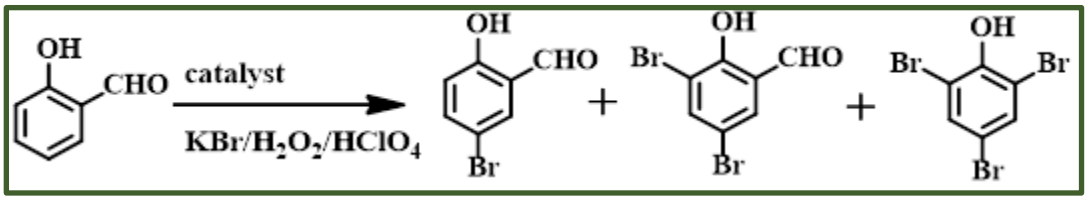

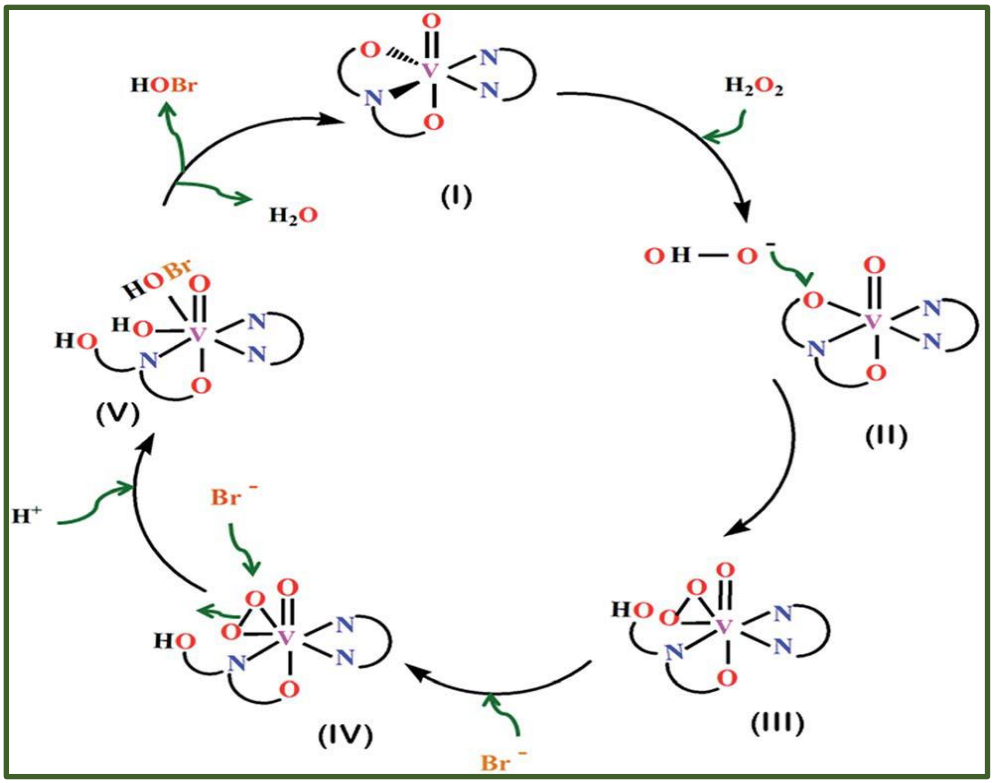

I.2.4. Chapter V

This chapter deals with the synthesis and characterization of two mononuclear oxidovanadium (IV) complexes having Coumarin and Naphthalene based two different Schiff base ligands. These two interesting EPR active vanadium complexes show biological activities (DNA and BSA interaction). Despite same type of coordination sites, complex 1 shows bromoperoxidase activity (phenol red to bromophenol blue).

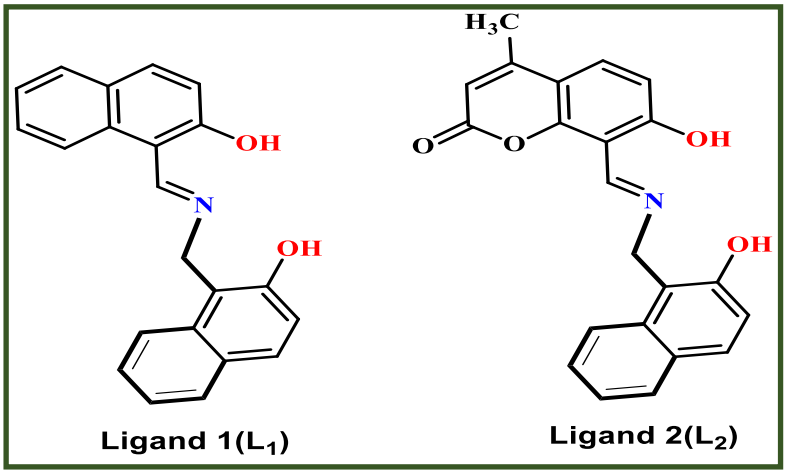

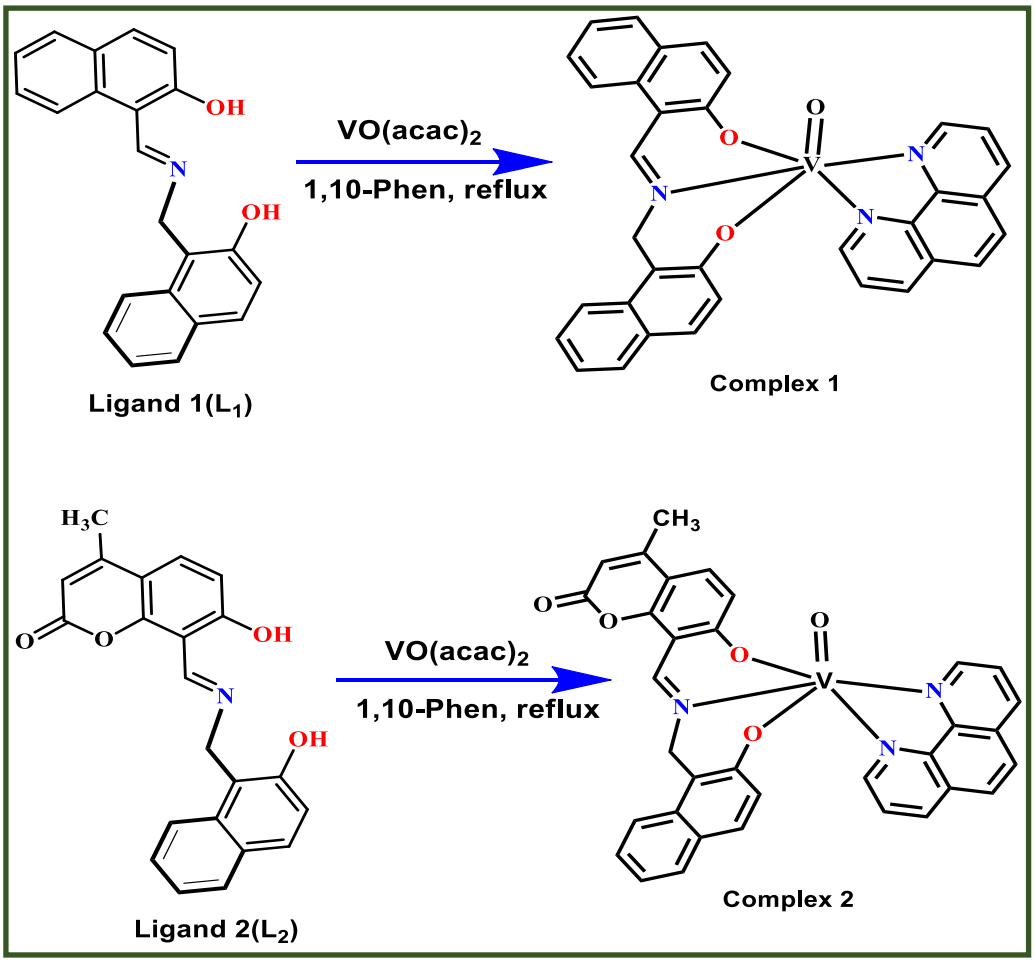

I.3 MEASUREMENTS

Various physical methods have been employed for the characterization and elucidation of the properties of the synthesized compounds and these are described in the subsequent chapters. These are briefly described below.

I.3.1 Elemental Analysis

The C, H, N content of the samples were determined with the help of a Perkin-Elmer 2400 Series II elemental analyzer which utilizes thermal conductivity data for gas (CO_2, H_2O, N_2) analysis. The sample (1.5-2.5 mg) was introduced into the combustion cell usually at a temperature in the range of 900–980^o C. For combustion, pure oxygen was used and pure helium was used as the driving gas.

I.3.2 Infrared Spectra

IR spectra were recorded in KBr disk with the help of a Perkin-Elmer L-0100 spectrometer.

I.3.3 Electronic Spectra

Electronic spectra were recorded on Perkin-Elmer LAMBDA EZ-301 and a LAMBDA 25 UV/VIS spectrometer (190-1100 nm). A matched pair of quartz cells of path length 1 cm was used.

I.3.4 Electrochemical Measurements

A CHI-620A electrochemical analyzer was used for electrochemical measurements. All experiments were performed under pure nitrogen atmosphere at 295 and 298 K. The potentials are referenced to the standard calomel electrode (SCE) without junction correction.

A three-electrode system consisting of a planar Beckman model 39273 platinum inlay working electrode, platinum wire auxiliary electrode and a saturated calomel electrode (SCE) were used. In every case care was taken to obtain a flat current-voltage base line over the required voltage range in the absence of the relevant electroactive species.

I.3.5 Fluorescence Spectra

The emission data were collected on Horiba Fluoromax-4 fluorescence spectrometer. For all luminescence measurements excitation and emission slit width of 5 nm were used. Cells are same as that of the electronic spectra.

I.3.6 EPR Spectra

X-band (9.1–9.2 GHz) EPR spectra were recorded on a Varion E-109 C spectrometer (magnetic field up to ~ 6000 G) using quartz sample tubes of 3 mm diameter. For measurements at 77 K, quartz Dewar flask was utilized. The Dewar was filled with liquid nitrogen and the quartz sample tube was immersed in it. During the measurements, the microwave cavity was continuously purged with pure and dry nitrogen. The spectra were calibrated with respect to diphenylpicrylhydrazyl (dpph, g = 2.0037).

I.3.7 MASS Spectra

Electrospray ionization mass spectrometry (ESI-MS) spectra of the samples were recorded on a Micromass Qtof YA 263 mass spectrometer.

I.3.8 NMR Spectra

^{1}H and ^{13}C NMR spectra were recorded in mainly $CDCl_3$, CD_3CN and DMSO-d_6 with the help of Bruker FT 300 MHz spectrometer and Bruker FT 400 MHz spectrometer, respectively using tetramethylsilane (TMS) as an internal standard depending upon the solubility of the products. Signals are assigned to individual protons on the basis of chemical shifts, spin-spin structure and substituent effects. The atom-numbering scheme used for ^{1}H and ^{13}C was same as that used in the crystallography.

I.3.9 Crystallographic Studies

The X-ray intensity data were collected on Bruker AXS SMART APEX CCD diffractometer (Mo Kα, λ = 0.71073 Å) at 293 K. The detector was placed at a distance 6.03 cm from the crystal. Total 606 frames were collected with a scan width of 0.3º in different settings of φ. The data were reduced in SAINTPLUS[86] and empirical absorption correction was applied using the SADABS package[87]. Metal atom was located by Patterson Method and the rest of the non-hydrogen atoms were emerged from successive Fourier synthesis. The structures were refined by full matrix least-square procedure on F2. All non-hydrogen atoms were refined anisotropically. All calculations

were performed using the SHELXTL V 6.14 program package[88]. Molecular structure plots were drawn using the Oak Ridge thermal ellipsoid plot (ORTEP)[89].

R1, wR2 and goodness-of-fit (GOF) are given by the following equations 1, 2 and 3 respectively.

$$R1 = \Sigma \big| |F_o| - |F_c| \big| / \Sigma |F_o| \qquad \ldots\ldots (1)$$

$$wR2 = [\Sigma[w(F_o^2 - F_c^2)^2] / \Sigma[w(F_o^2)^2]]^{1/2} \qquad \ldots\ldots (2)$$

$$GOF = S = [\Sigma[w(F_o^2 - F_c^2)^2] / (n_o - n_p)]^{1/2} \qquad \ldots\ldots (3)$$

n_o = **number of reflections**

n_p = **total number of parameters refined**

Specific details for each compound will be given in the concerned chapter.

I.3.10 DFT Study and Computational Details

All the quantum mechanical calculations were performed with the Gaussian 09W software package[90]. GaussSum 2.1 program[91] was used to calculate the molecular orbital contributions from groups or atoms. Figures showing MOs, NTOs and the difference density plots were prepared by using the Gauss View 5.1 software. All the calculations were carried out in IBM Intellistation Z Pro 922892A machine and Super-micro Super-server work station. The geometrical structures of the singlet ground state (S0) and the lowest lying triplet excited state (T1) were optimized by the DFT[92] method with B3LYP exchange correlation functional[93] approach. The geometry of the complexes was fully optimized in solution phase without any symmetry constraints.

In the calculation, the quasirelativistic pseudopotentials of rhenium atoms proposed by Hay and Wadt[94] with 14 valence electrons (outer-core [(5s25p6)] electrons and the ($5d^6$) valence electrons) were employed, and a "double-ξ"quality basis set LANL2DZ was adopted as the basis set for Re atoms. For H we used 6-31(g) basis set and the 6-31+G(d)[95] basis set for C, N, O, and Cl atoms for the optimization of the ground state geometries.

The vibrational frequency calculation was also performed for all the complexes to ensure that the optimized geometries represent the local minima and there are only positive eigen values. There was a good agreement between the theoretical and experimental structures.

On the basis of the optimized ground and excited state geometry structures, the absorption and emission spectra properties in a particular solvent media were calculated by time-dependent density functional theory (TDDFT)[96] approach associated with the conductor-like polarizable continuum model (CPCM)[97]. We computed the lowest 40 singlet – singlet transition and results of the TD calculations were qualitatively very similar. The TDDFT approach had been demonstrated to be reliable for calculating spectra properties of many transition metal complexes[98]. Due to the presence of electronic correlation in the TDDFT (B3LYP) method it can yield more accurate electronic excitation energies. Hence TDDFT had been shown to provide a reasonable spectral feature for our complex of investigation.

Finally to understand the nature of excited states involved in absorption and emission processes natural transition orbital (NTO) analysis had been performed for all complexes. This approach provides the most compact representation of the electronic transitions in terms of an expansion into single particle orbitals by diagonalizing the transition density matrix associated with each excitation. The spin density difference map calculations were also performed to explain their optical properties.

I.4 CHEMICALS AND SOLVENTS

All commercially available chemicals and solvents utilized in the present work were of analytical grade and were used without further purification. For the preparation of ligands, the solvents were dried in their usual method. Purification steps, where required, will be elaborated in appropriate chapters. The chemicals required for the synthesis of ligands were purchased from MERCK (India) and Sigma Aldrich chemicals limited.

All references in this thesis are given in the following format: Name of the author(s), Journal, year, volume, page.

I.5 REFERENCES

1. M. E. Weeks, H. M. Leicester, Discovery of elements, 7th Ed.; *Chemical Education Publishing, Easton, Pa.* 1968, 351.
2. F. A. Cotton, G. Wilkinson, C. A. Murillo, N. Bachmann, Advanced Inorganic Chemistry, 6th Ed.; *A Wiley-Interscience Publication*, 1999, 714.
3. J. J. R. Fraston da Silva, R. J. P. Williams, The Biological Chemistry of the elements.; *The Inorganic Chemistry of life.* 1991, 427.
4. L. V. Boas, J. C. Pessoa, in Comprehensive Coordination Chemistry.; *The Synthesis, Reaction, Properties and Application of Coordination Compounds.* Ed. Sir G. Wilkinson, 1987, 3, 454.
5. F. A. Cotton, G. Wilkinson, Advanced Inorganic Chemistry, 6th Ed.; *A Wiley-Interscience Publication*, 1988, 665.
6. M. Imtiaz, M. S. Rizwan, S. Xiong, H. Li, M. Ashraf, S. M. Shahzad, M. Shahzad, M. Rizwan, S. Tu, Vanadium, recent advancements and research prospects: A review.; *Environment International*. 2015, 80, 79-88.
7. H. Michibata, M. Yamaguchi, T. Uyama, T. Ueki, *Coord. Chem. Rev*. 2003, 237, 41.
8. (a) H. Michibata, T. Uyama, T. Ueki, K. Kanamori, *Microsc.Res. Technol*. 2002, 56, 421.
9. (b) D. Rheder, *Coord. Chem. Rev.*1999,182,297.
10. J. Chen, J. Christiansen, R. C. Tittsworth, B. J. Hales, S. J. George, D. Coucouvanis, S. P. Cramer, J. Am. Chem. Soc. 115(1993) 5509-5515.
11. H. Vitter in Metal ions in Biological Systems; (Eds.: H. Sigel, A. Sigel), METAL IONS IN BIOLOGICAL SYSTEMS Marcel Dekker: New York, 1995 Vol. 31, chapter 10.
12. J. N. Carter-Franklin, J. D. Parrish, R. A. Tschirret-Guth, R. D. Little, A. Butler, J. Am. Chem. Soc. 125 (2003) 3688.
13. (a) J. Littlechild, E. Garcia-Rodriguez, Coord. Chem. Rev. 237(2003) 65-76. (c) D. E. Carpio, L. Hernándeza, C. Ciangherotti, Coa, V. Villalobos, L. Jiménez, V. Lubes, G. Lubes, Coord. Chem. Reviews. 372(2018) 117-140. (d) M. Debnath, M. Dolai, K. Pal, S. Bhunya, A. Paul, H. M. Lee, M. Ali, Dalton Trans. 47(2018) 2799-2809.
14. A. Butler, A. H. Baldwin (Eds.: H. A. O. Hill, P. J. Salder, A. J. Thompson), Spingler-Verlag, Heidelberg, 1999, 108-132.

15. Bioinorganic Catalysis; (Ed.: J. Reedijk), Marcel Dekker, Inc.: New York, 1993, 425-445.
16. A. Butler, J. N. Carter-Franklin, National Library of Medicine, 2004, 21(1)180-8
17. (a) T. K. Si, S. S. Paul, M. G. B. Drew and K. K. Mukherjea, Dalton Trans. 2012, 41, 5805–5815; (b) S. Patra, S. Chatterjee, T. K. Si and K. K. Mukherjea, Dalton Trans. 2013, 42, 13425–13435.
18. (a) S. Rayati, N. Sadeghzadeh and H. R. Khavasi, Inorg. Chem. Commun., 2007, 10, 1545–1548; (b) H. S. Soedjak, J. V. Walker and A. Butler, Biochemistry, 1995, 34, 12689–12696; (c) B. B. Gangadhar, S. B. Prema and S. A. Patil, J. Enzyme Inhib. Med. Chem., 2009, 24, 381–394.
19. B. Rosenberg, Interdisc. Sci. Rev. (1978), 3, 134-147.
20. (a)V. Milacic, Q.P. Dou, Coord. Chem. Rev., 253 (2009), 1649-1660. (b)A.G. Quiroga, C.N. Ranninger, Coord. Chem. Rev., 248 (2004), 119-133.
21. L. Pellerito, L. Nagy, Coord. Chem. Rev., 224 (2002), 111-150.
22. C.X. Zhang, S.J. Lippard, Curr. Opin. Chem. Biol., 7 (2003), 481-489.
23. D. Rehder, J.C. Pessoa, C.F.G.C. Geraldes, T. Kabanos, T. Kiss, B. Meier, G. Micera, L. Pettersson, M. Rangel, A. Salifoglou, I. Turel, D. Wang, J. Biol. Inorg. Chem., 7 (2002), 384-396.
24. Y. Wei, C. Zhang, P. Zhao, X. Yang, K.J. Wang, Inorg. Biochem., 105 (2011),1081-1085.
25. J. Nilsson, A.A. Shteinman, D. Rehder, E. Nordlander, J. Inorg. Biochem., 105 (2011), 1795-1800
26. G.R. Willsky, L.-H. Chi, Z. Hu, D.C. Crans, Coord. Chem. Rev., 255 (2011), 2258-2269
27. A.A. Antipov, D.Y. Sorokin, N.P. L'Vov, J.G. Kuenen, Biochem. J., 369 (2003), 185-189.
28. J.H. McNeill, V.G. Yuen, H.R. Hoveyda, C. Orvig, J. Med. Chem., 35 (1992), 1489-1491.
29. P.K. Sasmal, A.K. Patra, A.R. Chakravarty, J. Inorg. Biochem., 102 (2008), 1463-1472
30. X. Liao, W. Pan, R. He, H. Guo, P. Ying, J. Lu, Chem. Biol. Drug Des., 83 (2014), 367-378
31. N.H. Khan, N. Pandya, N.C. Maity, M. Kumar, R.M. Patel, R.I. Kureshy, S.H.R. Abdi, S. Mishra, S. Das, H.C. Bajaj, Eur. J. Med. Chem., 46 (2011), 5074-5085
32. B. Banik, K. Somyajit, G. Nagaraju, A.R. Chakravarty, RSC Adv., 4 (2014), 40120-40131
33. B. Balaji, B. Balakrishnan, S. Perumalla, A.A. Karande, A.R. Chakravarty, Eur. J. Med. Chem., 85 (2014), 458-467.

34. J. C. Pessoa, I. Tomaz, Curr. Med. Chem. 2010, 17, 3701– 3738.
35. P. Köpf-Maier, D. Krahl, Chem.-Biol. Interact. 1983, 44, 317– 328.
36. P. Koepf-Maier, H. Koepf, Chem. Rev. 1987, 87, 1137– 1152.
37. R. K. Narla, C. L. Chen, Y. Dong, F. M. Uckun, Clin. Cancer Res. 2001, 7, 2124– 2133.
38. L. Andrezalova, H. Gbelcova, Z. Duraˇckova, J. Trace Elem. Med. Biol., 27 (2013), pp. 21-26
39. Z.H. Chohan, S.H. Sumrra, M.H. Youssoufi, T.B. Hadda, Eur. J. Med. Chem., 45 (2010), 2739-2747
40. J. Lu, H. Guo, X. Zeng, Y. Zhang, P. Zhao, J. Jiang, L. Zang, J. Inorg. Biochem., 112 (2012), 39-48
41. T. Yamaguchi, S. Watanabe, Y. Matsumura, Y. Tokuoka, A. Yokoyama, Bioorg. Med. Chem., 20 (2012), 3058-3064.
42. C. de Rosa, A. Melchior, M. Sanadar, M. Tolazzi, A. Giorgetti, R. P. Ribeiro, C. Nardon, F. Piccinelli, Inorg. Chem. 2020, 59, 12564– 12577.
43. A. Busemann, C. Araman, I. Flaspohler, A. Pratesi, X.-Q. Zhou, V. H. S. van Rixel, M. A. Siegler, L. Messori, S. I. van Kasteren, S Bonnet, Inorg. Chem. 2020, 59, 7710– 7720.
44. J. Lu, H. Guo, X. Zeng, Y. Zhang, P. Zhao, J. Jiang, L. J. Zang, Inorg. Biochem. 2012, 112, 39– 48.
45. Z. Kazemi, H. A. Rudbari, V. Mirkhani, M. Sahihi, M. Moghadam, S. Tangestaninejad, I. Mohammadpoor-Baltork, A. A. Kajani, G. Azimi, Eur. J. Med. Chem. 2017, 135, 230– 240.
46. S. A. Patra, M. Mohanty, A. Banerjee, S. Kesarwani, F. Henkel, H. Reuter, R. J. Dinda, Inorg. Biochem. 2021, 224, 111582.
47. S.P. Dash, S. Pasayat, S. Bhakat, H.R. Dash, S. Das, R.J. Butcher, R. Dinda, Polyhedron, 31 (2012), 524-529
48. T. Rosu, E. Pahontu, M. Reka-Stefana, D.-C. Ilies, R. Georgescu, S. Shova, A. Guleae
49. Polyhedron, 31 (2012), 352-360
50. N. Sharma, M. Kumari, V. Kumar, S.C. Chaudhry, S.S. Kanwar, J. Coord. Chem., 63 (2010), 1940-1950
51. K. Singh, P. Patel, A.K. Goswami, E-J. Chem., 5 (2008), 1144-1148
52. Y. Dong, R.K. Narla, E. Sudbeck, F.M. Uckun, J. Inorg. Biochem., 78 (2000), 321-330

53. A.M. Evangelou, Crit. Rev. Oncol. Hematol., 42 (2002), 249-265
54. C. Djordjevic, G.L. Wampler, J. Inorg. Biochem., 25 (1985), 51-55.
55. (a)G. Sahu, S. A. Patra, M. Mohanty, S. Lima, P. Das Pattanayak, W. Kaminsky, R. Dinda, Journal of Inorganic Biochemistry, 2022, 233, 111844. (b) S. Semiza, J Trace Elem Med Biol. 2022, 69, 126887. (c) H. Sakurai, Review Chem Rec, 2002, 2(4), 237-48.
56. D. Gambino, Coordination Chemistry Reviews, 255, 2011, 2193-2203.
57. (a)C. Xiong, M. Li, Q. Han, W. Zhao, L. Dai, Y. Ni, J. Mater. Sci. Technol., 97 (2022), 190-200. (b)C. Xiong, B. Li, C. Duan, L. Dai, S. Nie, C. Qin, Y. Xu, Y. Ni, Chem. Eng. J., 418 (2021), Article 129518
58. (a)C. Xiong, C. Zheng, S. Nie, C. Qin, L. Dai, Y. Xu, Y. Ni, Cellulose, 28 (6) (2021), 3733-3743. (b)C. Xiong, B. Li, H. Liu, W. Zhao, C. Duan, H. Wu, Y. Ni, J. Mater. Chem. A, 8 (21) (2020), 10898-10908
59. C. Xiong, M. Li, S. Nie, W. Dang, W. Zhao, L. Dai, Y. Ni, J. Power Sources, 471 (2020), Article 228448.
60. C. Diaz, G. Barrera, M. Segovia, M. L. Valenzuela, M. Osiak, C. O'Dwyer, Journal of Nanomaterials, 2015, 105157, 13.
61. (a) B.T. Op't Holt, M.A. Vance, L.M. Mirica, D.E. Heppner, T.D.P. Stack, E.I. Solomon, J. Am. Chem. Soc. 131 (2009), 6421. (b) S. Herres-Pawlis, P. Verma, R. Haase, P. Kang, C.T. Lyons, E.C. Wasinger, U. Florke, G, Henkel, T.D.P. Stack, J. Am. Chem. Soc. 131 (2009), 1154
62. (a) J.A. Halfen, S. Mahapatra, E.C. Wilkinson, S. Kaderli, V.G. Young, L. Que Jr., A.D. Zuberbuhler, W.B. Tolman, Science, 271 (1996), 1397. (b) V. Mahadevan, J.L. DuBois, B. Hedman, K.O. Hodgson, T.D.P. Stack, J. Am. Chem. Soc., 121 (1999), 5583.
63. (a) G. Blay, I. Fernandez, J.R. Pedro, R. Ruiz-Garcia, T. Temporal-Sanchez, E. Pardo, F. Lloret, M.C. Munoz, J. Mol. Catal. A: Chem. 250 (2006), 20. (b) K.S. Banu, T. Chattopadhyay, A. Banerjee, M. Mukherjee, S. Bhattacharya, G.K. Patra, E. Zangrando, D. Das, Dalton Trans. 40 (2009), 8755
64. (a) A. Jana, N. Aliaga-Alcalde, E. Ruiz, S. Mohanta, Inorg. Chem., 52 (2013), 7732. (b) P. Kar, R. Haldar, C.J. Gómez-García, A. Ghosh, Inorg. Chem., 51 (2012), 4265.
65. M. N. Akhtar, M. Shahid, M. S. Ahmad, W. Zierkiewicz, M. Michalczyk, M. B. Taj, M. Khalid, M. A. Hanif, Journal of Molecular Structure. 1252, 2022, 131685.

66. (a) L. Mandal, S. Sasmal, H.A. Sparkes, J.A.K. Howard, S. Mohanta, Inorg. Chim. Acta, 412 (2014), 38. (b) R. Modak, Y. Sikdar, S. Mandal, S. Goswami, Inorg. Chem. Commun., 37 (2013), 193. (c) S. Majumder, S. Mondal, P. Lemoine, S. Mohanta, Dalton Trans., 42 (2013), 4561. (d) L.I. Simandi, T. Barna, G. Argay, T.L. Simandi, Inorg. Chem., 34 (1995), 6337.
67. (a) M. Das, R. Nasani, M. Saha, S.M. Mobin, S. Mukhopadhyay, Dalton Trans., 44 (2015), 2299. (b) A. Guha, A. Banerjee, R. Mondol, E. Zangrando, D. Das, J. Coord. Chem., 64 (2011), 3872. (c) A. Guha, K.S. Banu, S. Das, T. Chattopadhyay, R. Sanyal, E. Zangrando, D. Das, Polyhedron, 52 (2013), 669. (d) A. Biswas, L.K. Das, M.G.B. Drew, G. Aromi, P. Gamez, A. Ghosh, Inorg. Chem., 51 (2012), 7993.
68. A. Guha, T. Chattopadhyay, N. D. Paul, M. Mukherjee, S. Goswami, T. K. Mondal, E. Zangrando, D. Das, Inorg. Chem. 51, 2012, 16, 8750–8759.
69. (a) B. Baruah, S. Das, A. Chakravorty, Inorg. Chem., (2002), 41, 4502-4508. (b) S. P. Rath, K. K. Rajak, A. Chakravorty, Inorg. Chem. 38(1999) 4376-4377.
70. J. S. Martinez, G. L. Carroll, R. A. Tschirret-Guth, G. Altenhoff, R. D. Little, A. Butler,J. Am. Chem. Soc. 123, 2001,14, 3289–3294.
71. J. N. Carter-Franklin, J. D. Parrish, R. A. Tschirret-Guth, R. D. Little, A. Butler, J. Am. Chem. Soc. 125, 2003, 13, 3688–3689.
72. (a)J. S. Martinez, G. L. Carroll, R. A. Tschirret-Guth, G. Altenhoff, R. D. Little, A. Butler, J. Am. Chem. Soc. 123, 2001, 3289−3294. (b) A. Butler, J. N. Carter, M. T. Simpson, In Handbook on Metalloproteins; I. Bertini, A. Sigel, H. Sigel, Eds. M. Dekker: New York, 2001; 153−179. (c)W. Hemrika, R. Renirie, H. Dekker, R. Wever, ACS Symp. Ser. 711, 1998, 216−227.
73. (a) E. Quin, J. R. Devlin, D. Cameron, K. M. Hannan, R. B. Pearson, R. D. Hannan, Biochim. Biophys. Acta, Mol. Basis Dis., 2014, 1842, 802–816. (b) A. Torgovnick, B. Schumacher, Front Genet. 6, 2015, 157. (c) C. Papalouka, M. Adamaki, P. Batsaki, P. Zoumpourlis, A. Tsintarakis, M. Goulielmaki, S. P. Fortis, C. N. Baxevanis, V. Zoumpourlis, Int. J. Mol. Sci. 24(3), 2023, 2760.
74. (a) J. D. Watson, F. H. C. Crick, Nature, 1953, 171, 737–738. (b) B. J. Pages, D. L. Ang, E. P. Wright, J. R. Aldrich-Wright, Dalton Trans. 44, 2015, 3505-3526.

75. N. C. Seeman, H. Wang, X. Yang, F. Liu, C. Mao, W. Sun, L. Wenzler, Z. Shen, R. Sha, H. Yan, M. H. Wong, P. Sa-Ardyen, B. Liu, H. Qiu, X. Li, J. Qi, S. M. Du, Y. Zhang, J. E. Mueller, T.-J. Fu, Y. Wang and J. Chen, Nanotechnology, 9,1998, 257–273
76. S. Arnott, Nature, 320,1986, 313.
77. (a) M. J. Hannon, V. Moreno, M. J. Prieto, E. Molderheim, E. Sletten, I. Meistermann, C. J. Isaac, K. J. Sanders and A. Rodger, Angew. Chem., Int. Ed., 2001, 40, 879–884. (b) S. Arnott, Nature, 1986, 320, 313.
78. C. Oguey, N. Foloppe, B. Hartmann, PLoS One, 2010, 5, 15931.
79. (a) D. Svozil, J. Kalina, M. Omelka, B. Schneider, Nucleic Acids Res., 2008, 36, 3690–3706. (b) V. R. Parvathy, S. R. Bhaumik, K. V. R. Chary, G. Govil, K. Liu, F. B. Howard, H. T. Miles, Nucleic Acids Res., 2002, 30, 1500–1511. (c) M. L. Bochman, K. Paeschke V. A. Zakian, Nat. Rev. Genet., 2012, 13, 770–780
80. T. Hollis, Methods Mol Biol. 363, 2007, 225-37.
81. E. R. Jamieson, S. J. Lippard, Chem. Rev. 99, 1999, 2467–2498.
82. S. Ishida, J. Lee, D. J. Thiele, I. Herskowitz, Proc. Natl. Acad. Sci. U. S. A., 99, 2002, 14298–14302.
83. Q. Lu, J. Med. Chem., 50, 2007, 2601–2604.
84. D. Carter, J.X. Ho, Advances in Protein Chemistry. Vol. 45, Academic Press, New York, 1994, pp. 153–203.
85. E.L. Gelamo, C.H.T.P. Silva, H. Imasato, M. Tabak, Biochimica et Biophysica Acta 1594, 2002, 84-99.
86. MART; SAINT; SADABS; XPREP; SHELXTL, Bruker AXS Inc., Madison, WI, 1998.
87. Sheldrick, G. M. SHELXTL, v. 6.14, Bruker AXS Inc., Madison, WI, 2003.
88. Johnson, C. K. ORTEP Report ORNL-5138, Oak Ridge National Laboratory, Oak Ridge, TN, 1976.
89. J. Wagler, D. Gerlach and G. Roewer, Inorg. Chim. Acta, 2007, 360, 1935–1942.
90. M. J. Frisch, G. W. Trucks, H. B. Schlegel, G. E. Scuseria, M. A. Robb, J. R. Cheeseman, G. Scalmani, V. Barone, B. Mennucci, G. A. Petersson, H. Nakatsuji, M. Caricato, X. Li, H. P. Hratchian, A. F. Izmaylov, J. Bloino, G. Zheng, J. L. Sonnenberg, M. Hada, M. Ehara, K. Toyota, R. Fukuda, J. Hasegawa, M. Ishida, T. Nakajima, Y. Honda, O. Kitao, H. Nakai, T. Vreven, J. A. Montgomery Jr., J. E. Peralta, F. Ogliaro, M. Bearpark, J. J. Heyd, E.

Brothers, K. N. Kudin, V. N. Staroverov, R. Kobayashi, J. Normand, K. Raghavachari, A. Rendell, J. C. Burant, S. S. Iyengar, J. Tomasi, M. Cossi, N. Rega, J. M. Millam, M. Klene, J. E. Knox, J. B. Cross, V. Bakken, C. Adamo, J. Jaramillo, R. Gomperts, R. E. Stratmann, O. Yazyev, A. J. Austin, R. Cammi, C. Pomelli, J. W. Ochterski, R. L. Martin, K. Morokuma, V.G. Zakrzewski, G.A. Voth, P. Salvador, J. J. Dannenberg, S. Dapprich, A. D. Daniels, O. Farkas, J. B. Foresman, J. V. Ortiz, J. Cioslowski, D. J. Fox, Gaussian 09, (Revision A.1), Gaussian, Inc., Wallingford, CT, 2009

91. N. M. O'Boyle, A. L. Tenderholt, K. M. Langner, J. Comput. Chem. 2008, 29, 839-845
92. E. Runge, E. K. U. Gross, Phys. Rev. Lett. 1984, 52, 997-1000
93. (a) A. D. Becke, J. Chem. Phys., 1993, 98, 5648-5652. (b) C. Lee, W. Yang, R. G. Parr, Phys. Rev. B., 1988, 37, 785-789.
94. (a) P. J. Hay, W. R. Wadt, J. Chem. Phys., 1985, 82, 270-283. (b) P. J. Hay, W. R. Wadt, J. Chem. Phys., 1985, 82, 299-310.
95. X. Gao, Y.Wang, Y. Wang, J. Jia, X. Su, Sci. Sin. Chim. 2011, 41, 1145-1155.
96. (a) M. E. Casida, C. Jamoroski, K. C. Casida, D. R. Salahub, J. Chem. Phys. 1998, 108, 4439-4449. (b) R. E. Stratmann, G. E. Scuseria, M. J. Frisch, J. Chem. Phys. 1998, 109, 8218-8224. (c) R. Bauernschmitt, R. Ahlrichs, Chem. Phys. Lett., 1996, 256, 454-464
97. (a) V. Barone, M. J. Cossi, Phys. Chem. A., 1998, 102, 1995-2001. (b) M. Cossi, V. J. Barone, Chem. Phys., 2001, 115, 4708-4717. (c) M. Cossi, N. Rega, G. Scalmani, V. J. Barone, Comp. Chem., 2003, 24, 669-681.
98. (a) T. Liu, H. -X. Zhang, B. -H. Xia, J. Phys. Chem. A., 2007, 111, 8724-8730. (b) X. Zhou, H. -X. Zhang, Q.-J. Pan, B. -H. Xia, Tang, A.-C. J. Phys. Chem. A., 2005, 109, 8809-8818. (c) X. Zhou, A. -M. Ren, J. -K. Feng, J. Organomet. Chem., 2005, 690, 338-347. (d) A. Albertino, C. Garino, S. Ghiani, R. Gobetto, C. Nervi, L. Salassa, E. Rosenverg, A. Sharmin, G. Viscardi, R. Buscaino, G. Cross, M. J. Milanesio, Organomet. Chem., 2007, 692, 1377-1391.

CHAPTER II

Oxidovanadium (V and IV) complexes incorporating coumarin based O^N^O ligand: synthesis, structure and catalytic activities†

ABSTRACT

The tridentate ligand **H_2L_1**, [(E)-7-Hydroxy-8-[(2-hydroxy-phenylimino)-methyl]-4-methyl-chromen-2-one] has been used in the present work towards the synthesis of mononuclear oxidovanadium complexes. Three mononuclear complexes [VOL_1(OMe)(MeOH)], **1**; [VO(L_1)(8-Hq)], **2** and [VO(L_1)(1,10-phen)], **3** have been successfully synthesized with high yields by reacting [VO(acac)$_2$] with **H_2L_1** in 1:1 ratio in methanol under refluxing conditions where 8-hydroxyquinoline and 1,10-phenanthroline were used as co-ligands in the synthesis of complex **2** and **3**. X-ray crystallographic studies reveal that in all the complexes synthesized in the present study, the ligand **H_2L_1** binds as O^N^O coordinating ligand. The synthesized complexes were well characterized by using UV-Vis, IR, NMR and Mass spectral techniques. The physiochemical properties have been well interpreted by density functional theory (DFT) and time dependent density functional theory (TDDFT) calculations. The synthesized complexes were established to show some distinctive properties e.g. oxidative bromination of aromatic aldehyde with high conversion rate and enhanced selectivity as well as high TON and TOF. The above properties were all well matched and demonstrated by using UV-visible and fluorescence as well as quenching studies. Complex **1** reacts with 3,5-DTBC catalytically in presence of molecular oxygen to generate corresponding ortho-benzoquinone.

II.1. INTRODUCTION

Vanadium ($3d^3 4s^2$) displays all oxidation states in the interval of -3 to +5. The states +2 to +5 can be sustained in aqueous solution and on the whole the most stable states are +4 and +5. The coordination chemistry of vanadium (IV) as well as Vanadium (V) with multidentate ligand has considered the great attention of many researchers for decades. Vanadium is an essential bio-metal which shows remarkable activities such as insulin mimetic agent, [1-3] catechol oxidize activity, anti-cancer activity and catalytic activity in haloperoxidase [4-6] and it also possess pharmacological properties [7]. Many marine algae [8-10], some lichens [11-12] and fungi [13-18] use vanadium-dependent haloperoxidase (VHPO) for the catalytic synthesis of organobromo compounds. It is assumed that the marine organisms use the organobromo compounds for their self-defense against predators. Vanadium haloperoxidase actually catalyse the halogenations of the organic compounds in presence of halide ions and peroxide under feasible reaction condition. Vanadium (V) acts as a strong Lewis acid to activate the peroxo group, which then undergoes nucleophilic attack by bromide to form the reactive "Br^+" intermediate. This intermediate then reacts with organic compounds containing alcohols or sulfide to form organobromo compounds. Monobromination of salicylaldehyde with relatively high yield is reported by many research groups but dibromination of salicylaldehyde with high yield up to 72% is rare. Herein, we report the formation of dibromo and tribromo salicylaldehyde via catalysis by complex 2 and 3. The oxidation of catechols to quinones in presence of molecular oxygen is an important biochemical transformation usually catalyzed by binuclear copper. In such copper complexes the rate of formation of quinones from catechol is in the order of 10^{-2} to 10^{-1} min^{-1} [19-20]. Various model systems of Vanadium complexes have been published to illuminate the mechanism of the catechol-quinone conversion. In this present work, the vanadium (V) complexes show relatively higher rate of conversion than other vanadium containing complexes have been reported [21].

The present work is concerned with the successful synthesis of mononuclear oxidovanadium complexes bearing tridentate O^N^O coordinating Schiff base synthesized from 7-hydroxy-4-methyl-2-oxo-2H-chromene-8-carbaldehyde and 2-aminophenol. The complexes were well characterized using different spectral techniques such as UV-Vis, IR, NMR, Mass etc. Crystal structure of two complexes has been determined. The electrochemical behaviour of the complexes was also examined. The bromoperoxidase activity and the catecholase were studied.

Here, we also present a full density functional theory (**DFT**) and time-dependent density functional theory **(TDDFT**) investigation to get better insight into the geometry, electronic structure, and optical properties of these systems, with good accuracy. Geometry optimizations of the singlet ground-state were carried out by means of DFT calculations. TDDFT calculations of several singlet states have been performed for better understanding of the electronic origin of the absorption spectra.

II.2. EXPERIMENTAL SECTION

A. Materials

Vanadyl sulphate was purchased from S D Fine-Chem Limited, 4-Methylumbelliferone and 1,10-Phenanthroline were purchased from Sigma-Aldrich. 8-Hydroxyquinoline was purchased from Alfa-Aesar. Potassium Bromide was purchased from Fischer scientific and Hydrogen peroxide (30% V/V) was obtained from Merck. $VO(acac)_2$ was prepared according to the literature. [22] Analytically pure solvents and chemicals are used throughout the study. All the reactions with metal salts are carried out under open air atmosphere.

B. Preparation of Compounds

Ligand

Synthesis of (E)-7-Hydroxy-8-[(2-hydroxyphenylimino)-methyl]-4-methyl-chromen-2-one [H_2L_1]:

7-Hydroxy-4-methyl coumarin (3.08g, 15mmol) which was prepared above was dissolved in 15mL methanol. Then 2-aminophenol (1.64g, 15.0mmol) was added to the solution and the mixture was heated and stirred for 6 h affording a deep orange coloured precipitate of the targeted Schiff base ligand (**H_2L_1**). After that the orange solid was filtered and washed with mother liquor, and kept under vacuum. Yield: 3.11g (70%), ^{1}H NMR ($CDCl_3$, 300 MHz):δ 10.26 (s, 1H); 9.33 (s, 1H); 7.73 (d, 1H, J=9.5 Hz), 7.60 (s, 1H), 7.17 (s, 1H), 7.08-6.92 (m, 3H), 6.79 (d, 1H, J= 9.1Hz), 6.16 (s, 1H), 2.38 (s, 3H,for $–CH_3$), Elemental anal. calcd. for $C_{17}H_{13}NO_4$: C, 69.15; H, 4.44; N,

4.74, O, 21.67. Found: C, 69.25; H, 4.55; N, 4.60, O, 21.60. IR (KBr, cm^{-1}): ***ν*** (O–H): 3043; ***ν*** (imine C=N): 1622, 1603 (lactone). ESI-MS (CH_2Cl_2): m/z 296.092 $[M+H]^+$,Found: 296.0958.

Complexes

$[V^VO(L_1)(OMe)(MeOH)]$, complex 1

The ligand $\mathbf{H_2L_1}$ (1.5g, 5 mmol) and $[V^{IV}O(acac)_2]$ (1.33g, 5 mmol) both were dissolved in 7.5mL methanol respectively. Then the two solutions were mixed and heated under reflux for 8h. The resulting clear brown coloured solution was cooled and kept in air for slow evaporation. After two days black crystals were generated suitable for X-ray diffraction analysis. Yield: 1.03 g (81%). ^1H NMR ($CDCl_3$, 400 MHz): δ 9.79 (s, 1H); 7.89 (s, 1H); 7.75 (s, 1H), 7. 46 (s, 1H), 7.23 (s, 1H), 7.0 (m, 1H), 6.77 (m, 1H), 6.40 (d, 1H, J=8Hz), 6.19 (s, 1H), 2.50 (s, 3H, for –CH3), 1.61 (s, 6H). Elemental anal calcd for $C_{19}H_{18}NO_7V$: Theo: C, 53.91; H, 4.29; N, 3.31, O, 26.46, V, 12.03. Found: C, 53.45; H, 4.65; N, 3.21; O, 26.23; V, 12.21. IR (KBr, cm^{-1}): ν (O–H): 3033 (from bound MeOH moiety); ν (imine C=N): 1624, 1604 (lactone), 933 (V=O stretch). ESI-MS (CH_2Cl_2): m/z 423.052 Found: 408.138. $[M-CH_3]^+$.

$[V^VO(L_1)(8\text{-Hq})]$. Complex 2

Ligand $\mathbf{H_2L_1}$ (1.5g, 5 mmol), $[V^{IV}O(acac)_2]$ (1.33g, 5 mmol) and 8-Hydroxyquinoline (0.73g, 5 mmol) were added in 15 mL methanol and were heated under reflux for 8h with stirring. Then the deep violet solution was cooled and kept in air 2 days for slow evaporation, a diamond shaped black coloured crystals were formed suitable for single crystal X-ray diffraction analysis. Yield: 0.36g (75%) ^1H NMR ($CDCl_3$, 300 MHz): δ 8.15 (s, 1H), 7.80 (s, 1H), 7.66 (t, 2H, J = 8.85 Hz); 7.50 (d, 1H, J = 5.94 Hz), 7.28-7.21 (m, 5H), 6.89-6.77 (m, 2H), 6.53 (d, 1H, J = 8.1Hz); 6.19 (s, 1H), 2.41 (s, 3H, for -CH_3). Elemental anal. calcd. for $C_{26}H_{17}N_2O_6V$: C, 61.92; H, 3.40; N, 5.55, O, 19.03, V, 10.10 Found: C, 61.98; H, 3.62; N, 5.35, O, 19.12, V, 10.04. IR (cm-1): ν (imine C=N): 1622, 1599 (lactone), 963 (V=O stretch). ESI-MS (CH_2Cl_2): m/z 504.053 Found for $[M+H]^+$: 505.064.

$[V^{IV}O(L_1)$(1,10-phenanthroline)], Complex 3

Ligand $\mathbf{H_2L_1}$(1.5g, 5 mmol), $[V^{IV}O(acac)_2]$ (1.33g, 5 mmol) and 1,10-phenanthroline (0.9g, 5 mmol) were dissolved in 20 mL methanol solution and were heated under reflux for 12h with stirring affording a red colored precipitate. The precipitate was filtered and washed with methanol and kept under vacuum. After that re-crystallization had been done and found crystalline product. Unfortunately, despite several atoms we hardly achieved good quality single crystal which can be diffracted. Yield: 0.5g (77%), Elemental Anal. Calcd. for $C_{29}H_{19}N_3O_5V$: C, 64.45; H, 3.54; N, 7.78; O, 14.80; V, 9.43. Found: C, 64.58; H, 3.51; N, 7.48, O, 14.65 V, 9.23; IR (cm-1): ν (imine C=N): 1626, (lactone) 1586, 948 (V=O stretch). ESI-MS (CH_2Cl_2): m/z 540.076 $[M]^+$, Found: 540.114. The complex is paramagnetic, having magnetic moment **1.75 BM** at room temperature.

C. X-Ray Structure Determination

The single crystal suitable for X-ray crystallographic analysis of the complex was obtained by slow evaporation of methanol solution of the complex. The X-ray intensity data were collected on Bruker AXS SMART APEX CCD diffractometer (Mo Kα, λ = 0.71073 Å) at 293 K. The detector was placed at a distance 6.03 cm from the crystal. Total 606 frames were collected with a scan width of 0.3° in different settings of ϕ. The data were reduced in SAINTPLUS [23] and empirical absorption correction was applied using the SADABS package. Metal atom was located by Patterson Method and the rest of the non-hydrogen atoms were emerged from successive Fourier synthesis. The structures were refined by full matrix least-square procedure on F2. All non-hydrogen atoms were refined anisotropically.

All calculations were performed using the SHELXTL V 6.14program package [24]. Molecular structure plots were drawn using the Oak Ridge thermal ellipsoid plot (ORTEP) [25]. The CCDC numbers are **1914360** and **1920471** for **1** and **2** respectively (**Table 1**).

Table 1: Crystal Data and Structure Refinement Parameters for complex 1 and 2.

	Complex 1	**Complex 2**
Formula	$C_{19}H_{18}NO_7V$	$C_{26}H_{17}N_2O_6V$
M_r	423.29	504.36
Crystal system	triclinic	Orthorhombic
Space group	P-1	$Pca2_1$
a/ Å	8.4009 (17)	38.2320 (4)
b/ Å	10.7220 (2)	8.9445 (7)
c/ Å	11.7100 (2)	12.7294 (12)
α/°	107.03 (3)	90.00
β/°	91.43 (3)	90.00
γ/°	90.48 (3)	90.00
V/ Å^3	1008.1 (4)	4353.0 (7)
Z	2	8
D_{calcd} /g cm^{-3}	1.497	1.539
μ/mm^{-1}	0.531	0.504
θ/°	1.820 - 27.500	1.922 – 27.148
T/K	293 (2)	273 (2)
Reflns collected	3494	4197
R^1, wR^2 [I>2σ(I)]	0.0491, 0.1562	0.0812, 0.2530
GOF on F^2	0.988	0.970

$^{a}R1 = \Sigma \big| |F_o| - |F_c| \big| / \Sigma |F_o|$. ^{b} $wR2 = [\Sigma[w(F_o^2 - F_c^2)^2] / \Sigma[w(F_o^2)^2]]^{1/2}$

D.Physical Measurements

All physical measurements that included elemental analysis, IR, ^{1}H NMR, Absorption spectra, ESI mass spectra, emission spectra, were done as described in Chaptrer 1.

II.3. RESULT AND DISCUSSION

1. Synthesis

Ligand(H_2L_1)

The journey towards the synthesis of tridentate (O^N^O) ligand (H_2L_1) was accompanied by two steps as depicted in scheme 1. Initially 4-methyl-7-hydroxy coumarin was formylated according to the literature reported procedure. [26] In the second step, the formylated product was allowed to react with the methanolic solution of 2-aminophenol for 8h under refluxing condition to afford the desired tridentate Schiff base ligand as an orange colored solid in good yield. The synthesized ligand (Scheme 1) was well characterized by using 1H NMR, IR, Mass spectral analysis.

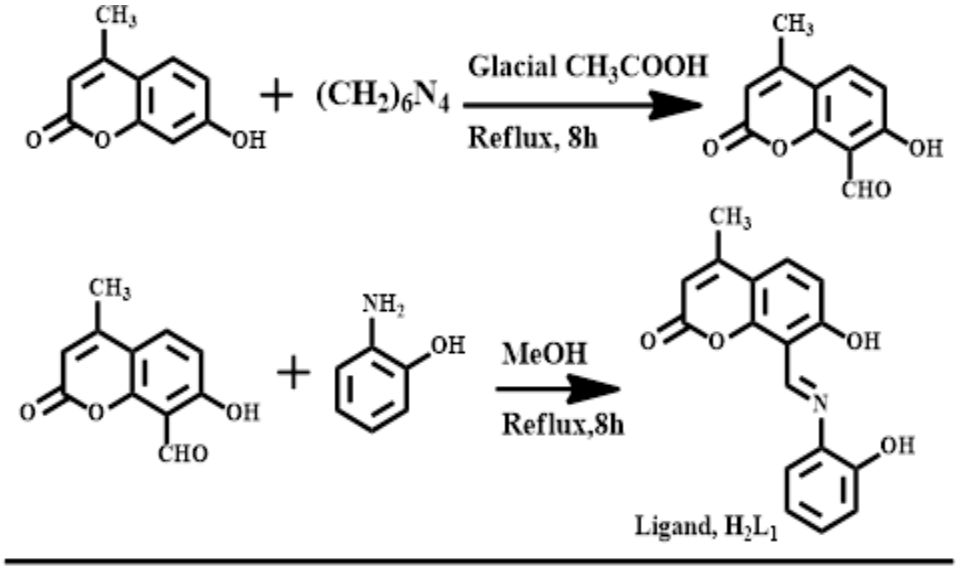

Scheme 1: Synthesis of the ligand, H_2L_1.

Complexes

The stoichiometric reaction of $[V^{IV}O(acac)_2]$ with ligand (H_2L_1) were dissolved in methanol under refluxing condition for 8h afforded complex 1. Complex 2 and 3 was obtained by reacting complex **1** with 8-Hydroxyquinoline and 1,10-phenanthroline (co-ligands) under refluxing condition. The synthetic roots were given in Scheme 2.

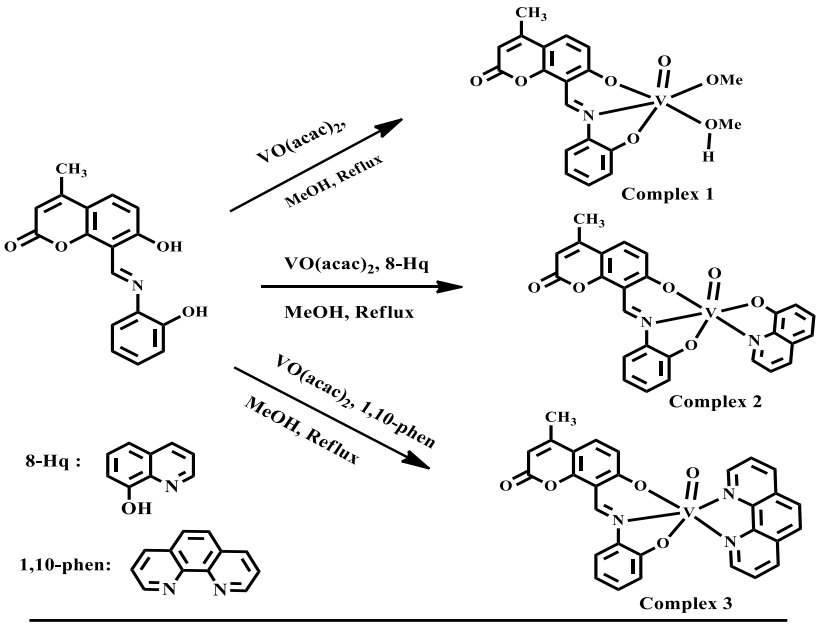

Scheme 2: Synthetic routes towards complex **1, 2** and **3.**

2. Characterization

NMR Spectra: The synthesized ligand and all the complexes except complex **3** are diamagnetic in nature and display well resolved NMR spectra in $CDCl_3$ solution and the spectral data are given in the experimental section. The assigning of NMR peaks is done on the basis of the intensity and spin–spin splitting pattern. The appearance of singlet peak at 10.26 ppm which disappears upon the addition of D_2O confirms the presence of phenolic hydrogen. A singlet corresponding to the azomethine hydrogen atom was observed at 9.33 ppm in the ligand, complexes **1** and **2**.

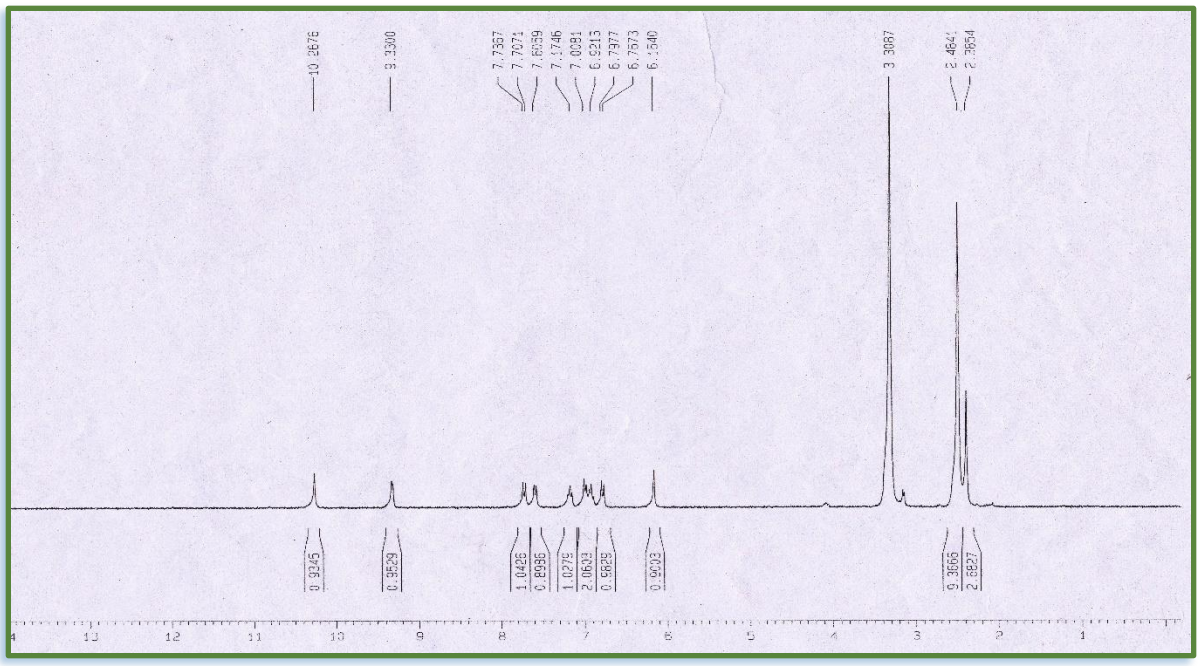

Figure 1: ^{1}H NMR spectrum of ligand.

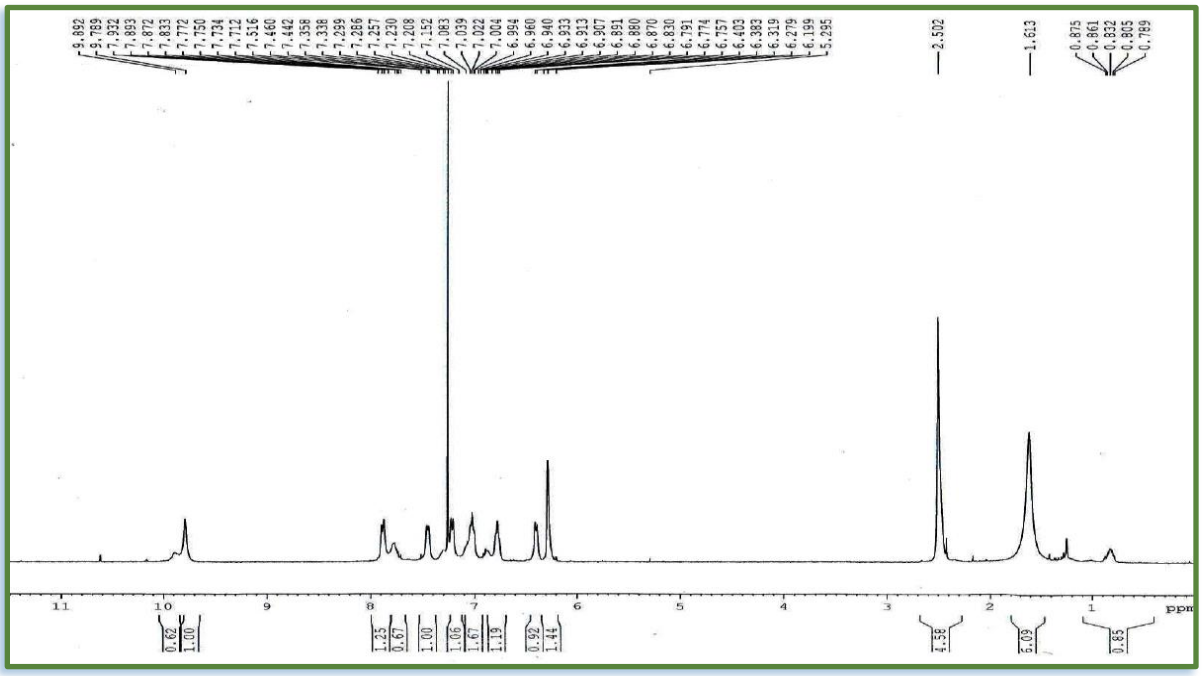

Figure 2: ^{1}H NMR spectrum of Complex **1**.

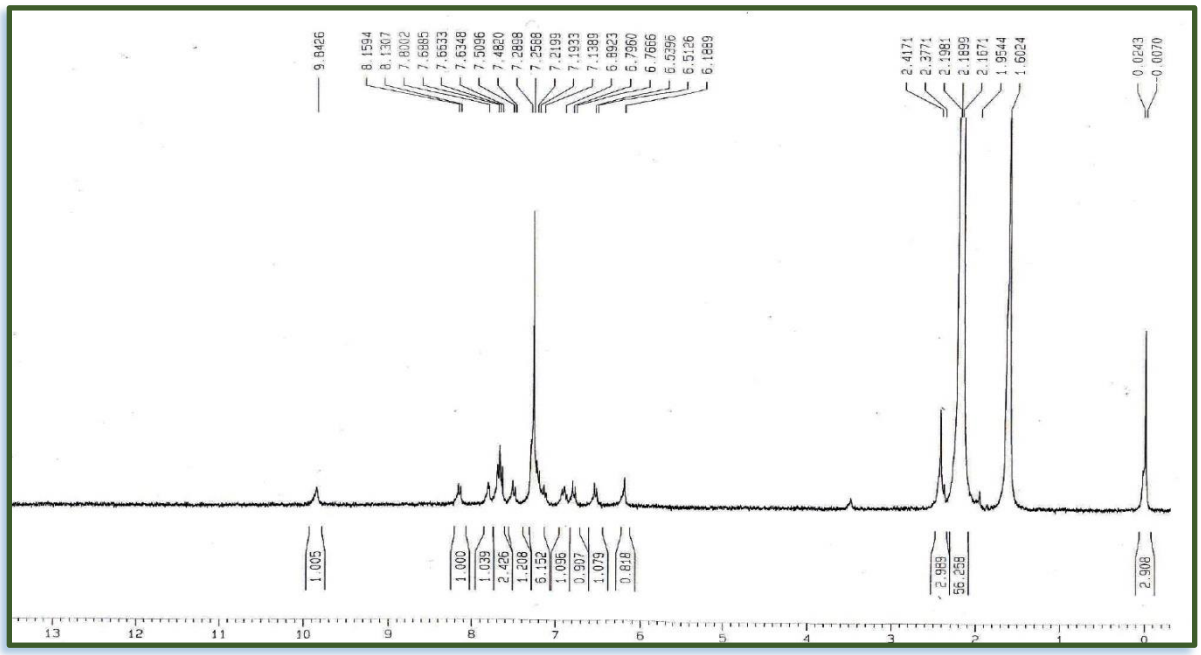

Figure 3: ^{1}H NMR spectrum of Complex **2**.

EPR spectra: Complex 3 exhibits one unpaired electron due to the presence of vanadium in it's +IV oxidation state having the magnetic moment 1.75 Bohr magneton (μB). The paramagnetism corresponds to 3dxy1 configuration. Complexes 3 exhibits hyperfine EPR spectra owing to the ^{51}V(I = 7/2) nucleus, and the simulated g values are 1.9696, which is consistent with the existence of oxidovanadium(IV) ions in complex 3 depicted in figure 4. The average hyperfine splitting (A) is 95.25 G and line width of 2.1 mT.40 The calculated hyperfine splitting value 76.67 G, from DFT study is usually lower than the experimental value.

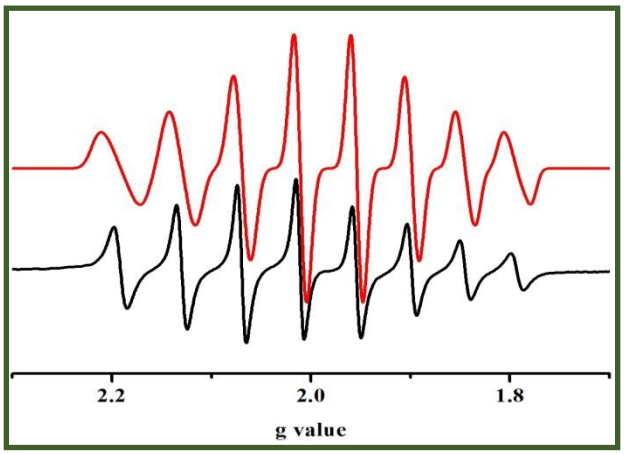

Figure 4: X-band EPR spectra of complex 3 in CH_2Cl_2 (dichloromethane) solution at 298 K (black, experimental; red, simulated).

Electrochemical studies: All the complexes are electroactive in acetonitrile solution. The cyclic voltammogram were recorded with scan rate of 50 mV/sec. Vanadium (V) exhibits one quasi-reversible vanadium (V)/(IV) couple. Complex 1 displays 0.674V (ΔEp = 90 mV) where as that of 2 displays at 0.0V (ΔEp = 200 mV). The more negative value for 2 is associated with higher stabilization of (+V) oxidation state than the (+IV) state. In case of complex 3 the quasi-reversible vanadium (IV)/(V) couple displays at 0.375V (ΔEp = 75 mV). The respective cyclic voltammogram are shown in Figure **5**.

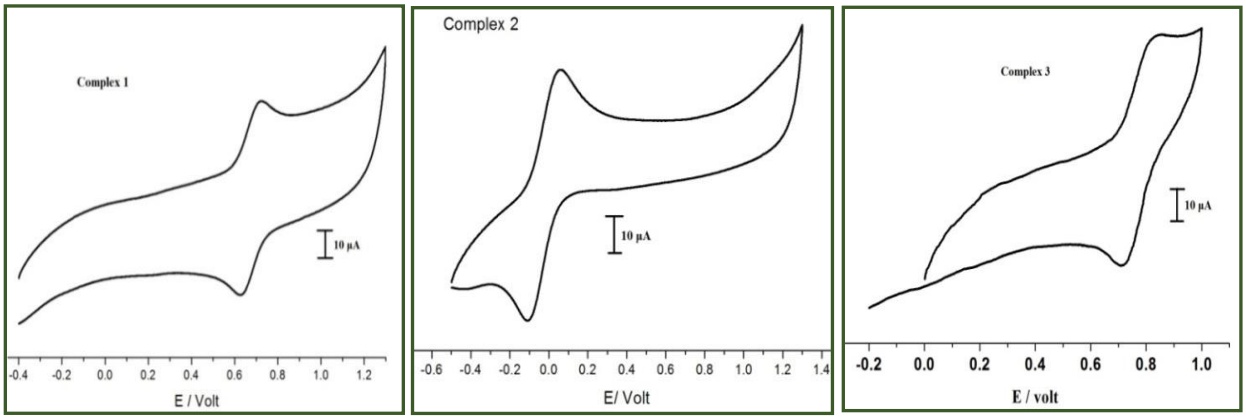

Figure 5: Cyclic voltammogram plots of complex 1, 2 and 3. (Scan rate: 50 mV/s) in CH_3CN solvent at 298K. Conditions: 0.20M $[N(n\text{-}Bu)_4]PF_6$ used as supporting electrolyte and Pt working electrodes.

Mass Spectra: Electrospray ionization mass spectrometry (ESI-MS) of the ligand and the complexes was done. Ligand displayed the highest peak at 296.092 $[M+H]^+$ and the complex 1,2 and 3 displayed the highest m/z peak at 408.138 $[M\text{-}CH_3]^+$, 505.064$[M+H]^+$ and, 540.114$[M]^+$respectively.

IR Spectra: The IR spectra of the ligand and its corresponding metal complexes were recorded in a KBr disk. The appearance of the spectral bands near 1622 cm^{-1} and 1603 cm^{-1} clearly indicates the presence of imine, C=N and lactone moiety respectively. The broad absorption band at 3043 cm^{-1} attributes to the stretching frequency of "free OH" moiety. This spectral data matches satisfactorily with the synthesized ligand.

All the vanadium complexes exhibited spectral bands in the range of 1630-1620 cm^{-1} and 1608-1603 cm^{-1} arising from the imine and lactone moiety vibrations. The spectral bands in the range of

1000 cm^{-1}– 850 cm^{-1} indicates the presence of V=O moiety in the Vanadium (IV/V) complexes and the small band near 500 cm^{-1} relates the presence of V-O moiety. [28] The strong vibrations at 1451 cm^{-1} and 743 cm^{-1} are due to ν(C-N stretch) of the co-ordinated 1,10-phenanthroline moiety in complex 3, the non-coordinated ν(C-N stretch) of 1,10-phenanthroline appears at 1421 cm^{-1} and 731 cm^{-1} respectively.

Crystal Structure: The molecular structures of the complexes [VVO(OMe)(MeOH)(L1)], 1 and [VVO(L1)(8-HQ)], 2, have been determined by using single crystal X-ray diffractometer. The molecular structures of **1** and **2** and **3** are shown below. The selected bond lengths and bond angles are depicted in Table **2**.

Complex 1 crystallizes in the triclinic crystal system with P^{-1} space group. Here the ligand binds with the metal centre as an O^N^O coordinating dianionic ligand in tridentate mode. The ligand possesses two phenoxide groups and imine nitrogen, which are directly bound to the metal centre in a meridional fashion. The fourth coordination site of vanadium is occupied by oxo oxygen atom. The vanadium is occupied by oxo oxygen atom.The remaining two vacant coordination sites of vanadium are occupied by methoxy group and methanol respectively owing to the formation of distorted octahedral geometry.[3f,3h] The V1-O1 bond length (1.58 Å) characterizes the presence of V=O moiety. The elongated V-O bond (2.27 Å) indicates the presence of the attached solvent moiety with the metal centre.

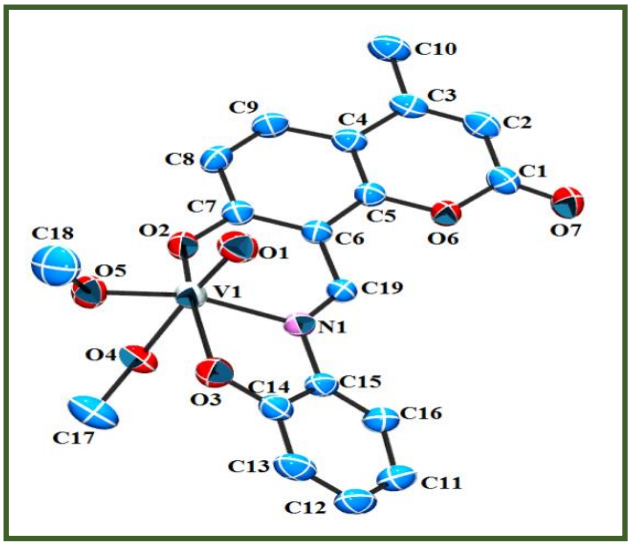

Figure 6: ORTEP plot of complex 1 [VVO(OMe)(MeOH)(L1)]. H atoms and solvent moiety are omitted for clarity.

Complex **2** also crystallizes in the orthorhombic crystal system with space group $Pca2_1$. Here also the four coordination sites of the metal were occupied in the similar fashion, whereas the remaining two vacant sites were occupied by the nitrogen and oxygen atom of the 8-Hq moiety. The nitrogen atom of 8-hyroxyquinoline lies trans to the oxo oxygen atom. The metal complex thus attains distorted octahedral geometry as in the previous case.

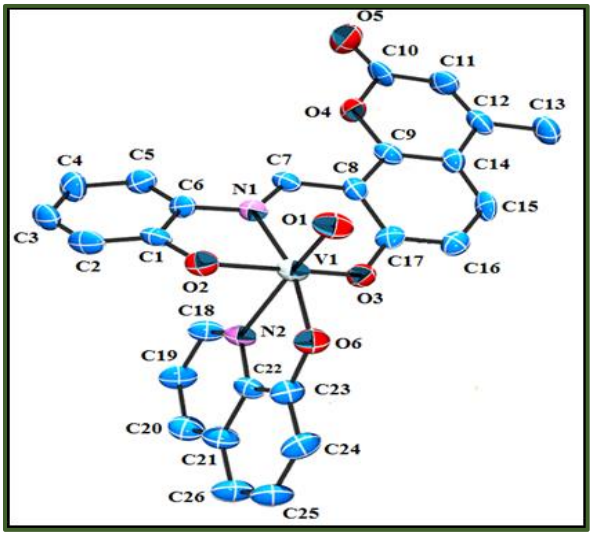

Figure 7: ORTEP plot of complex **2** [$V^{V}O(L_1)$(8-HQ)]. H atoms and solvent moiety are omitted for clarity.

For complex **3**, we have tried several methods but suitable crystal for X-Ray diffraction study was not obtained. Although we have performed DFT studies to get an optimized stable geometry. However, the proposed structure of complex **3** is optimized with the help of DFT and the structural parameters are given in Table **1** and the depicted structure in [fig.**8**]**.**

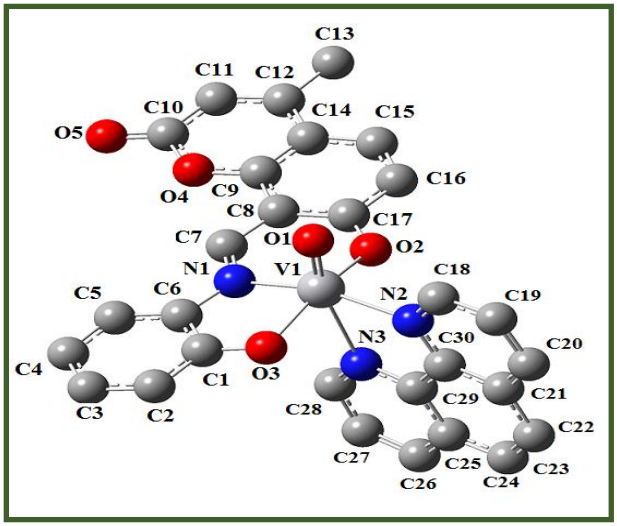

Figure 8: Optimized structure of complex 3 [$VO(L_1)$(1,10-phen)].

Table 2: Selected bond lengths and bond angles of complexes 1, 2 and 3.

Complex 1		Complex 2		Complex 3 (optimized)	
Bond Length (Å)					
V1-O1	1.5843 (19)	V1-O1	1.5920 (11)	V1-O1	1.6000
V1-O2	1.8964 (18)	V1-O2	1.8860 (12)	V1-O2	1.9823
V1-O3	1.9106 (19)	V1-O3	1.8890 (11)	V1-O3	1.9540
V1-O4	2.272 (2)	V1-O6	1.8500 (11)	V1-N1	2.0841
V1-O5	1.7651 (19)	V1-N1	2.1110 (13)	V1-N2	2.4152
V1-N1	2.157 (2)	V1-N2	2.3500 (12)	V1-N3	2.1815
C19-N1	1.279 (3)	C7-N1	1.2980 (18)	C7-N1	1.3054
Bond angles (°)					
O1-V1-O2	97.95 (10)	O1-V1-O2	100.9 (6)	O1-V1-O2	100.0
O1-V1-O3	100.85 (10)	O1-V1-O3	96.8 (6)	O1-V1-O3	103.3
O1-V1-O4	172.25 (9)	O1-V1-O6	101.2 (6)	O1-V1-N1	103.6
O1-V1-O5	102.19 (10)	O1-V1-N1	98.7 (6)	O1-V1-N2	165.1
O1-V1-N1	93.31 (9)	O1-V1-N2	177.6 (6)	O1-V1-N3	93.5
O2-V1-O3	152.92 (9)	O2-V1-O3	156.3 (5)	O2-V1-O3	150.5
O2-V1-O4	77.03 (8)	O2-V1-O6	95.9 (5)	O2-V1-N1	86.9
O2-V1-O5	101.74 (9)	O2-V1-N1	78.9 (5)	O2-V1-N2	78.9
O2-V1-N1	82.05 (8)	O2-V1-N2	80.6 (5)	O2-V1-N3	93.9
O3-V1-O4	82.04 (8)	O3-V1-O6	95.9 (5)	O3-V1-N1	80.6
O3-V1-O5	93.16 (9)	O3-V1-N1	83.0 (5)	O3-V1-N2	80.2
O3-V1-N1	77.60 (8)	O3-V1-N2	82.2 (5)	O3-V1-N3	91.6
O5-V1-O4	84.73 (8)	O6-V1-N1	160.1 (5)	N1-V1-N2	91.0
O4-V1-N1	80.23 (7)	O6-V1-N2	76.7 (5)	N1-V1-N3	162.3
O5-V1-N1	163.27 (9)	N1-V1-N2	83.5 (4)	N2-V1-N3	72.0

3. *Geometry optimization, electronic structure, charge distribution*

Geometrical optimizations for complexes **1** and **2** are accomplished in presence of solvent. The main geometrical optimized structure of complexes **1**, **2** and **3** are given below.

Complex 1

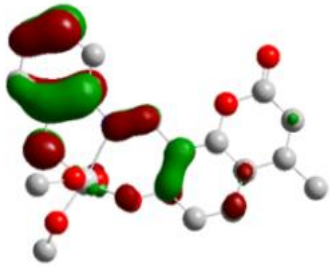

HOMO

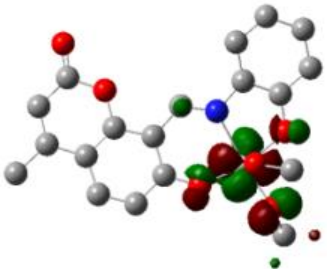

LUMO

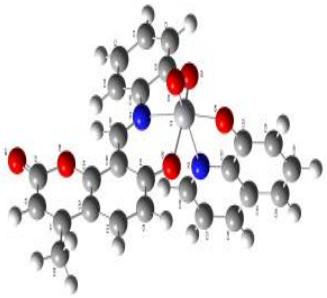

Complex 2

HOMO

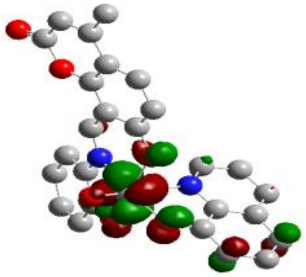

LUMO

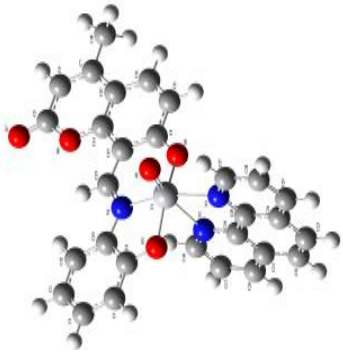

Complex 3

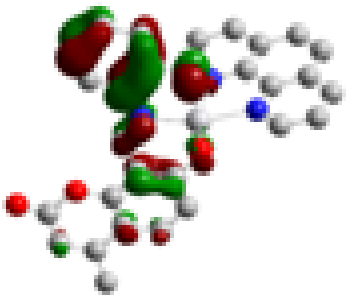

HOMO

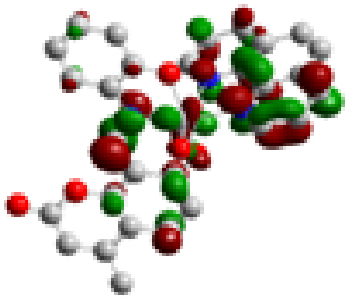

LUMO

The geometries retain a distorted octahedral arrangement around the vanadium (V) metal centre. The optimized structures of these complexes are well matched to the experimentally observed structures, which were determined using single crystal XRD studies. A slight variation in structural parameters may occur due real molecules. [29] The V–N and V–O bond lengths are in the range of

1.58–2.27 Å in both the theoretical calculation and experimental observation. The isodensity plot of some selected frontier molecular orbitals in their singlet ground state (S_0) is listed in **Table 3**. A partial molecular orbital diagram with the HOMO and LUMO to crystal lattice distortion in for all the three complexes is shown in **Fig. 9**. In the ground state (S_0), the HOMO of complexes **1** and **2** are similar in energy whereas that of complex **3** is slightly higher. But we can see the variation in the energies of LUMO for the complexes in their ground state. The LUMO of complex **3** is energetically much higher than complex **1** and **2**. The HOMO - LUMO energy gaps in all the mononuclear complexes are in the close resemblance to each other and the values are 2.89 eV, 2.51 eV and 3.09 eV for complexes **1**, **2** and **3** respectively. The corresponding orbital contribution for the three complexes is givenin **Table 4**. The electron density in the HOMO of all the complexes mainly resides on the coumarin moiety (in the rangeof 20–21%) and phenol moiety (in the range of 68-69%). On the other hand, for the LUMO, the electron densitymainly resides on the vanadium centre (in the range 65-68%)and the π* orbitals of the attached methanol (complex **1**) and 8-hydroxyquinoline (complex **2**) (in the range of 14-19%). For complex 3 the LUMO is distributed over the metal centre (9%), imine bond (18%), phenanthroline (48%) and coumarin moiety (17%). This data depicts a very low density around the metal centre.

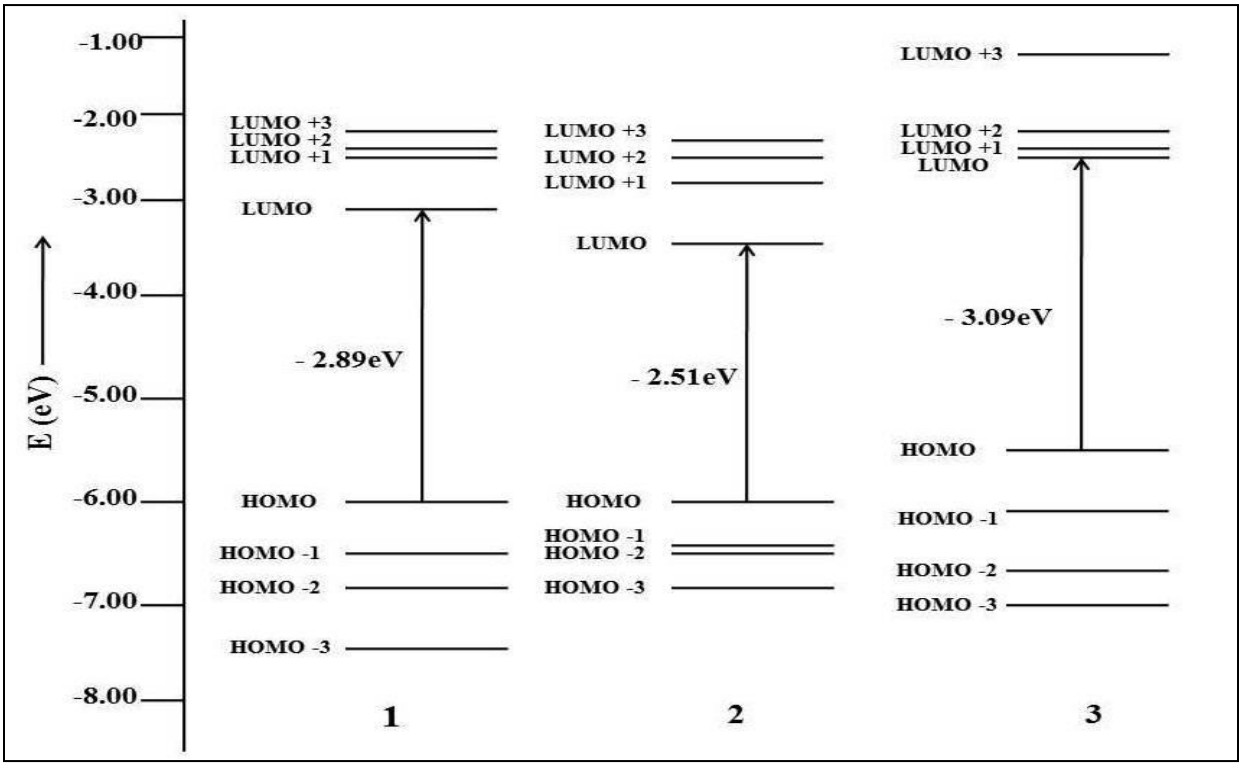

Figure 9: Partial orbital molecular diagram of complex **1, 2** and **3.**

Table **3**: Isodensity plot of some frontier molecular orbital of the complexes.

	Complex 1	Complex 2	Complex 3
LUMO + 3	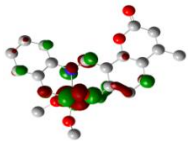	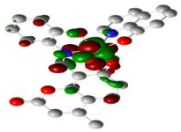	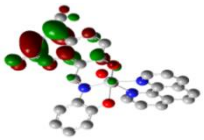
LUMO + 2	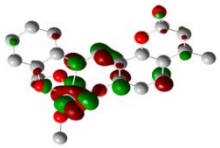	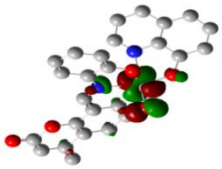	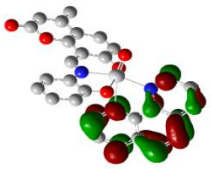
LUMO +1	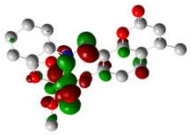	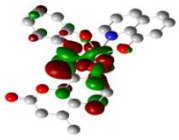	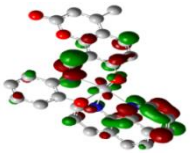
LUMO	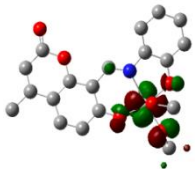	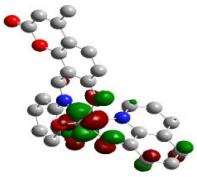	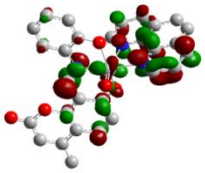
HOMO	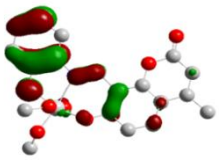	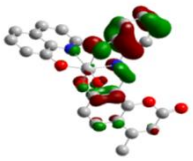	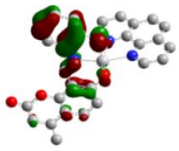
HOMO - 1	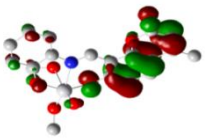	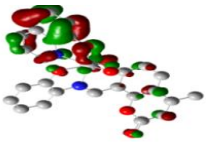	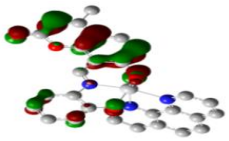
HOMO - 2	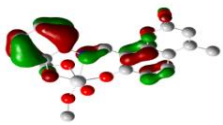	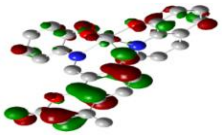	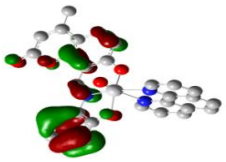
HOMO - 3	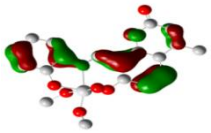	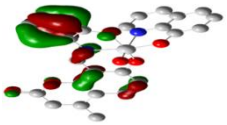	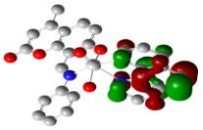

Table 4: Composition of the frontier molecular orbitals of complexes **1-3**:

Complex 1		**% contribution**						**Main bond type**
MO		**Ph**	**Oxo**	**MeOH**	**Coum**	**Azometh**	**V**	
108	**L+3**	12	13	1	15	11	50	d(V)+ π*(coum)+ π*(oxo)
107	**L+2**	9	12	2	22	10	45	d(V)+ π*(coum)+ π*(oxo)
106	**L+1**	5	15	3	13	17	46	d(V)+ π*(azometh)+ π*(oxo)
105	**LUMO**	5	3	14	7	2	68	d(V)+ π*(MeOH)
104	**HOMO**	68	2	1	20	9	1	π(ph)+ π(coum)
103	**H-1**	13	1	0	83	1	1	π(ph)+ π(coum)
102	**H-2**	68	1	0	25	6	0	π(ph)+ π(coum)
101	**H-3**	28	0	0	64	7	0	π(ph)+ π(coum)

Complex 2		**% contribution**						**Main bond type**
MO		**Ph**	**Oxo**	**Hq**	**Coum**	**Azometh**	**V**	
128	**L+3**	11	12	5	12	12	47	d(V)+ π*(coum)+ π*(oxo) + π*(ph) + π*(azometh)
127	**L+2**	3	19	3	10	4	61	d(V)+ π*(coum)+ π*(oxo)
126	**L+1**	11	9	2	26	28	24	d(V)+ π*(azometh)+ π*(coum)
125	**LUMO**	5	1	19	8	1	65	d(V)+ π*(hq)
124	**HOMO**	66	2	4	20	7	1	π(ph)+ π(coum)
123	**H-1**	4	0	71	20	0	5	π(hq)+ π(coum)
122	**H-2**	13	2	17	65	1	2	π(ph)+ π(coum) + π(hq)
121	**H-3**	68	1	0	24	7	0	π(ph)+ π(coum)

Complex 3		**% contribution**						**Main bond type**
MO		**Ph**	**Oxo**	**Phen**	**Coum**	**Azometh**	**V**	
137	**L+3**	1	1	0	92	3	3	π*(coum)
136	**L+2**	1	0	97	2	0	1	π*(phen)
135	**L+1**	8	1	44	20	21	5	π*(phen)+ π*(coum) +π*(azometh)
134	**LUMO**	7	1	48	17	18	9	d(V)+ π*(phen)+ π*(azometh)+ π*(coum)
133	**HOMO**	69	1	1	21	7	1	π(ph)+ π(coum)
132	**H-1**	19	2	1	75	2	0	π(ph)+ π(coum)
131	**H-2**	63	1	0	30	7	0	π(ph)+ π(coum)
130	**H-3**	0	0	99	0	0	1	π(phen)

4. *Absorption spectral properties*

The UV- Visible spectral behaviour of the ligand and its corresponding complexes **1, 2** and **3** are recorded in dichloromethane solution at room temperature. The spectral parameters with the experimental molar extinction coefficient (ε) value of $\mathbf{H_2L_1}$ and complexes **1–3** are listed in Table **2**. The relevant electronic spectra are depicted in **Fig. 10**. Ligand shows only one characteristic peak near 350 nm which may arise due to intramolecular n–π* and π–π* charge transfer transitions. The complexes **1, 2** and **3** display a strong peak varying between 300 and 525 nm having molar extinction coefficient in the range of 6400 – 42810 $M^{-1}cm^{-1}$. The bands in the longer wavelength region of these complexes can be attributed to the ligand to metal charge transfer [$H_2L_1 \rightarrow V(d\pi)$] transition. Only complex **3** shows low intense intra-ligand charge transfer transition.

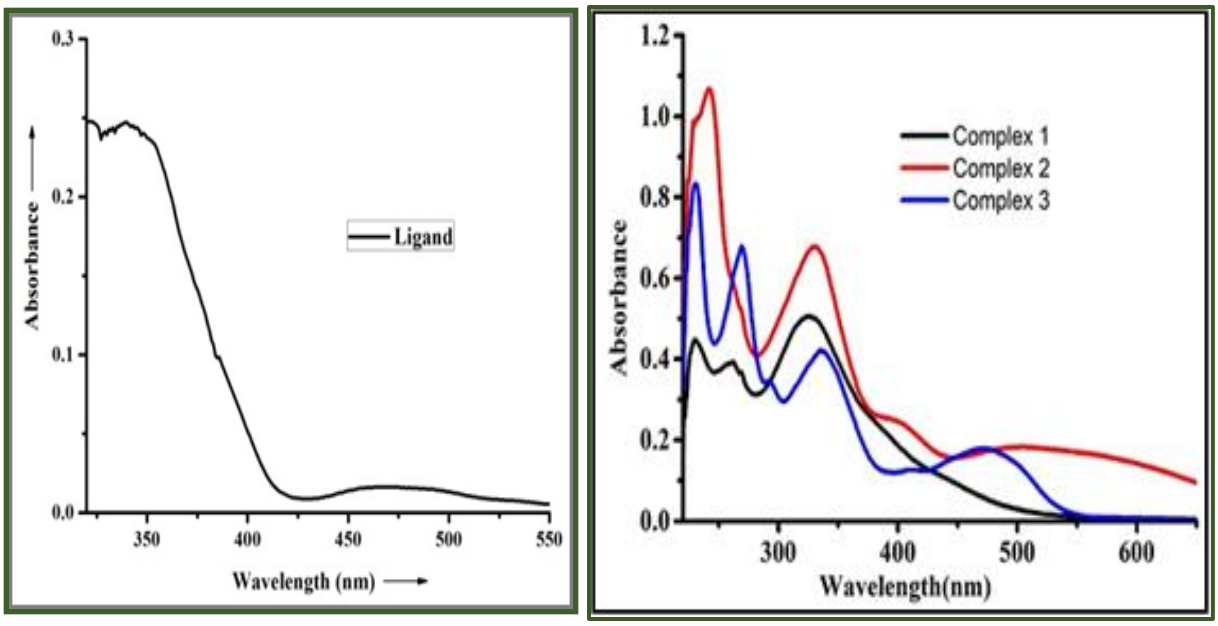

Figure 10: Absorption Spectra of ligand and complexes **1**, **2** and **3** in dichloromethane, at room temperature.

Table 5: Main calculated optical transitions for complexes in DCM:

Compound	Electronic transition	Composition	Excitation Energy(eV)	Oscillator Strength (f)	Configuration Interaction (CI)	Assign	λ_{exp} in nm (ε in $M^{-1}cm^{-1}$)
1	$S_0 \rightarrow S_7$	H→L-3	3.1578 (392 nm)	0.2672	0.5942	**^{1}LMCT**	400 (22502)
	$S_0 \rightarrow S_{13}$	H-2→L+2	3.6936 (335 nm)	0.3001	0.6102	**^{1}LMCT**	327 (42810)
	$S_0 \rightarrow S_{31}$	H-1→L+5	4.6699 (265 nm)	0.0977	0.4261	**^{1}LMCT**	261 (19575)
2	$S_0 \rightarrow S_3$	H-1→L	2.3615 (525 nm)	0.2574	0.4971	**^{1}LMCT**	505 (7845)
	$S_0 \rightarrow S_{10}$	H→L+3	3.0645 (404 nm)	0.1893	0.6341	**^{1}LMCT**	401 (10955)
	$S_0 \rightarrow S_{20}$	H-3→L+2	3.6924 (335 nm)	0.1150	0.6622	**^{1}LMCT**	330 (29225)
3	$S_0 \rightarrow S_6$	H→L+1	2.2661 (472 nm)	0.0905	0.8131	**^{1}LLCT**	472 (6410)
	$S_0 \rightarrow S_{32}$	H→L+5	3.6534 (339 nm)	0.0751	0.4781	**^{1}LMCT**	336 (12485)
	$S_0 \rightarrow S_7$	H→L-3	3.1578 (392 nm)	0.2672	0.5942	**^{1}LMCT**	400 (22502)

5. Catalytic activities

Oxidative bromination of Salicylaldehyde: In the present study oxidative bromination of salicylaldehyde was carried out in presence of synthesized vanadium complexes as catalysts in presence of H_2O_2 (120 mmol), Water (40 mL) in each case was used as solvent. Other conditions were taken as standard: Salicylaldehyde (20 mmol), KBr (50 mmol), $HClO_4$ (80 mmol), Vanadium complexes **1-3** as catalyst (15 mg). The catalytic oxidative bromination reaction afforded three compounds viz. 5-Bromosalicylaldehyde, 3,5-dibromo salicylaldehyde and 2,4,6-tribromophenol. The addition of $HClO_4$ was done in four equal portions during the progress of the reaction, which was found to be necessary to prevent the decomposition of the complex and maximize the

conversion of the substrate. Using similar reaction conditions, maximum 99 percent conversion was accomplished with complex **1** giving mono-bromo derivative as the main product. Selectivity order is as follows; 5-Bromosalicylaldehyde (75%)> 3,5-dibromosalicylaldehyde (24%)> 2,4,6-tribromophenol (1%). Complex **2** and **3** also possesses very high conversion with dibromo derivative (72% and 65% respectively) as the main product. It was also depicted that, if complex **2** was used in the bromination reaction; 2,4,6-tribromophenol was formed as bromination product with low yield (24%). Table **3** provides the percentage conversion of salicylaldehyde and selectivity of the products formed using equivalent reaction conditions for complexes **1, 2** and **3**.Interestingly, when the reaction was performed in the absence of catalyst, the reaction mixture gave very low conversion of salicylaldehyde with the selectivity order of the products as: 5-Bromosalicylaldehyde (85%)> 3,5-dibromosalicylaldehyde (28%)> 2,4,6- tribromophenol (13%).

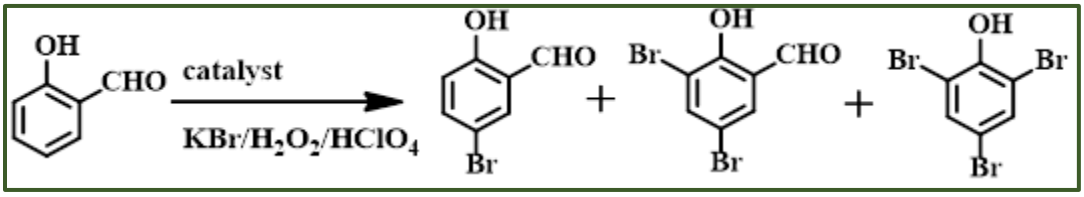

Scheme 3: Oxidative bromination of salicylaldehyde using model vanadium complexes as catalyst.

Table 6: Different experimental findings of bromination reaction by vanadium complexes:

Complex	KBr (g,mmol)	H_2O_2 (g,mmol)	$HClO_4$ (g,mmol)	Complex as catalyst (g)	H_2O (mL)	% Conv.	TON	TOF (h^{-1})	% Selectivity		
									Mono bromo	**Di-bromo**	**Tri-bromo**
1	5.95, 50	15, 120	4.02, 80	0.015	40	**99**	2716	679	75	24	1
2	5.95, 50	15, 120	4.02, 80	0.015	40	**99**	**3136**	**784**	4	**72**	24
3	5.95, 50	15, 120	4.02, 80	0.015	40	**99**	**3140**	**785**	25	**67**	8
Blank Reaction				0.000		35			**85**	2	13

Catechol Oxidation: All the vanadium complexes are stable in their solid state under ambient conditions. But for complex 1, [VO(L1)(OMe)(MeOH)], due to presence of two weak V-O bonds originating from the attached methoxy group and the solvent moiety, the complex is slightly less stable compared to complexes 2 and 3 and is labile to be attacked by cis-diol type of compounds. To examine the assumption, we have treated the complex 1 with 3, 5-ditert-butyl catechol (3, 5-DTBC), an aromatic cis-diol and accordingly a new deep blue coloured complex 1a were formed in O_2 saturated acetone. The deep blue colour of the complex got progressively bleached in presence of molecular oxygen proves the oxidation of catechol in presence of complex 1. The mononuclear vanadium complex is converted to the oxygen bridged dinuclear complex with subsequent release of the bound catechol moiety as ortho- benzoquinone. To proof the reversibility of the reaction, when the dinuclear complex is treated with 3, 5-DTBC again, the mononuclear vanadium complex incorporating the ligand and the cis-diol moiety was formed. The detailed reactions occurring are depicted in scheme **4**.

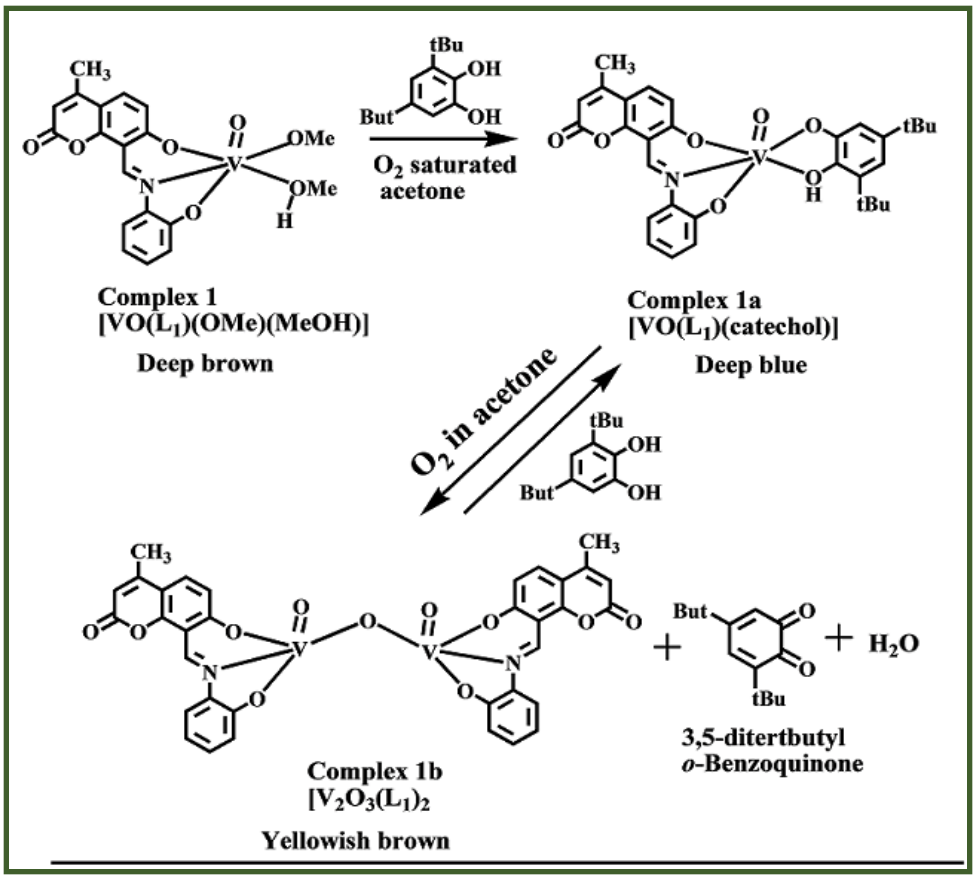

Scheme 4: Probable reaction pathway of complex **1a** with oxygen.

The reaction has been quantitated for complex **1** in acetone solution. The progress of the reaction is observable in both UV-Vis spectra and ^{1}H-NMR spectra. [30] Time dependent UV-spectral studies were performed in dichloromethane to gain better insight into the rate of the reaction in the presence of oxygen. The absorption band at 676 nm of **1a** diminishes gradually and the band at 395 nm increases progressively with advancement of reaction time with a presence of an isobestic point at 469 nm. This spectral change can be attributed to the generation of o-benzoquinone and gradual transformation of the mononuclear complex towards dinuclear vanadium compound. The time dependent spectral plot of decolourization of the deep blue solution to brown is given in Fig. **11**. The plot of $\mathbf{A_{676}/A_{395}}$ vs. time (min) gives a straight line with R^2 value 0.99 which corroborates with the gradual decay of the mononuclear form with respect to time. In oxygen saturated acetone solution, the reaction is found to be pseudo-first order and the calculated rate constant is found to be $\mathbf{2.9 \times 10^{-2}\ min^{-1}}$. The rate is comparable with other reported complexes.

Consequently, proton NMR studies were also performed in O_2 saturated acetone-d_6 solution to observe the progress of reaction with time.[27] The *tert*- butyl signals at δ 1.22, 1.53 ppm and δ 1.37 ppm are due to the co-ordinated ligand moiety in complex **1a** and free catechol moiety (remains in slight excess initially) respectively. At the time of completion (after 2h) the peaks at δ 1.22, 1.53 and 1.37 decays whereas the peak at δ 1.25 ppm increased significantly which clearly states the complete conversion of 3,5-DTBC to corresponding benzoquinone.

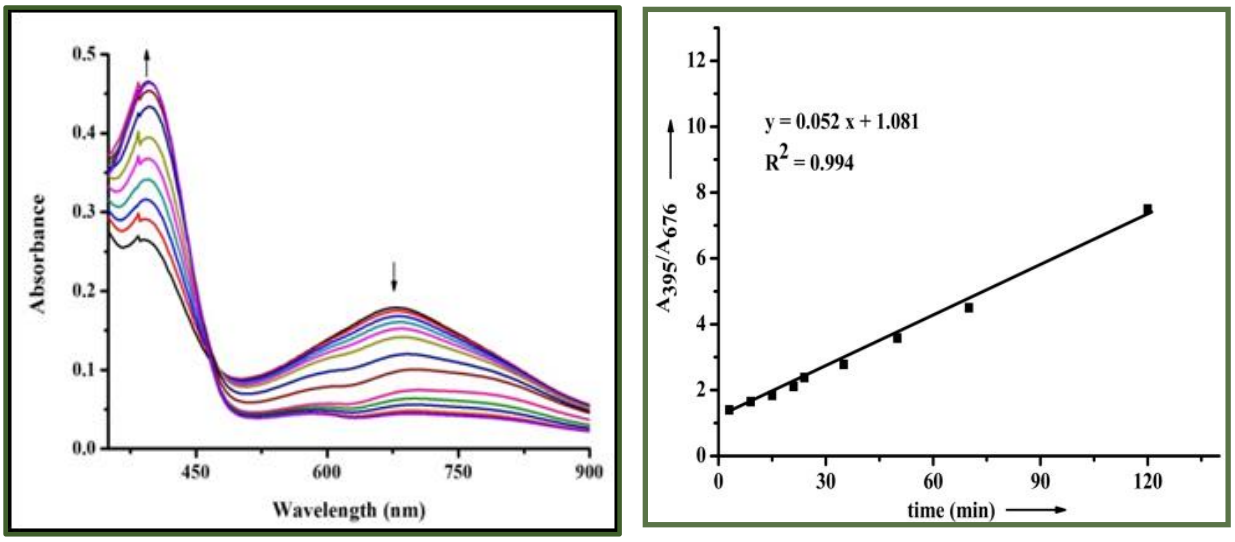

Figure 11:(Left) Time evolution spectra (UV-Vis) of complex 1a, [VO(L_1)(3,5-DTBC)] in O_2 saturated DCM solution at 298K.(Right) Ratiometric plot of A_{395} / A_{676} vs. time (min.)

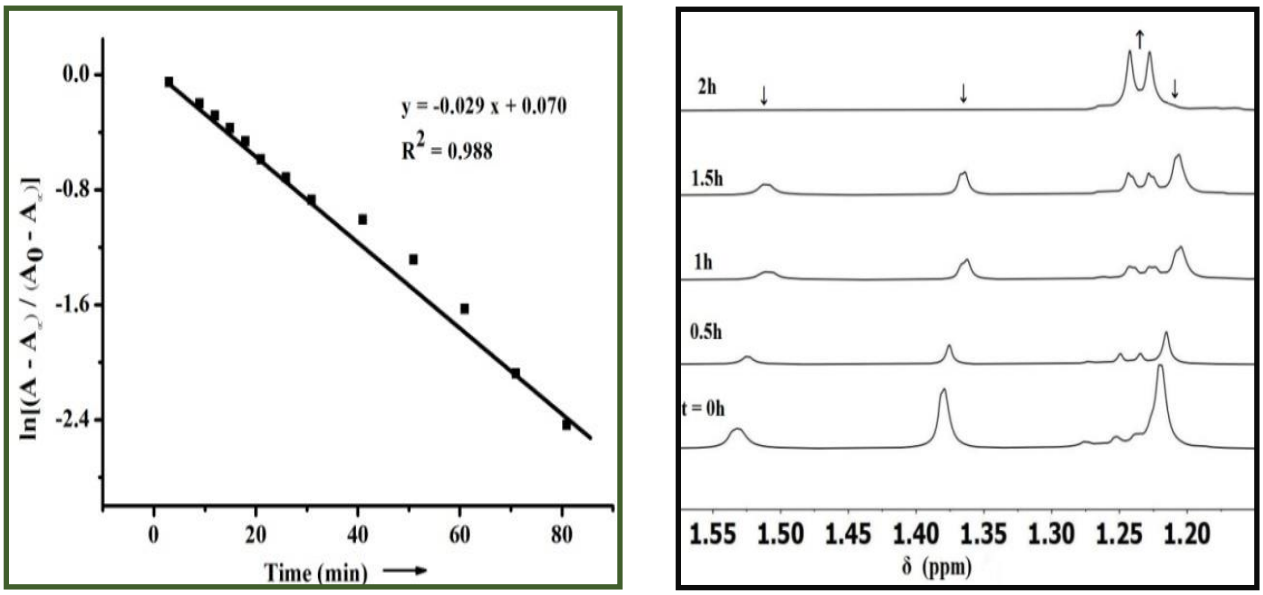

Figure 12: (Left) Plot of ln $[(A - A_\infty)/(A_0 - A_\infty)]$ vs. time (monitored at 395 nm). **(**Right): Time evolution of tert-butyl signals in Complex 1a in O_2 saturated acetone-d_6**.**

II.4. CONCLUSION

To summarize, we have successfully synthesized a new tridentate O^N^O donor ligand to generate oxidovanadium (V and IV) complexes of our choice. Using the ligand three complexes bearing oxidovanadium moiety have been prepared and well characterized by single crystal X-ray diffraction studies and spectral techniques like UV-Vis, IR, NMR, ESI-Mass etc. To attain better insights on the electronic transition properties as well as theoretically stable structural features, detailed density functional theoretical (DFT) as well as time dependent density functional theoretical (TDDFT) calculations were performed and the results are in good agreement with the experimental findings.

Present work has been aimed to generate pentavalent and tetravalent oxidovanadium complexes. The electrochemical as well the redox properties of the synthesized complexes were also studied extensively. Model catalytic bromination reaction of an aromatic aldehyde, salicylaldehyde was examined using the complexes to establish the halo-peroxidase mimicking activities of those. The experimental findings presented herein provide valuable insights into the planning of the preparation of strategically important complexes in the field of oxidovanadium chemistry.

II.5. REFERENCES

1. D. C. Crans, J. J. Smee, E. Gaidamauskas, L. Yang, Chem. Rev. 104(2004) 849-902.

2. (a) A. K. Goldfine, M. –E. Patti, L. Zuberi, B. J. Goldstein, R. LeBlanc, E. J. Landaker, Z. Y. Jiang, G. R. Willsky, C. R. Kahn, Metabolism.49(2000) 400. and the references therein.

3. (a) D. C. Crans, L. Yang, T. Jakusch, T. Kiss, Inorg. Chem. 39 (2000) 4409-4416. (b) K. H. Thompson, V. G. Yuen, J. McNeill, C. Orvig, Chem. Rev. 99(1999) 2561-2572. (c) K. H. Thompson, V. G. Yuen, J. McNeill, C. Orvig in Vanadium Compounds: Chemistry and Biochemistry and Therapeutic Applications. (Eds.: D. C. Crans, A.S. Tracey), Oxford University Press, New York, Ny, 1998, pp. 329.

4. (a) J. Littlechild, E. Garcia-Rodriguez, Coord. Chem. Rev. 237(2003) 65-76. (c) D. E. Carpio, L. Hernándeza, C. Ciangherotti, Coa, V. Villalobos, L. Jiménez, V. Lubes, G. Lubes, Coord. Chem. Reviews. 372(2018) 117-140. (d) M. Debnath, M. Dolai, K. Pal, S. Bhunya, A. Paul, H. M. Lee, M. Ali, Dalton Trans. 47(2018) 2799-2809.

5. A. Butler, A. H. Baldwin in Metal Sites in Protein and Model, Phosphatases, Lewis Acids and Vanadium; (Eds.: H. A. O. Hill, P. J. Salder, A. J. Thompson), Spingler- Verlag, Heidelberg, 1999, pp. 108-132.

6. Bioinorganic Catalysis, (Ed.: J. Reedijk), Marcel Dekker, Inc. New York, 1993, pp. 425-445.

7. S. Treviño, A. Díaz, E. Sánchez-Lara, B. L. Sanchez-Gaytan, J. M. Perez-Aguilar, E. González-Vergara, Biol Trace Elem Res. 188(1) (2019) 68–98.

8. A. Butler, In Comprehensive Biological Catalysis, Sinnott, M. Ed. British Academic Press, Oxford, U.K. (1997) p 427.

9. Vilter, H. Met. Ions Biol. Syst. 31(1995) 325.

10. Butler, A. Walker, J. V. Chem. Rev. 93(1993) 1937.

11. Butler, A. In Bioinorganic Catalysis Reedijk, J. Ed. Marcel Dekker, New York. (1993) p 425.

12. Wever, R. Krenn, B. E. Vanadium Haloperoxidases. In Vanadium in Biological Systems Chasteen, N. D. Ed. Kluwer Academic Publishers: Dordrecht, The Netherlands. (1990) p 81.

13. Weyand, M. Hecht, H. J. Kieß, M. Liaud, M. F. Vilter, H. Schomburg, D. J. Mol. Biol. 293(1999) 595.

14. Isupov, M. I. Dalby, A. R. Brindley, A. A. Izumi, Y. Tanabe, T. Murshudov, G. N. Littlechild, J. A. J. Mol. Biol. 299(2000) 1035.

15. M. Schmidt, A. Wever, R. Proc. Natl. Acad. Sci. U.S.A. 93(1996) 392.

16. Almeida, M. G. Humanes, M. Melo, R. Silva, J. A. da Silva, J. J. R. F. Wever, R. Phytochemistry. 54(2000) 5.

17. Almeida, M. Humanes, M. Melo, R. Silva, J. A. da Silva, J. J. R. F. Vilter, H. Wever, R. Phytochemistry.48(1998) 229.

18. Hara, I. Sakurai, T. J. Inorg. Biochem. 72(1998) 23.

19. A. Vijayaraj, R. Prabu, R. Suresh, N. Mathivanan & V. Narayanan, Synthesis and Reactivity in Inorganic, Metal-Organic, and Nano-Metal Chemistry.45(2015) 1647-1654.

20. A. Banerjee, R. Singh, E. Colacio, K. K. Rajak, Eur. J. Inorg. Chem. (2009) 277–284

21. D. M. Manidhar, K. U. M. Rao, N. B. Reddy, Ch. S. Sundar, C. S. Reddy, J. Kor. Chem. Soc. 56(4) (2012) 459-463.

22. (a) M. Mohamadi, S. Y. Ebrahimipour, M. T. –Mahani, S. Foro, A. Akbari, RSC Adv., (2015), 5, 101063-101075. (b) U. Saha, K. K. Mukherjea, RSC Adv. 5(2015) 94462-94473.

23. E. Palmajumder, S. Patra, M. G. B. Drew, K. K. Mukherjea, New J. Chem. 40(2016) 8696-8703.

24. (a) B. Baruah, S. Das, A. Chakravorty, Inorg. Chem., (2002), 41, 4502-4508. (b) S. P. Rath, K. K. Rajak, A. Chakravorty, Inorg. Chem. 38(1999) 4376-4377.

25. R. A. Rowe, M. M. Jones, Inorg. Synth. 5(1957) 113.

26. (a) A. D. Becke, Density-functional thermochemistry. III. The role of exact exchange, J. Chem. Phys. 98(1993) 5648–5652; (b) C. Lee, W. Yang, R. G. Parr, Phys. Rev. B: Condens. Matter. 37(1988) 785–789.

27. (a) M. E. Casida, C. Jamoroski, K. C. Casida, D. R. Salahub, J. Chem. Phys. 108(1998) 4439–4449;(b) R. E. Stratmann, G. E. Scuseria, M. J. Frisch, J. Chem. Phys. 109(1998) 8218–8224. (c) R. Bauernschmitt, R. Ahlrichs, Chem. Phys. Lett. 256(1996) 454–464.

28. (a) P. J. Hay, W. R. Wadt, J. Chem. Phys. 82(1985) 270–283; (b) P. J. Hay, W. R. Wadt, J. Chem. Phys. 82(1985) 299–310.

29. G. M. Sheldrick, SHELXTL, v. 6.14, Bruker AXS Inc., Madison, WI, 2003.

30. C. K. Johnson, ORTEP Report ORNL-5138, Oak Ridge National Laboratory, Oak Ridge, TN, 1976.

CHAPTER III

Synthesis, characterization and Theoretical Studies of a novel Tridentate ligand and Vanadium (IV)/(V) complexes.

ABSTRACT

The tridentate Schiff base ligand **H_2L_1**, [(Z)-3-((2-hydroxybenzylidene)amino)dibenzo[b,d]furan-2-ol], synthesized by the typical condensation reaction of [3-aminodibenzo[b,d]furan-2-ol] with salicyldehyde has been used in the present work towards the synthesis of mononuclear oxidovanadium complexes. Three mononuclear oxidovanadium complexes [$VOL_1(OMe)$],**1**; [$VO(L_1)$(8-Hq)], **2** and [$VO(L_1)$(1,10-phen)], **3** have been successfully synthesized with high yields using [$VO(acac)_2$]. 8-hydroxyquinoline and 1,10-phenanthroline were used as co-ligands in the synthesis of complex **2** and **3**. X-ray crystallographic studies revealed that the ligand **H_2L_1** binds in tridentate fashion. The synthesized complexes were well characterized by using different spectral techniques. The physiochemical properties have been well interpreted by density functional theory (DFT) and time dependent density functional theory (TDDFT) calculations.

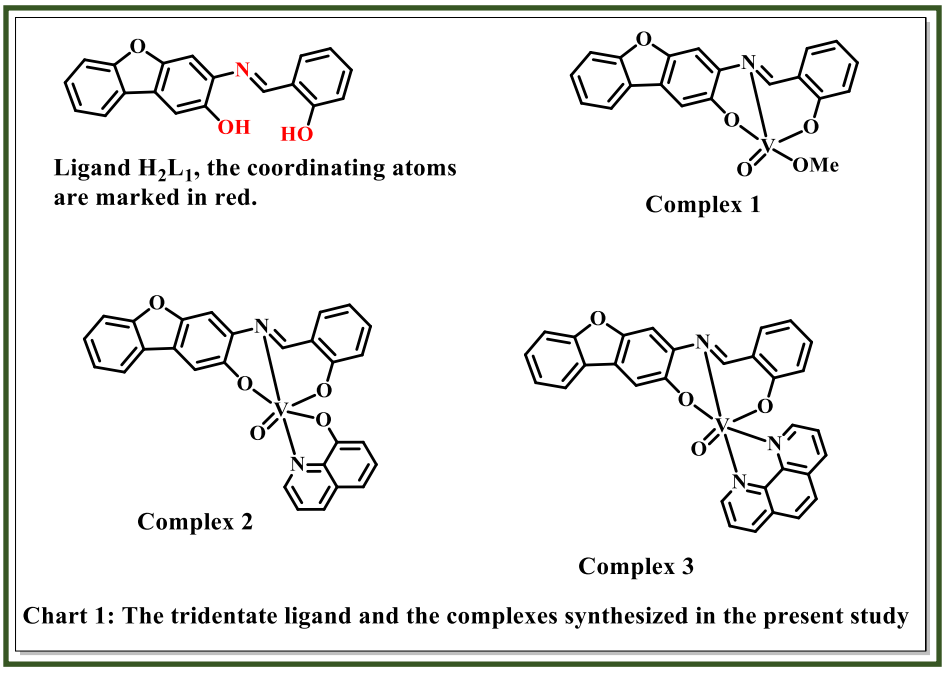

Chart 1: The tridentate ligand and the complexes synthesized in the present study

III.1. INTRODUCTION

Vanadium ($3d^3 4s^2$) displays all oxidation states in the interval of -3 to +5. The states +2 to +5 can be sustained in aqueous solution and on the whole the most stable states are +4 and +5. Vanadium, in nature, exists under physiological conditions predominantly in the anionic vanadate, HVO_4^{2-} form (oxidation state +5) or as the Vanadyl (+4) cation (VO^{2+}) though oligomeric and protonated V(v) species ($H_2VO_4^-$) are possible depending on the pH and concentration. [1] Mononuclear and multinuclear oxidovanadium complexes incorporating non-porphyrinic O/N-coordinating ligands are of abiding interest. [2-4] The most widespread applications of vanadium complexes are due to its insulin mimicking activity [5-7] and as an effective industrial catalyst. [8] Vanadium has also been recognized as an essential element in some living organism, [9-13]but the biological roles of vanadium are still not clear. [14-15] Two categories of vanadium containing enzymes, nitrogenase (V-Nase) [16-18] and halo-peroxidase (VHPO) [19-21] have been isolated and characterized. Vanadium mediated enzymatic oxidative (halo-peroxidase) and reductive (nitrogenase) transformations signify the importance of +5 and +4 oxidation states of vanadium.

There are several literature reports regarding the synthesis of vanadium complexes and their role in different type of enzymatic as well as biological activities. The present study consists of successful synthesis of three mononuclear oxidovanadium complexes bearing tridentate O^N^O schiff base ligand having dibenzofurane moeity. The interesting feature of the designated ligand is that it has two pendant –OH groups along with imine moeity (C=N) constituting the O^N^O coordination pattern. The single crystal X-Ray diffraction studies as well as the optimized geometries obtained from the theoretical calculations (by means of DFT) of the complexes also reveal the similar co-ordinating pattern. All the complexes as well as the ligand were characterized by means of different spectrochemical techniques. Catalytic activities such as bromoperoxidase was well interpretated through GC-MS.

Here, we also present a full density functional theory (**DFT**) and time-dependent density functional theory **(TDDFT**) studies to get better understanding of the geometry, electronic structure, and optical properties of these complex molecules, with good accuracy. Geometry optimizations of the singlet ground-state were carried out by means of DFT calculations. TDDFT calculations of several singlet states have been performed to gain a better insight on the electronic origin of the

absorption spectra.The theoretically obtained results and experimental findings are found to be in good agreement.

III.2. EXPERIMENTAL SECTION

A.Materials

Vanadyl sulphate was purchased from S D Fine-Chem Limited, Salicylaldehyde,3-amino-2-methoxy-dibenzofuran; 1,10-Phenanthroline; were purchased from Sigma-Aldrich. 8-Hydroxyquinoline was purchased from Alfa-Aesar. Potassium Bromide was purchased from Fischer scientific and Hydrogen peroxide (30% V/V) was obtained from Merck. $[VO(acac)_2]$ was prepared according to the literature. [22] Analytically pure solvents and chemicals are used throughout the study. All the reactions with metal salts are carried out under open air atmosphere.

B.Preparation of Compounds

Ligand

Synthesis of $[H_2L_1]$:

Initially 3-amino-dibenzo[b,d]furan-2-ol (2.0g, 10mmol) was dissolved in 15mL methanol. Then salicylaldehyde (1.22g, 10.0mmol) was added to the solution drop wise and the mixture was heated to reflux in a water bath and stirred for 6 h. This afforded a deep orange coloured precipitate of the targeted Schiff base ligand (**H_2L_1**). After that the orange solid was filtered and washed with mother liquor, and kept under vacuum. Yield: 70% (2.12g, 7mmol), ^{1}H NMR ($CDCl_3$, 300 MHz):δ 13.73 (s, 1H); 9.83 (s, 1H); 9.08 (s, 1H Characteristic of =C-H); 8.06 (s, 1H), 7.79 (s, 1H), 7.65-6.94 (m, 8H), Elemental anal. calcd. for $C_{19}H_{13}NO_3$: C, 75.24; H, 4.32; N, 4.62, O, 15.82. Found: C, 75.13; H, 4.23; N, 4.71, O, 15.93 IR (KBr, cm^{-1}): ***ν*** (O–H): 3040; ***ν*** (imine C=N): 1625, ESI-MS (CH_2Cl_2): m/z 303.090 $[M+H]^+$, Found: 304.0869.

Complexes

$[V^{V}O(L_1)(OMe)]$, complex 1:

The ligand **$[H_2L_1]$** (1.52g, 5mmol) and vanadium precursor complex $[V^{V}O(acac)_2]$ (1.33g, 5mmol) both were dissolved in 10mL methanol separately in a beaker. Then the two solutions were mixed gently and the solution mixture was heated under reflux for 8h. The resulting clear brown coloured solution was cooled and kept in air for slow evaporation. After two days' black crystals suitable for single crystal X-Ray diffraction study were generated. Yield: 1.03g (81%) ^{1}H NMR ($CDCl_3$, 500 MHz): δ 9.15 (s, 1H, Characteristic of =C-H); 7.92 (s, 1H); 7.82-7-66 (m, 4H); 7.65 (s, 1H); 7.46-7.17 (m, 1H); 3.49(s, 3H, for $–OCH_3$). Anal. Calcd for $C_{20}H_{14}NO_5V$: C, 60.16; H, 3.53; N, 3.51, O, 20.04, V, 12.76. Found: C, 60.02; H, 3.93; N, 3.43; O, 20.10; V, 12.52; IR (cm^{-1}): ν (V=O): 850; ν (imine C=N): 1625, 1603. ESI-MS (CH_2Cl_2): m/z, 399.03 Found: $[M+Na]^+$, 421.9956.

$[V^{V}O(L_1)(8\text{-}Hq)]$, complex 2:

Initially, the ligand **H_2L_1** (1.52g, 5mmol) was dissolved in minimum volume of methanol. Similarly, the vanadium precursor $[V^{V}O(acac)_2]$ (1.33g, 5 mmol) was also dissolved in minimum volume of same solvent system. Now, the two solutions were mixed thoroughly and heated to form a clear brown coloured solution. At this point, 10 mL methanolic solution of 8-hydroxyquinoline (0.73g, 5mmol), which acts as a co-ligand was added. Finally, the reaction mixture was heated under refluxing conditions for 8h. Then the clear brown coloured solution was cooled and kept in air 2 days for slow evaporation, resulted in the formation of deep violet coloured diamond shaped crystals which were suitable for single crystal X-ray diffraction analysis. Yield: 0.36g (75%) ^{1}H NMR ($CDCl_3$, 500 MHz): δ 9.12 (s, 1H); 8.11 (d, 1H, J=10.0Hz); 8.09 (s, 1H); 7.72-7.67 (m, 3H); 7.65-7.50 (m, 3H); 7.40(s, 1H); 7.50-7.40 (m, 4H); 7.27-6.87 (m, 3H). Anal.Calcd. for $C_{28}H_{17}N_2O_5V$: C, 65.63; H, 3.34; N, 5.47, O, 15.61, V, 9.94. Found: C, 65.52; H, 3.54; N, 5.20, O, 15.92, V, 9.82 IR (cm^{-1}): *ν* (imine C=N): 1605, 950 (V=O stretch). ESI-MS (CH_2Cl_2): m/z 512.06, Found: $[M+H]^+$,513.033.

$[V^{V}O(L_1)(1,10\text{-phen})]$, complex 3:

At first, both the ligand $\mathbf{H_2L_1}$ (1.52g, 5mmol) and vanadium precursor complex $[VO(acac)_2]$ (1.33g, 5 mmol)were dissolved in minimum volume of methanol respectively. The two homogeneous solutions were mixed carefully and the resulting solution was gently heated. Now, to this pre-heated solution, methanolic solution of 1,10-phenanthroline (0.9g, 5mmol) was added. The solution mixture was then stirred under refluxing conditions overnight. A red coloured precipitate was formed. The precipitate was filtered and washed thoroughly with methanol and kept under vacuum. After re-crystallisation, we found a red crystalline product. Unfortunately, after several attempts we are unable to get single crystals suitable for X-Ray diffraction study. Yield: 0.45g (77%), Elemental Anal. Calcd. for $C_{31}H_{19}N_3O_4V$: C, 67.89; H, 3.49; N, 7.66; O, 11.67; V, 9.23. Found: C, 67.62; H, 3.69; N, 7.60, O, 11.75; V, 9.34; IR (cm-1): ν (imine C=N): 1626, 948 (V=O stretch).ESI-MS (CH_2Cl_2): m/z 548.08, Found: $[M]^+$548.2103. The complex is paramagnetic, having magnetic moment **1.92 BM** at room temperature.

C.X-Ray Structure Determination

The single crystal suitable for X-ray crystallographic analysis of the complex was obtained by slow evaporation of methanol solution of the complex. The X-ray intensity data were collected on Bruker AXS SMART APEX CCD diffractometer (Mo Kα, λ = 0.71073 Å) at 296 K. The detector was placed at a distance 6.03 cm from the crystal. Total 606 frames were collected with a scan width of 0.3˚ in different settings of φ. The data were reduced in SAINTPLUS [23] and empirical absorption correction was applied using the SADABS package. Metal atom was located by Patterson Method and the rest of the non-hydrogen atoms were emerged from successive Fourier synthesis. The structures were refined by full matrix least-square procedure on F2. All non-hydrogen atoms were refined anisotropically. All calculations were performed using the SHELXTL V 6.14program package. [24] Molecular structure plots were drawn using the Oak Ridge thermal ellipsoid plot (ORTEP) [25] The CCDC numbers are **1949622** and **1949623** for **1** and **2** respectively **(Table 1)**.

Table 1: **Crystal data and structure refinement parameters of complexes 1 and 2:**

	Complex 1	**Complex 2**
Formula	$C_{20}H_{14}NO_5V$	$C_{28}H_{17}N_2O_5V$
M_r	399.26	512.37
Crystal system	monoclinic	monoclinic
Space group	C c	P 21/c
a/ Å	24.8830(9)	15.9541(8)
b/ Å	7.3970(3)	10.2282(5)
c/ Å	19.4450(8)	13.8216(7)
α/°	90	90
β/°	106.77(2)	90.209(3)
γ/°	90	90
V/ Å^3	3427(2)	2255.42(19)
Z	8	4
D_{calcd} /g cm^{-3}	1.548	1.509
μ/mm^{-1}	0.612	0.485
θ/°	2.356 – 27.496	2.365– 27.493
T/K	296(2)	296(2)
Reflns collected	7729	5185
R^1, wR^2 [I>2σ(I)]	0.0591, 0.1753	0.0479, 0.1616
GOF on F^2	0.947	0.996

$^{a}R1 = \Sigma \big| \, |F_o| - |F_c| \, \big| / \Sigma \, |F_o| \, . \; ^{b}\, wR2 = [\Sigma[w(F_o^2 - F_c^2)^2] / \Sigma[w(F_o^2)^2]]^{1/2}$

D.Physical Measurements

All physical measurements that included elemental analysis, IR, ^{1}H NMR, Absorption spectra, ESI mass spectra, emission spectra, were done as described in Chaptrer 1.

II.3. RESULT AND DISCUSSION

1. Synthesis

Ligand(H_2L_1)

Initially, 3-Amino-dibenzofuran-2-ol was synthesized from 3-amino-2-methoxy-dibenzofuran according to the literature reported method. In brief, 3-amino-2-methoxy-dibenzofuran (5 g, 23.5 mmol) was dissolved in dry dichloromethane and the temperature was maintained at 0°c to 5°c. Then, boron tribromide (70 mL, 1 M in CH_2Cl_2) was added drop wise from a dropping funnel while stirring at ice cold condition. After the addition was complete, the mixture was allowed to come to room temperature over 1 hour and then quenched with water followed by potassium carbonate (14 g). The resulting solid was recovered by vacuum filtration and dried. The hydroxyl dibenzofuran is a white solid (4.4 g, 22 mmol). In the second step, the as synthesized amino substituted dibenzofuran-2-ol was condensed with methanolic solution of salicylaldehyde under refluxing conditions to form our desired Schiff base tridentate O^N^O co-ordinating ligand, H_2L_1as an orange coloured solid in good yield. The synthesized ligand (Scheme **1**) was well characterized using different spectral techniques and the found data are listed in experimental section.

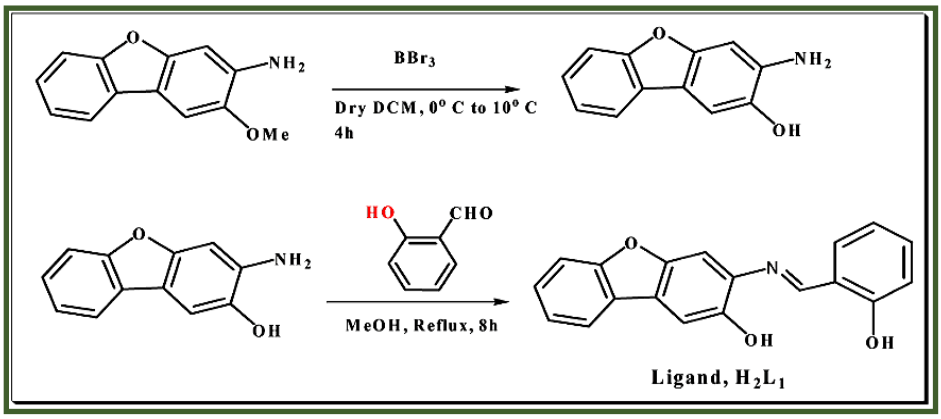

Scheme 1: Synthesis of desired Schiff base ligand, H_2L_1

Complexes

The stoichiometric reaction of the synthesized Schiff base ligand with vanadium precursor, [VO(acac)$_2$] in presence of methanol, 8-Hydroxyquinoline and 1,10-phenanthroline in methanol solvent under refluxing conditions afforded complexes **1**, **2** and **3** respectively. The synthesized ligand and the corresponding mononuclear oxovanadium complexes are portrayed in chart 1.

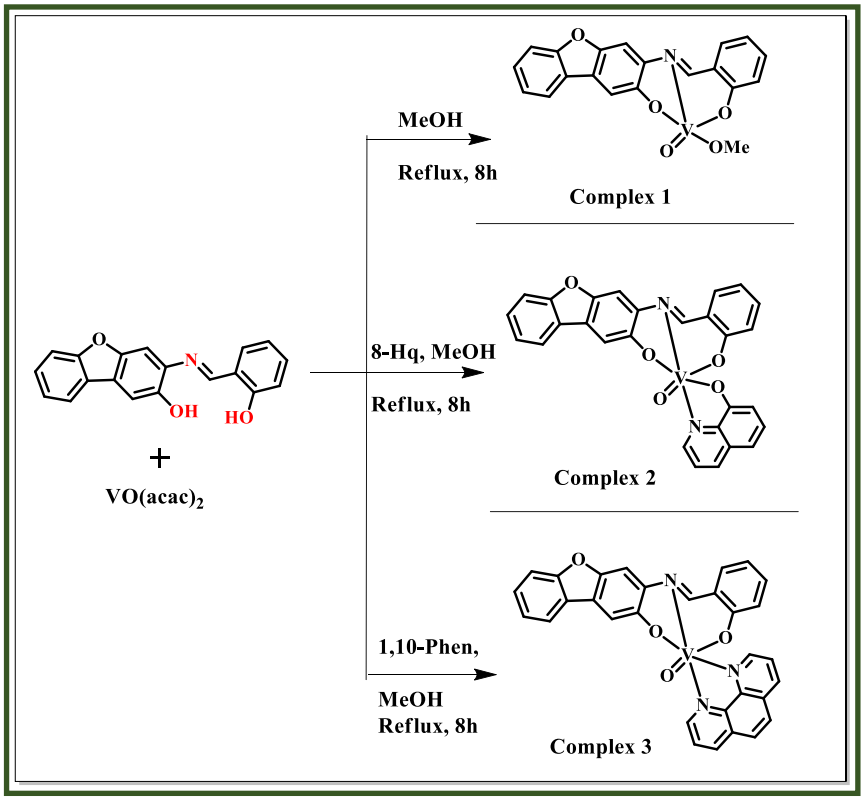

Scheme 2: Synthetic routes towards complex **1**, **2** and **3.**

2. Characterization

NMR Spectra: The synthesized ligand and the mononuclear oxovanadium complexes except complex 3 (EPR active, +4 oxidation state) are diamagnetic in nature and display well resolved NMR spectra in CDCl3 solution. The spectral data are given in the experimental section. The assigning of NMR peaks is done on the basis of the intensity and spin–spin splitting pattern. The appearance of singlet peak at 13.74 ppm which disappears upon the addition of D_2O confirms the presence of phenolic hydrogen. A singlet corresponding to the azomethine hydrogen atom was

observed at 9.08 ppm in the ligand, 9.15 ppm for complexes 1 and 9.12 for complex 2. Complex 2 also shows a characteristics peak at 8.11 ppm the proton adjacent to the 'N' moiety in 8-hydroxyquinoline. The relevant electronic spectra are depicted in Figure (**1-3**).

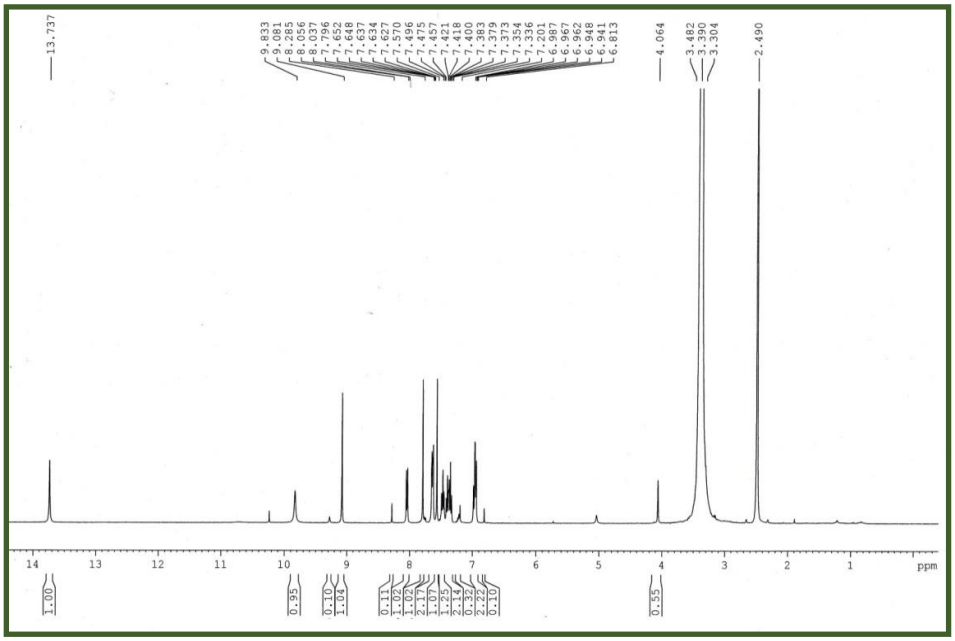

Figure 1: ^{1}H NMR spectra of ligand.

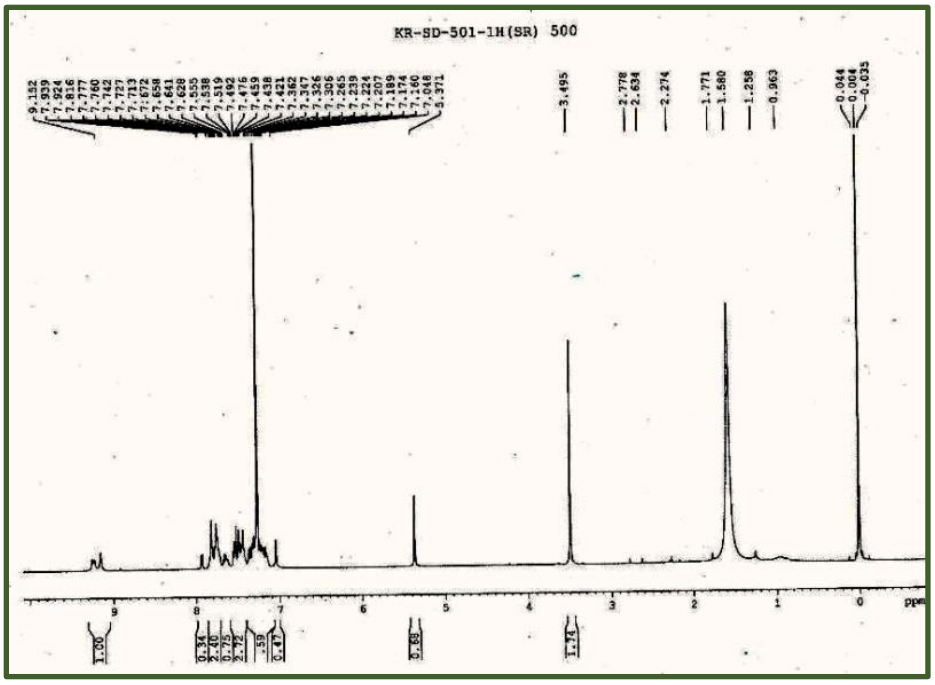

Figure 2: ^{1}H NMR spectra of complex 1.

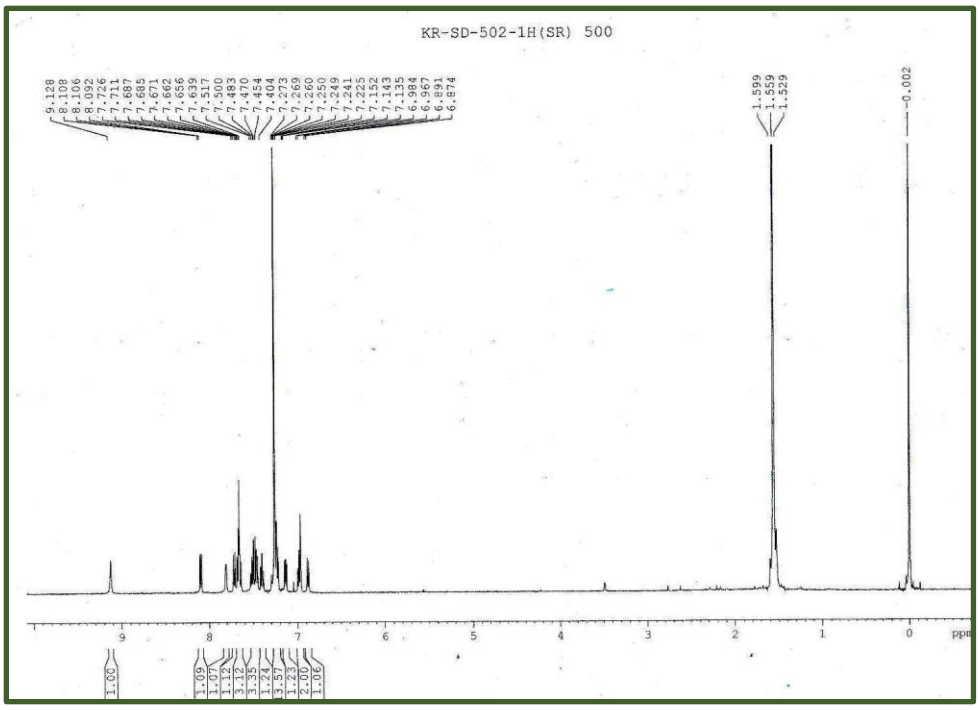

Figure 3: ^{1}H NMR spectra of complex 2.

EPR Spectra: Complex 3 exhibits one unpaired electron due to the presence of vanadium metal in it's +IV oxidation state. Generally, the paramagnetism corresponds to $3d_{xy}^{1}$ configuration. Complex 3 is EPR active in CH_2Cl_2 solution at room temperature and the representative spectrum of the EPR study is given in Fig **4**. The average hyperfine splitting is 95.28 G and central field g-value is 1.9682 with line width of 2.09 mT.

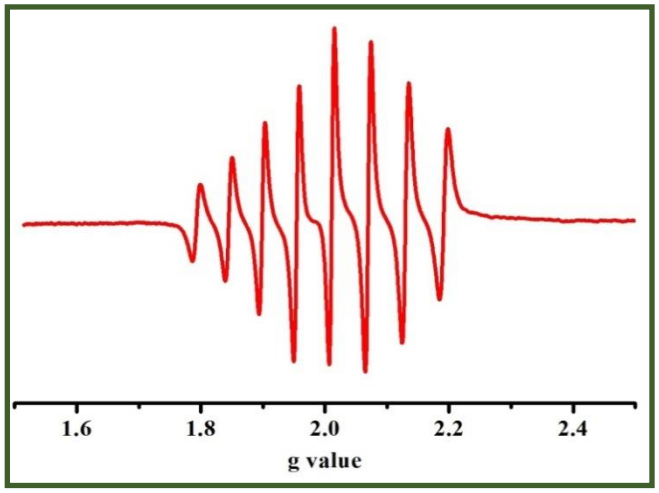

Figure 4: EPR spectrum of complex 3 in DCM/Toluene solution at 298 K

IR Spectra: The IR spectra of the ligand and its corresponding metal complexes were recorded in a KBr disk. The appearance of the spectral bands near 1625 cm^{-1} clearly proves the presence of imine, C=N moiety. The broad absorption band at 3040 cm^{-1} attributes to the stretching frequency of "free OH" moiety. This spectral data matches satisfactorily with the synthesized ligand.

All the vanadium complexes exhibited spectral bands in the range of 1630-1620 cm^{-1} arising from the stretching vibrations of the imine moiety and the range of 1000 cm^{-1}– 850 cm^{-1} indicates the presence of V=O moiety of the complexes [3h] and the small band near 500 cm^{-1} relates the presence of V-O moiety. [25] The strong vibrations at 1451 cm^{-1} and 743 cm^{-1} are due to ν(C-N stretch) of the co-ordinated 1,10-phenanthroline moiety in complex 3, the non-coordinated ν(C-N stretch) of 1,10-phenanthroline appears at 1431 cm^{-1} and 731 cm^{-1} respectively.

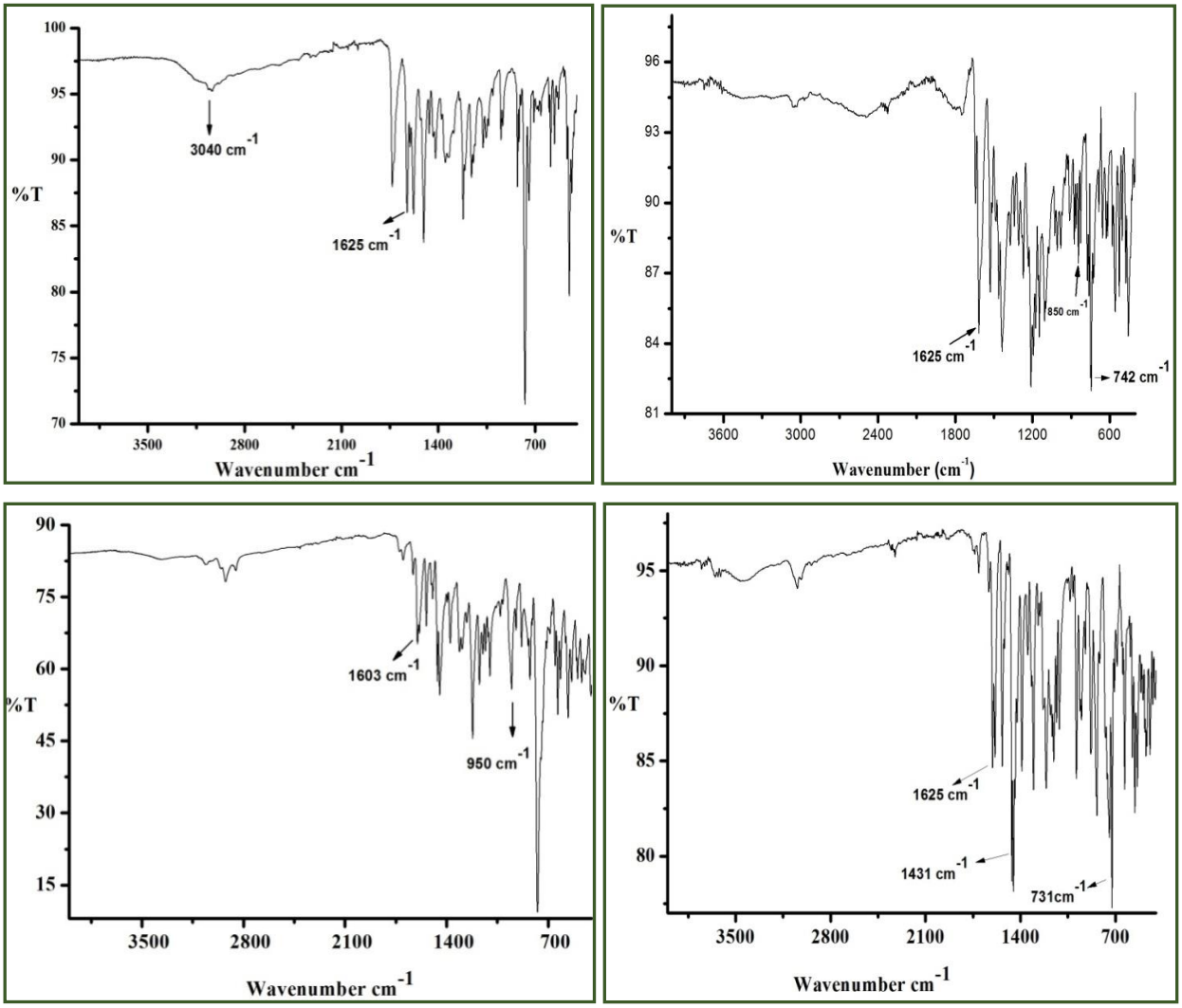

Figure 5: IR spectrum of the ligand and the complexes **1**, **2** and **3**.

Mass Spectra: Electrospray ionization mass spectrometry (ESI-MS) of the ligand and the complexes was done. Ligand displayed the highest peak at ESI-MS (CH_2Cl_2): m/z 303.090 [M+H]+, Found: 304.0869.and for the complex 1, displayed the highest m/z peak at ESI-MS (CH2Cl2): m/z, 399.03 Found: [M+Na]+. For Complex 2, highest peak ESI-MS (CH2Cl2): m/z 512.06, Found: [M+H]+,513.033. and for Complex 3 highest peak ESI-MS (CH2Cl2): m/z 548.08, Found: [M]+548.21.

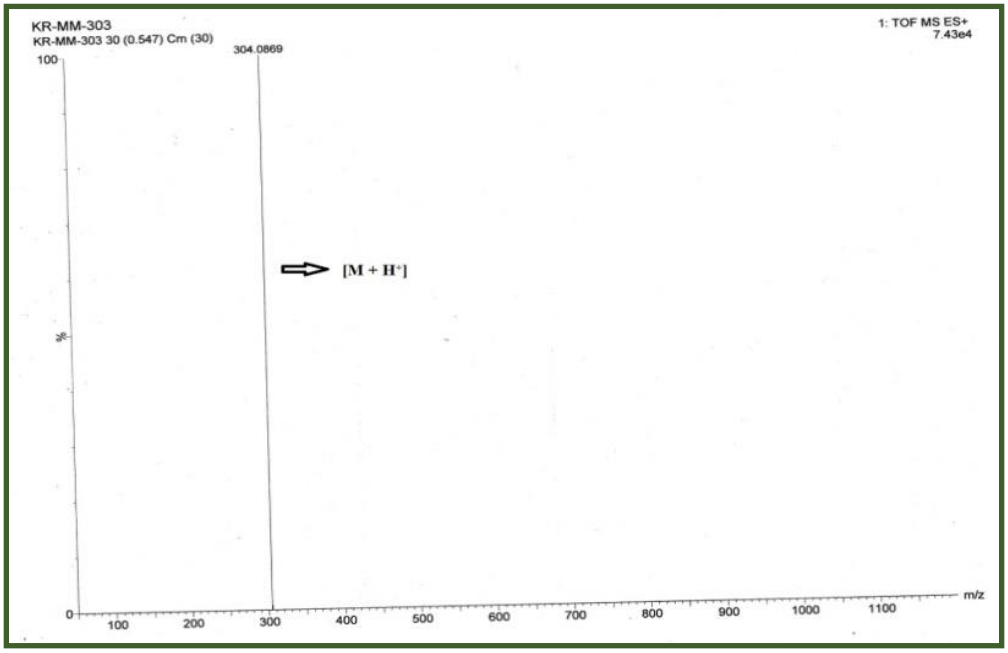

Figure 6: ESI-MS spectra of ligand.

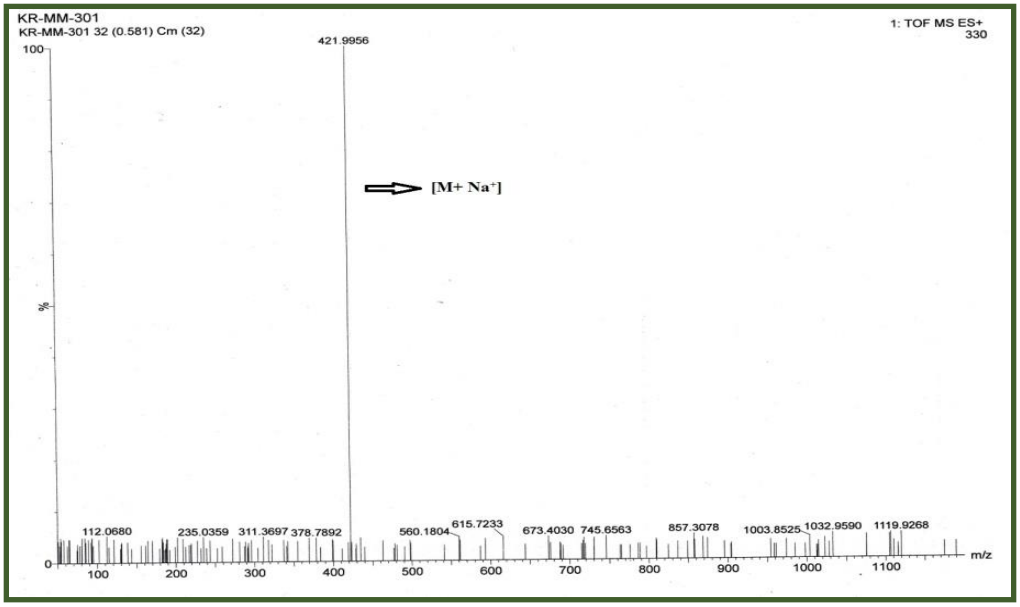

Figure 7: ESI-MS spectra of Complex 1.

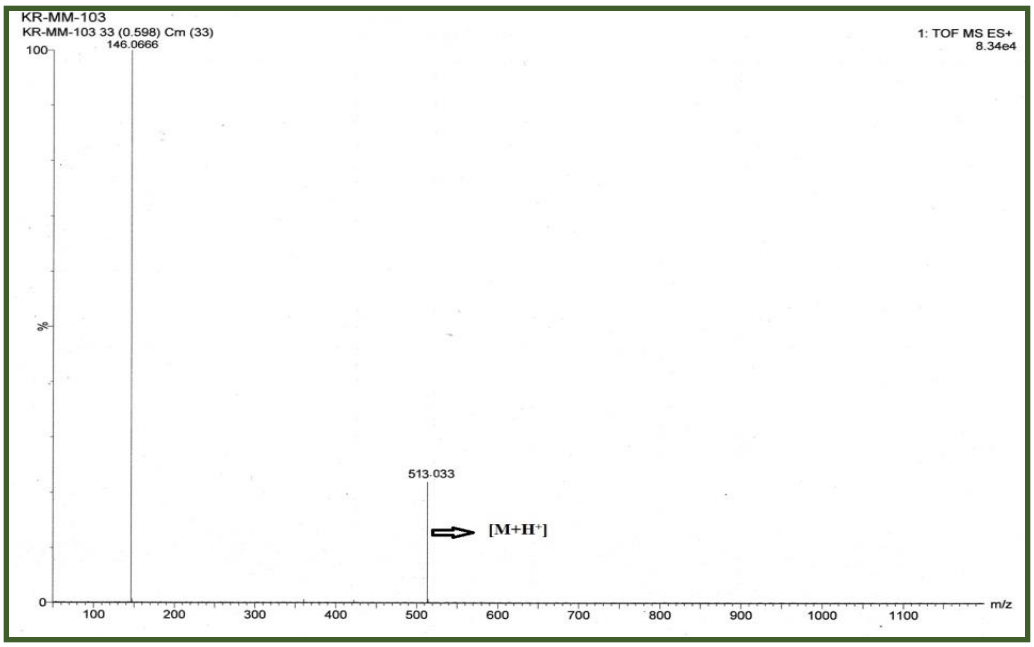

Figure 8: ESI-MS spectra of Complex 2

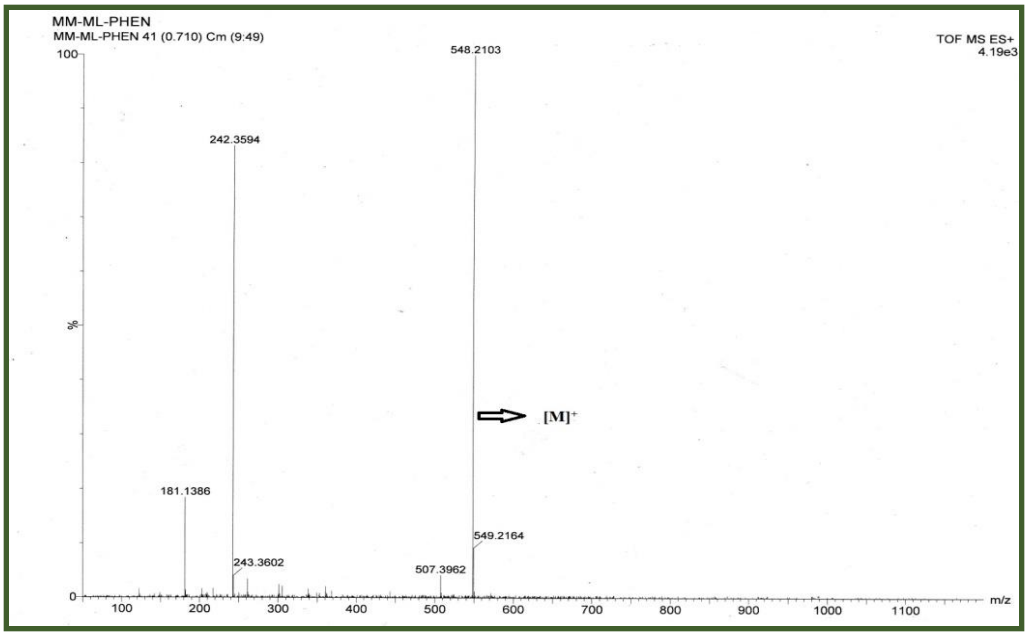

Figure 9: ESI-MS spectra of Complex 3.

Crystal Structure: The molecular structures of the complexes [VVO(OMe)L1)], 1 and [VVO(L1)(8-HQ)], 2, have been determined by using single crystal X-ray diffractometer. The molecular structures of 1 and 2 are shown in Fig.2-3respectively.The selected bond lengths and bond angles are depicted in Table **3.**

Complex **1** crystallizes in the monoclinic crystal system with Cc space group. The dibenzofuran based **H_2L_1** co-ordinates with the metal centre as an O^N^O donating dianionic ligand. The synthesized Schiff base ligand possesses two pendent phenoxide moeity and imine nitrogen in the close vicinity, which makes the ligand as a very promising O^N^O co-ordinating in nature. In the co-ordination sphere, the phenolic –OH moeity and the imine nitrogen are directly bound to the vanadium centre in a *meridional* fashion. The fourth coordination site of vanadium is occupied by an oxo oxygen atom, which comes from the vanadium precursor complex, $[VO(acac)_2]$. The remaining vacant coordination sites of vanadium are occupied by methoxy group arising from methanol, the solvent used in the synthetic route owing to the formation of distorted square pyramidal geometry with (The trigonality index(τ)=0.21) [26]. The V1-O1 bond length (1.58 Å) establishes the presence of V=O moiety. The elongated V-O bond (1.880 Å) indicates the presence of the attached methoxy moiety with the metal centre. The ORTEP view of the single crystal X-Ray structure is shown in figure **10**.

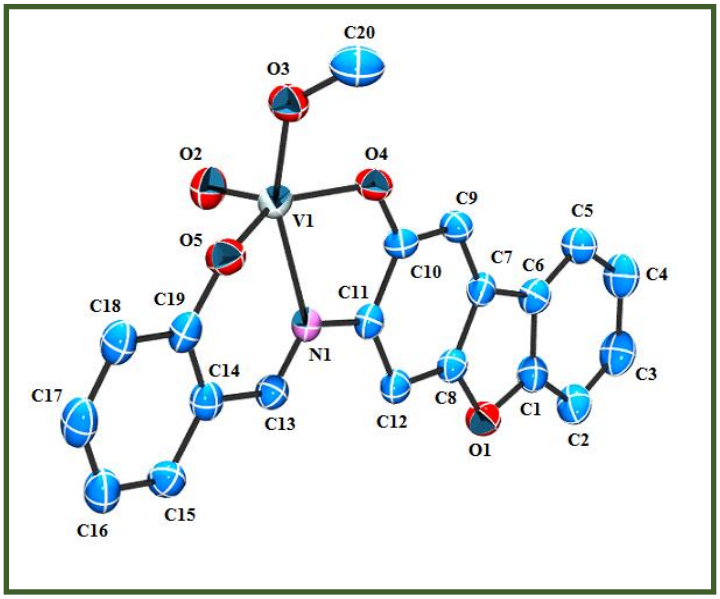

Figure 10: ORTEP plot of complex **1** showing essential numbering.

Complex 2 also crystallizes in the monoclinic crystal system with space group P21/c. Here also the four coordination sites of the metal center were occupied in the similar way; the phenolic –OH moiety and the imine nitrogen are directly bound to the vanadium center in a meridional fashion, whereas the remaining two vacant sites were occupied by the nitrogen and oxygen atom respectively of the 8-Hq moiety. The nitrogen atom of 8-hyroxyquinoline lies trans to the oxo oxygen atom. The dihedral angle between the oxo oxygen atom and the nitrogen atom of 8-

hyroxyquinoline (176.33°) proves the above fact. The imine nitrogen and the nitrogen atom of 8-hydroxyquinoline lies very close towards perpendicular position (86.83°). Thus the metal complex hereby attains distorted octahedral geometry as in the previous case.

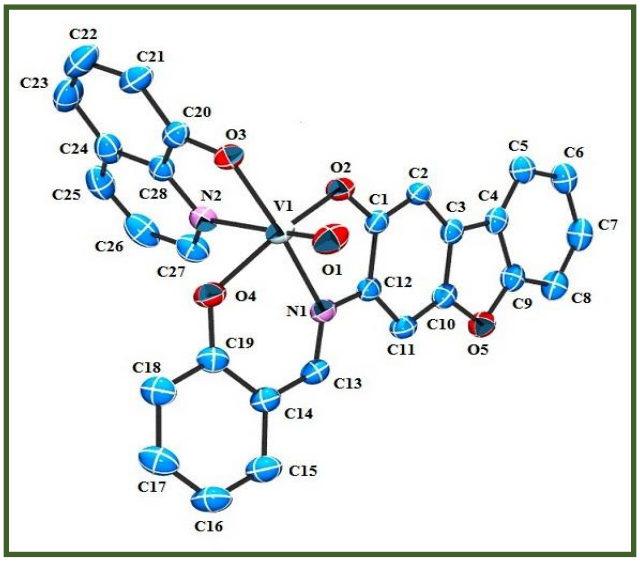

Figure 11: ORTEP plot of complex **2** showing essential numbering.

For complex 3, initially we have found a red colored precipitate and after recrystallization we have found a crystalline form. We have tried several methods but suitable crystal for X-Ray diffraction study was not obtained. However, the proposed structure of complex 3 is optimized with the help of DFT and the structural parameters are given in **Table 2.**

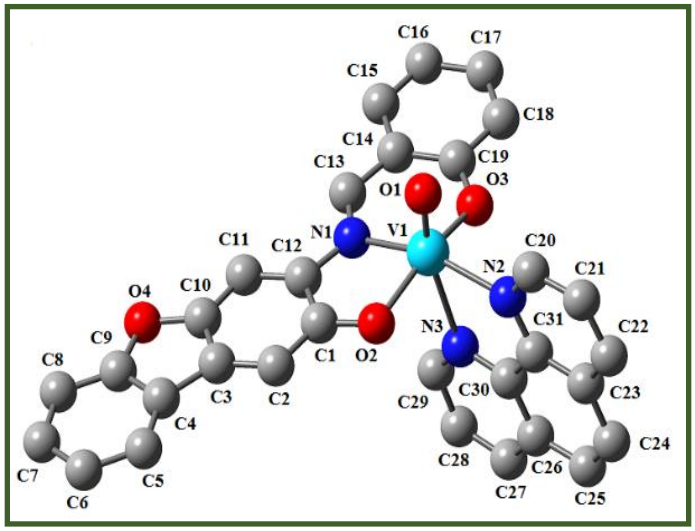

Figure 12. Optimized structure of complex **3.**

Geometrical studies: Geometrical optimizations for complexes 1 and 2 are performed in presence of solvent. The geometrical optimized structure of complexes 1, 2 and 3 are given below.

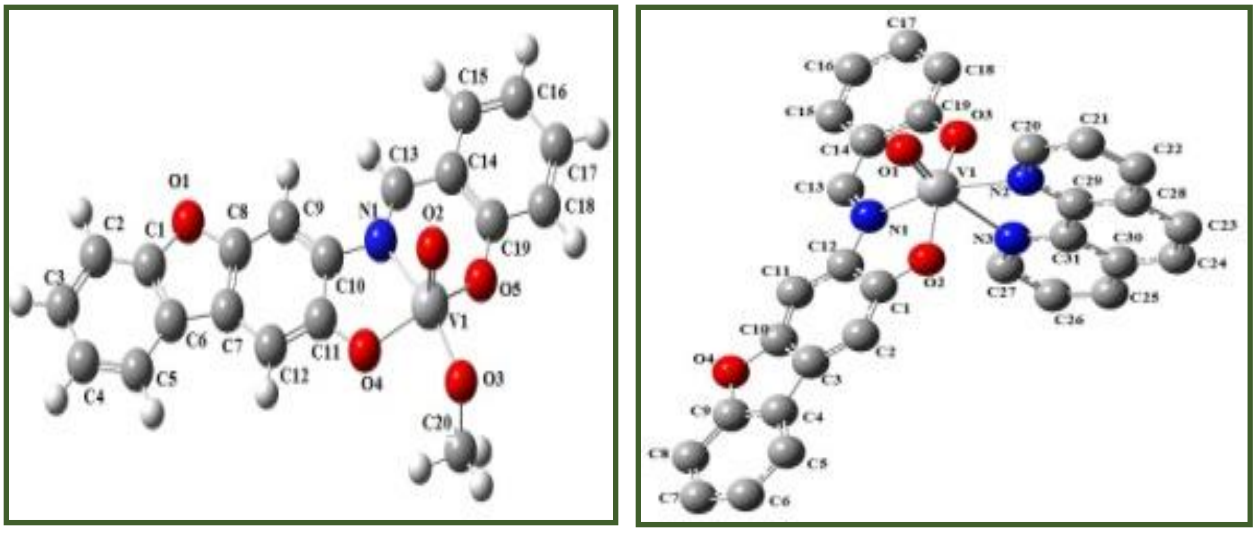

Figure 13: Optimized Structure of the Complex **1** and **2**.

The optimized geometry reveals that the complexes have a distorted octahedral arrangement around the vanadium (V) metal center. The optimized structures of these complexes are in good agreement with the experimentally observed structures and results, which were determined using single crystal XRD studies. A slight variation in structural parameters may occur due to crystal lattice distortion in real molecules. [27] The V–N and V–O bond lengths are in the range of 1.56–2.50 Å in both the theoretical calculation and experimental observation.

The isodensity plot of some selected frontier molecular orbitals in their singlet ground state (S_0) is listed in (Table 2). A partial molecular orbital diagram with the HOMO and LUMO for all the three complexes is shown in Fig. 4. In the ground state (S0), the HOMO of complexes 1 and 2 are quite similar in energy whereas that of complex 3 is slightly higher. But we can see the variation in the energies of LUMO for the complexes in their ground state.

The LUMO of complex **3** is energetically much higher than complex **1** and **2**. The HOMO - LUMO energy gaps in the complexes are in the range of 2.5 eV to 3.00 eV. The values are inclose resemblance to each other and the HOMO – LUMO energy gaps are 2.75 eV, 2.33 eV and 2.97 eV for complexes **1**, **2** and **3** respectively. The corresponding orbital contribution for the three complexes is given in (**Table 3)**.

Table 2. Selected bond lengths and bond angles of complexes 1, 2 and 3

Complex 1	Complex 2	Complex 3 (Optimized)			
Bond length (Å)					
V1-O2	1.5680 (7)	**V1-O1**	1.5890 (2)	**V1-O1**	1.6028
V1-O3	1.7550 (6)	**V1-O2**	1.8816 (19)	**V1-O2**	1.9551
V1-O4	1.8430 (7)	**V1-O3**	1.8395 (17)	**V1-O3**	1.9691
V1-O5	1.8800 (6)	**V1-O4**	1.8833 (19)	**V1-N1**	2.0857
V1- N1	2.1340(7)	**V1-N1**	2.1170 (2)	**V1-N2**	2.1856
C13- N1	1.2690 (10)	**V1-N2**	2.3640 (2)	**V1-N3**	2.4233
		C13-N1	1.2940 (3)	**C13-N1**	1.3077
Bond angles (°)					
O2-V1-O3	107.10 (3)	**O1-V1-O2**	100.90 (10)	**O1-V1-O2**	103.1537
O2-V1-O4	106.90 (3)	**O1-V1-O3**	100.49 (9)	**O1-V1-O3**	100.5708
O2-V1-O5	106.40 (3)	**O1-V1-O4**	98.78(10)	**O1-V1-N1**	103.6840
O3-V1-O4	88.80 (3)	**O1-V1-N1**	96.39(9)	**O1-V1-N2**	93.4440
O3-V1-O5	96.30 (3)	**O1-V1-N2**	176.33(10)	**O1-V1-N3**	165.0309
O3-V1-N1	155.80 (3)	**O2-V1-O3**	95.40(8)	**O2-V1-O3**	155.3269
O4-V1- N1	77.90 (2)	**O2-V1-O4**	154.42(8)	**O2-V1-N1**	80.2873
O2-V1- N1	96.20 (3)	**O2-V1-N1**	78.28(8)	**O2-V1-N2**	91.8488
O5-V1-N1	83.10 (3)	**O2-V1-N2**	81.44(8)	**O2-V1-N3**	79.9253
O4-V1-O5	143.00 (3)	**O3-V1-O4**	96.93(8)	**O3-V1-N1**	87.6537
		O3-V1-N1	162.84(8)	**O3-V1-N2**	93.4074
		O3-V1-N2	76.40(8)	**O3-V1-N3**	78.8984
		O4-V1-N1	83.44(8)	**N1-V1-N2**	162.3568
		O4-V1-N2	79.81(8)	**N1-V1-N3**	91.2609
		N1-V1-N2	86.83(8)	**N2-V1-N3**	71.7227

The electron density in the HOMO of all the complexes mainly resides on the dibenzofuran moiety (in the rangeof 74-79 %) and salicylaldehyde moiety (in the range of 11-17%). On the other hand, for the LUMO, the electron density mainly resides on the vanadium centre (70%)and the π^* orbitals of the attached methoxy group (14%, complex **1**). Similarly, for complex **2**, electron density is maximum over metal centred d-orbitals (66%) and attached 8-hydroxyquinoline moeity

(19%).For complex **3** the LUMO is distributed over the imine bond (35%), salicylaldehyde (28%) and dibenzofuran moiety (22%). This data depicts a very low density around the metal centre.

Table 3: Optimized geometries, HOMO-LUMO contour plots of metal complexes at the B3LYP/6-31G* level.

	Complex 1	Complex 2	Complex 3
Optimized geometries at the B3LYP/631G* level	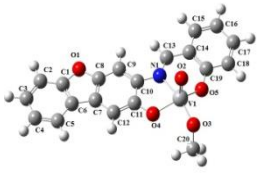	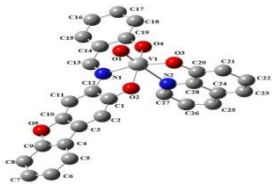	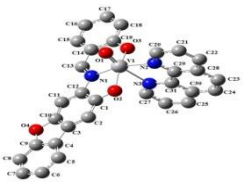
LUMO + 2	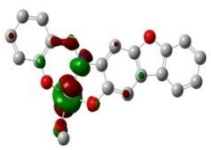	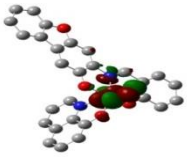	
LUMO +1		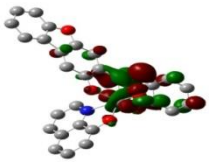	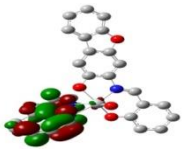
LUMO	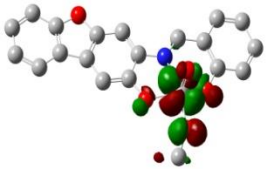		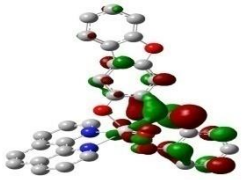
HOMO	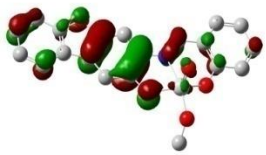	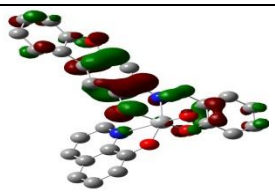	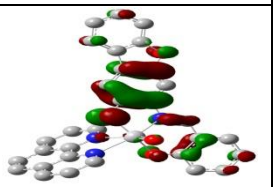
HOMO - 1	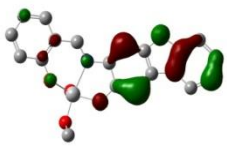		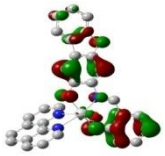
HOMO - 2	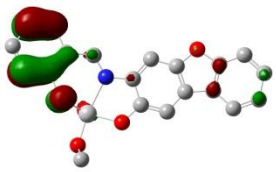	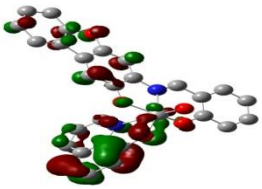	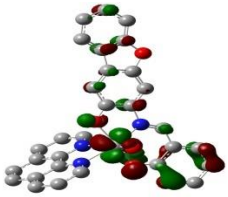

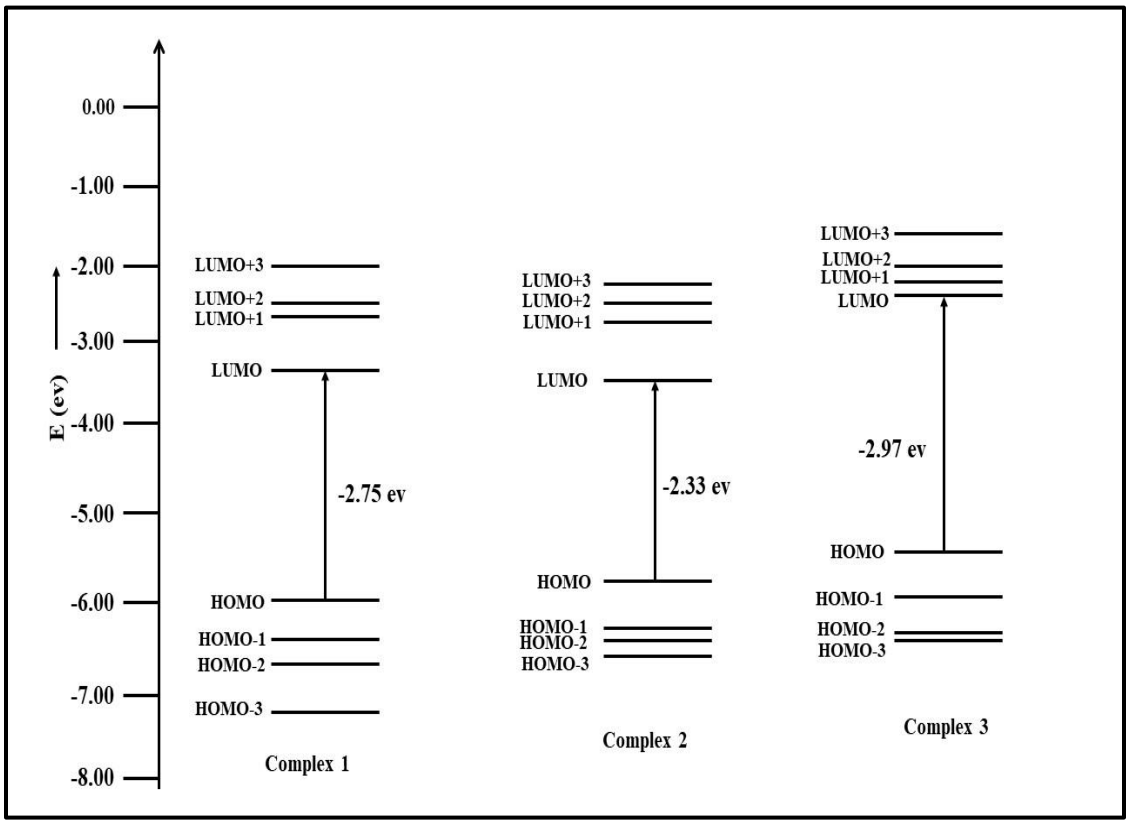

Figure 14: Partial molecular orbital diagram of all the complexes.

Table 4: Composition of the frontier molecular orbitals of complexes 1-3:

Complex 1		**% contribution**						**Main bond type**
MO		Sal	V	oxo	azometh	dbf	OMe	
101	L+3	7	65	18	1	9	0	d(V)+ π*(oxo)
100	L+2	6	58	14	10	10	3	d(V)+ π*(oxo)
99	L+1	25	15	5	33	20	2	d(V)+ π*(azometh)+ π*(sal)+ π*(dbf)
98	LUMO	8	70	2	2	4	14	d(V)+ π*(OMe)
97	HOMO	11	2	2	7	79	0	π(dbf)+ π(sal)
96	H-1	11	0	1	2	86	0	π(dbf)+ π(sal)
95	H-2	80	1	1	3	14	0	π(dbf)+ π(sal)
94	H-3	1	0	1	0	98	0	π(dbf)

Complex 2		% contribution						Main bond type
MO		Sal	V	oxo	azometh	dbf	Hq	
130	L+3	11	45	12	9	18	4	d(V)+ π*(sal)+ π*(oxo)+ π*(dbf)
129	L+2	5	60	19	6	7	3	d(V)+ π*(oxo)
128	L+1	21	26	10	26	15	2	d(V)+ π*(sal)+ π*(dbf)+ π*(azometh)
127	LUMO	8	66	1	1	6	19	d(V)+ π*(Hq)
126	HOMO	15	1	1	6	75	2	π(Sal)+ π(dbf)
125	H-1	16	1	1	2	53	27	π(Sal)+ π(dbf)+ π(Hq)
124	H-2	4	5	1	1	28	62	π(dbf)+ π(Hq)
123	H-3	68	1	1	3	24	2	π(Sal)+ π(dbf)

Complex 3		% contribution						Main bond type
MO		Sal	V	oxo	azometh	dbf	Phen	
140	L+3	1	63	21	2	11	2	d(V)+ π*(dbf)+ π*(oxo)
139	L+2	1	1	0	0	1	97	π*(Phen)
138	L+1	0	0	0	2	0	98	π*(Phen)
137	LUMO	28	8	4	35	22	3	π*(Sal)+ π*(dbf)+ π*(azometh)
136	HOMO	17	1	1	6	74	1	π(Sal)+ π(dbf)
135	H-1	42	1	2	4	50	0	π(Sal)+ π(dbf)
134	H-2	26	44	2	2	20	7	π(Sal)+ π(dbf)+ d(V)
133	H-3	32	19	0	2	43	3	π(Sal)+ π(dbf)+ d(V)

UV-Vis spectra and DFT studies: The UV- Visible spectral behavior of the ligand and its corresponding complexes**1**and **3** are recorded in dichloromethane solution, whereas for complex **2**, methanol was used for better solubility at room temperature. The spectral parameters with the experimental molar extinction coefficient (ε) value of $\mathbf{H_2L_1}$ and complexes **1–3** are listed in **(Table 5)**. The Ligand shows only one characteristic peak near 373 nm which may arise due to intramolecular n–π* and π–π* charge transfer transitions. The complexes**1, 2** and **3** display a strong peak varying between 350 and 500 nm having molar extinction coefficient in the range of 19200 – 36450 $M^{-1}cm^{-1}$. The bands in the longer wavelength region of these complexes can be attributed to the ligand to metal charge transfer [$H_2L_1 \rightarrow V(d\pi)$] transition. Only complex **3** shows low intense intra-ligand charge transfer transition. The corresponding spectra of the ligand and the complexes are shown in figure 1**5**.

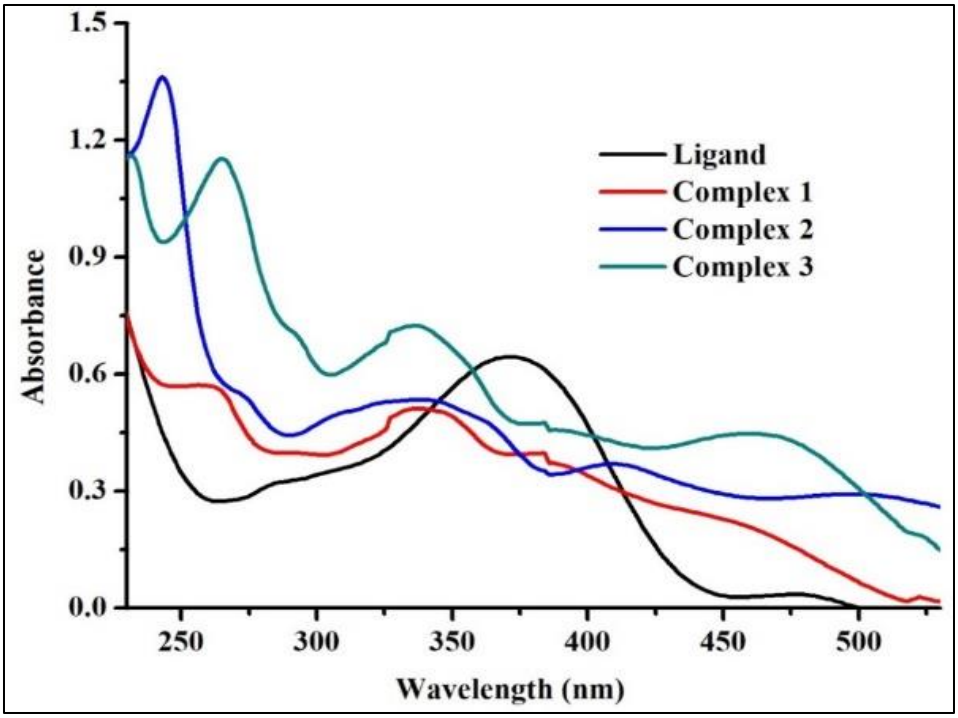

Figure 15: UV-Visible spectra of Ligand and corresponding complexes.

To get a better insight in the UV-Visible spectrum of the metal complexes, detailed theoretical calculations were performed in presence of solvent (DFT studies) and the results are depicted in **Table 5.**

Table 5: **Calculated optical transitions for complexes 1-3**

Compound	Electronic transition	Composition	Excitation Energy(eV)	Oscillator Strength (f)	Configuration Interaction (CI)	Assign	λ_{exp} in nm (ε in $M^{-1}cm^{-1}$)
1	$S_0 \rightarrow S_{24}$	H-7→L+1	3.6278 (341 nm)	0.0170	0.5942	^{1}LLCT	350 (25395)
	$S_0 \rightarrow S_{50}$	H-12→L+1	4.7605 (260 nm)	0.3001	0.6102	^{1}LLCT	261 (28450)
2	$S_0 \rightarrow S_{10}$	H-1→L+2	3.0260 (409 nm)	0.0382	0.4101	^{1}LMCT	410 (19200)
	$S_0 \rightarrow S_{20}$	H-7→L	3.6214 (342 nm)	0.0484	0.6425	^{1}MMCT	338 (27000)
3	$S_0 \rightarrow S_{10}$	H-2→L	2.6795 (462 nm)	0.0290	0.5535	^{1}LLCT	463 (22350)
	$S_0 \rightarrow S_{33}$	H-3→L	3.6679 (338 nm)	0.1376	0.5564	^{1}LMCT	336 (36450)

III.4. CONCLUTION

To summarize, we have successfully synthesized a new dibenzofuran based tridentate O^N^O donor ligand to generate mononuclear oxovanadium (V and IV) complexes. The co-ordinating behaviour of the ligand was used to synthesize three complexes bearing oxovanadium moiety successfully with good yields and well characterized by single crystal X-ray diffraction studies and spectral techniques viz. UV-Vis, IR, NMR, ESI-Mass etc. To support experimental values DFT as well as TDDFT calculations were performed. The experimental findings presented herein provide valuable insights into the planning of the preparation of strategically important complexes in the field of oxidovanadium chemistry. Further research aimed at the synthesis of polynuclear vanadium complexes using different polydentate ligands is currently under progress.

III.5. REFERENCES

1. D. Rehder, John Wiley & Sons, New York, 2008.
2. (a) A. Mondal, S. Sarkar, D. Chopra, T. N. Guru Row, K. Pramanik, K. K. Rajak, Inorg. Chem. 44 (2005) 703-708. (b) F. Wolf, C. Lorber, R. Choukroun, B. Donnadieu, Inorg. Chem. 42 (2003) 7839-7845. (c) K. K. Rajak, B. Baruah, S. P.Rath, A. Chakravorty, Inorg. Chem. 39 (2000) 1598-1601. (d) K. K. Rajak, S. P. Rath, A. Chakravorty, Carbohydrate Inorg. Chem. 38 (1999) 3283-3289. (e)K. K. Rajak, S. P. Rath, A. Chakravorty, J. Chem. Soc. Dalton Trans. (1999) 2537-2540. (f) S. Mondal, S. P. Rath, K. K. Rajak, A. Chakravorty, Inorg. Chem. 37 (1998) 1713-1719. (g) S. P. Rath, K. K. Rajak, S. Mondal, A. Chakravorty, J. Chem. Soc. Dalton Trans. (1998) 2097-2102.
3. (a) T. Otieno, L. Mokry, M. R. Bond, C. J. Carrano, N. S. Dean, Inorg. Chem. 35 (1996) 850-856. (b) R. Codd, T. W. Hambley, P. A. Lay, Inorg. Chem. 34 (1995) 877-882.
4. (a) M. A. Neelakantan, P. C. Balakrishnan, K. V. Selvarani, Polyhedron. 145 (2018) 191-199. (b) S. A. Talouki, G. Grivani, A. D. Khalaji, , Appl. Organometal. Chem. 32 (2018) e4078. (c) Saswati, P. Adão, S. Majumder, S. P. Dash, S. Roy, M. L. Kuznetsov, J. C. Pessoa, C. S. B. Gomes, M. R. Hardikar, E. R. T. Tiekink, R. Dinda, Dalton Trans. 47

(2018) 11358-11374. (d) S. Roy, M. Böhme, S. P. Dash, M. Mohanty, A. Buchholz, W. Plass, S. Majumder, S. Kulanthaivel, I. Banerjee, H. Reuter, W. Kaminsky, R. Dinda, Inorg. Chem. 57 (2018) 5767-5781. (e) M. R. Maurya, B. Uprety, F. Avecilla, P. Adão, M. L. Kuznetsov, J. C. Pessoa, Eur. J. Inorg. Chem. (2017) 3087. (f) S. P. Dash, A. K. Panda, S. Dhaka, S. Pasayat, A. Biswas, M. R. Maurya, P. K. Majhi, A. Crochet, R. Dinda, Dalton Trans. 45 (2016) 18292-18307. (g) J. C. Pessoa, S. Etcheverry, D. Gambino, Coord. Chem. Reviews. 301-302 (2015) 24-48 and the references there in. (h) M. R. Maurya, B. Uprety, F. Avecilla, P. Adãoc, J. C. Pessoa, Dalton Trans. 44 (2015) 17736-17755. (i) C. Das, P. Adak, S. Mondal, R. Sekiya, R. Kuroda, S. I. Gorelsky, S. K. Chattopadhyay, Inorg. Chem. 53 (2014) 11426-11437. (j) P. B. Chatterjee, N. Kundu, S. Bhattacharya, Ki-Y. Choi, A. Endo, M. Chaudhury, Inorg. Chem. 46 (2007) 5483-5485. (k) P. B. Chatterjee, D. Mandal, A. Audhya, Ki-Y. Choi, A. Endo, M. Chaudhury, Inorg. Chem. 47 (2008) 3709-3718. (l) M. Shit, S. Bera, S. Maity, T. Weyhermüller, P. Ghosh, New J. Chem. 41 (2017) 4564-4572. (m) C. Leblanc, H. Vilter, J.-B. Fournier, L. Delage, P. Potin, E. Rebuffet, G. Michel, P. L. Solari, M. C. Feiters, M.Czjzek, Coord. Chem. Reviews. 301-302 (2015) 134.

5. D. C. Crans, J. J. Smee, E. Gaidamauskas, L. Yang, Chem. Rev. 104 (2004) 849-902.

6. (a) A. K. Goldfine, M. –E. Patti, L. Zuberi, B. J. Goldstein, R. LeBlanc, E. J. Landaker, Z. Y. Jiang, G. R. Willsky, C. R. Kahn, Metabolism, Complementary and Alternative Medicine Therapies for Diabetes. 49 (2000) 400.

7. (a) D. C. Crans, L. Yang, T. Jakusch, T. Kiss, Inorg. Chem. 39 (2000) 4409-4416. (b) K. H. Thompson, V. G. Yuen, J. McNeill, C. Orvig, Chem. Rev. 99(1999) 2561-2572. (c) K. H.Thompson, V. G. Yuen, J. McNeill, C.Orvig, Oxford University Press, New York, Ny, 1998, 329.

8. M. T. Sananes, G. J. Hutchings, J. C. Volta, J. Chem. Soc, Chem. Commun. 243-244(1995).

9. H. Michibata, N. Yamaguchi, T. Uyama, T. Ueki, Coord. Chem. Rev. 237 (2003) 41-51.

10. H. Michibata, T. Uyama, T. Ueki, K. Kanamori, Microsc. Res. Technol. 56(2002) 421.

11. D. Rehder, Coord. Chem. Rev. 182(1999) 297-322.

12. H. Michibata, H. Sakurai, Kulwer Academic Publishers, Boston, 1990.

13. K. Kustin, G. C. McLeod, T. R. Gilbert, L. B. R. T. Briggs, Struct. Bonding.53 (1983) 139.

14. H. Michibata, T. Terada, N. Ananda, K. Yamakawa, T. Numakunai, Biol. Bull. 171(1986) 672.

15. D. J. Rehder, Inorg. Biochem. 80 (2000) 133.

16. J. Chen, J. Christiansen, R. C. Tittsworth, B. J. Hales, S. J. George, D. Coucouvanis, S. P. Cramer, J. Am. Chem. Soc. 115(1993) 5509-5515.

17. H. Vitter in Metal ions in Biological Systems; (Eds.: H. Sigel, A. Sigel), METAL IONS IN BIOLOGICAL SYSTEMS Marcel Dekker: New York, 1995 Vol. 31, chapter 10.

18. J. N. Carter-Franklin, J. D. Parrish, R. A. Tschirret-Guth, R. D. Little, A. Butler, J. Am. Chem. Soc. 125 (2003) 3688.

19. (a) J. Littlechild, E. Garcia-Rodriguez, Coord. Chem. Rev. 237(2003) 65-76. (c) D. E. Carpio, L. Hernándeza, C. Ciangherotti, Coa, V. Villalobos, L. Jiménez, V. Lubes, G. Lubes, Coord. Chem. Reviews. 372(2018) 117-140. (d) M. Debnath, M. Dolai, K. Pal, S. Bhunya, A. Paul, H. M. Lee, M. Ali, Dalton Trans. 47(2018) 2799-2809.

20. A. Butler, A. H. Baldwin (Eds.: H. A. O. Hill, P. J. Salder, A. J. Thompson), Spingler-Verlag, Heidelberg, 1999, 108-132.

21. Bioinorganic Catalysis; (Ed.: J. Reedijk), Marcel Dekker, Inc.: New York, 1993, 425-445.

22. R. A. Rowe, M. M. Jones, Inorg. Synth. 5 (1957) 113.

23. Reference for Gaussian 09w Package: M. J. Frisch, G. W. Trucks, H. B. Schlegel, G. E. Scuseria, M. A. Robb, J. R. Cheeseman, G. Scalmani, V. Barone, B. Mennucci, G. A. Petersson, H. Nakatsuji, M. Caricato, X. Li, H. P. Hratchian, A. F. Izmaylov, J. Bloino, G. Zheng, J. L. Sonnenberg, M. Hada, M. Ehara, K. Toyota, R. Fukuda, J. Hasegawa, M. Ishida, T. Nakajima, Y. Honda, O. Kitao, H. Nakai, T. Vreven, J. A. Montgomery Jr., J. E. Peralta, F. Ogliaro, M. Bearpark, J. J. Heyd, E. Brothers, K. N. Kudin, V. N. Staroverov, R. Kobayashi, J. Normand, K. Raghavachari, A. Rendell, J. C. Burant, S. S. Iyengar, J.

Tomasi, M. Cossi, N. Rega, J. M. Millam, M. Klene, J. E. Knox, J. B. Cross, V. Bakken, C. Adamo, J. Jaramillo, R. Gomperts, R. E. Stratmann, O. Yazyev, A. J. Austin, R. Cammi, C. Pomelli, J. W. Ochterski, R. L. Martin, K. Morokuma, V. G. Zakrzewski, G. A. Voth, P. Salvador, J. J. Dannenberg, S. Dapprich, A. D. Daniels, Ö. Farkas, J. B. Foresman, J. V. Ortiz, J. Cioslowski and D. J. Fox, GAUSSIAN 09 (Revision A.1), Gaussian, Inc., Wallingford, CT, 2009.

24. N. M. O'Boyle, A. L. Tenderholt, K. M. Langner, J. Comput. Chem. 29(2008) 839–845.
25. G. M. Sheldrick, SHELXTL, v. 6.14, Bruker AXS Inc., Madison, WI, 2003.
26. C. K. Johnson, ORTEP Report ORNL-5138, Oak Ridge National Laboratory, Oak Ridge, TN, 1976.
27. Atanu Banerjee, Sumana Sarkar, Deepak Chopra, Enrique Colacio, and Kajal Krishna Rajak, *Inorg. Chem.***47**4023-4031.

CHAPTER IV

A study of DNA/BSA interaction and catalytic potential of oxidovanadium (V, IV) complexes incorporating dibenzofuran based O^N^O ligand.

ABSTRACT

The tridentate Schiff base ligand **H_2L_1**, [(Z)-3-((2-hydroxybenzylidene)amino)dibenzo[b,d]furan-2-ol], synthesized by the typical condensation reaction of [3-aminodibenzo[b,d]furan-2-ol] with salicyldehyde has been used in the present work towards the synthesis of mononuclear oxidovanadium complexes. Three mononuclear oxidovanadium complexes [$VOL_1(OMe)$],**1**; [$VO(L_1)$(8-Hq)], **2** and [$VO(L_1)$(1,10-phen)], **3** have been successfully synthesized with high yields using [$VO(acac)_2$]. 8-hydroxyquinoline and 1,10-phenanthroline were used as co-ligands in the synthesis of complexes **1**, **2** and **3**. In this chapter we have discussed about the biological and catalytic activity of the complexes **1**, **2** and **3** (the synthesis, characterization and the DFT studies are described in the previous chapter). DNA/BSA interaction study was performed using UV-Vis spectroscopy, Fluorescence spectroscopy, circular dichroism, viscometer measurements, FRET and Molecular docking study. It is revealed that the complexes bind with DNA through intercalation resulting in shortening of DNA length. Among all the complexes, complex 3 shows the strongest binding ability with DNA and the binding constant (K_b) was found to be 6.2×10^5 M^{-1}. Complex **2** showed highest binding affinity with the BSA protein ($K_{BSA}= 3.7 \times 10^6$ M^{-1}). The energy transfers between BSA and the complexes are feasible in a static quenching interaction. They were also proven to show bromoperoxidase activity with high conversion rate and enhanced selectivity.

IV.1. INTRODUCTION

Owing to the broad application of vanadium complexes in biological fields and catalysis it has been a center of interest among many researchers over decades. [1-3] Vanadium has also been recognized as an essential element in some living organism**.** [4-8] Due to such occurrence oxidovanadium complexes are often shows insulin mimicking activity**,** [9-11] various enzymatic activity such as nitrogenase (V-Nase), [12-14] halo-peroxidase (VHPO) [15-17] as well as anticancer and antimicrobial activity**.**

DNA is the storehouse of genetic information which is needed for an organism to develop, survive and reproduce. By using these information DNA plays a pivotal role to synthesis of proteins which are complex molecules that affect different processes and functions in our body and has a strong impact on our health. Thus DNA binding study is useful for the development of new therapeutic reagents and drugs. Metal complexes bind with DNA mainly through covalent and non-covalent interactions such as major and minor groove binding, intercalation and electrostatic interactions [18]. There is also a possibility that the interaction with metal complexes leads to the destruction of DNA which in turn helps to destroy cancerous cells. [19]

In biological fluids, there is a major contribution of serum albumin in circulatory system and has importance in physiological and pharmacological functions. Bovine serum albumin (BSA) can be taken as a model protein as it contains 76% sequence homology as Human serum albumin (HSA). [20] So, BSA binding study with metal complexes is also important for the successful implementation of drug delivery.

The present study consists of successful synthesis of three mononuclear oxovanadium complexes bearing tridentate O^N^O schiff base ligand having dibenzofuran moeity. The binding ability and nature of interaction of these complexes with DNA/BSA has been evaluated by absorption titration, emission titration, circular dichroism, and viscosity measurements and Forster resonance energy transfer (FRET) studies. Besides this, the complexes used here are able to show significant bromoperoxidase activity with high yield in mono-bromo complexes. Molecular docking studies were done for the better insight into the binding mechanism of oxidovanadium complexes with DNA and BSA.

IV.2. EXPERIMENTAL SECTION

A.Materials

Vanadyl sulphate was purchased from S D Fine-Chem Limited, Sodium salt of CT-DNA and ethidium bromide were purchased from Sigma-Aldrich. BSA was purchased from sigma. Tris-(hydroxymethyl)-aminomethane, 99.9% ultrapure grade was taken from Aldrich. 8-Hydroxyquinoline was purchased from Alfa-Asser. Potassium Bromide was purchased from Fischer scientific and Hydrogen peroxide (30% V/V) was obtained from Merck. Analytically pure solvents and chemicals were used throughout the study. All the reactions with metal salt was carried out under open air atmosphere.

Tris–HCl buffer solution was prepared from tris(hydroxymethyl)aminomethane hydrochloride and pH adjusted to 7.4. The stock solution of ct-DNA was prepared by dissolving approximately 1–2 mg of ct-DNA fibres in 2.0 mL Tris–HCl buffer (50 mM) by shaking gently and stored for 24 h at 4°C. The concentration of ct-DNA in stock solution (2.0×10^{-3}) was expressed in monomer units, as determined by spectrophotometry at 260 nm using an extinction coefficient (εp) of 6600 M^{-1} cm^{-1} [21].

B. Bromo-peroxidase activity

Catalytic oxidative bromination of salicylaldehyde: The oxidative bromination reaction of salicylaldehyde in aqueous medium was performed by using complexes 1, 2 and 3 [salicylaldehyde (2.44g, 20.0 mmol), KBr (5.95g, 50 mmol), H_2O_2 (15g, 120 mmol) and water (40mL) were taken]. Complexes 1, 2 and 3 were used as three different catalysts which were added with a constant amount of 0.015 g. To initiate the reaction, $HClO_4$ (4.02 g, 80 mmol) was added and the mixture was stirred at room temperature. An additional 240 mmol of $HClO_4$ was added in three equal portions at regular intervals of fifteen minutes. After 2h the reaction mixture was extracted with dichloromethane, washed with brine (NaCl) solution and dried over anhydrous Na_2SO_4. The products were analysed and identified by GC-MS.

C. DNA binding studies

UV-Vis spectroscopy and Fluorescence spectroscopic study: UV absorption spectral titration was done in the range 200-800 nm. The concentration of the complex (25μM) was maintained constant initially and CT-DNA concentrations were varied from 0 to 140 μM and vice-versa. EtBr fluorescence displacement assays were carried out using EtBr bound CT-DNA solution (EtBr =10 μM and DNA = 100 μM) as the reference solutions. The excitation wavelength of EtBr was 510 nm. The emitted fluorescence intensity was observed at 610 nm for EtBr at room temperature. All the DNA experiments were performed in 50mM Tris-HCl buffer at pH = 7.4.

Viscosity measurements: Viscosity experiments were conceded on the Ubbelohde viscometer at a fixed temperature (26±0.1°C). Complexes were added with a micropipette to the DNA solution (10 μmol·L−1). Flow time was recorded for the increasing concentration of the compounds (0–10 μM) and data were graphically presented as $(\eta/\eta_o)^{1/3}$ versus the binding ratio of the concentration of compounds to DNA. Where η was the viscosity of the DNA in the presence of the complex and η_o was the viscosity of the DNA alone. The relative viscosity η was calculated using the following equation [22]:

$$\eta = \frac{(t - t_0)}{t_0}$$

Where, t and t_o represent the flow time of the buffer solution through the capillary and the observed flow time for the DNA in the presence and absence of the complexes correspondingly. The mean of replicate measurements was used to evaluate the viscosity of the samples.

Circular dichroism measurements: For the purpose of recording DNA CD spectra, an JASCO spectropolarimeter was used in the presence and absence of the V(IV)/(V) complexes at temperature 26˚C, with a 0.1 cm path length quartz cell at a scan speed of 100 nm min^{-1}. In the CD experiment, the spectral change of the protein was examined by recording the spectra of free BSA (60 μM), upon successive addition of complexes **1, 2 and 3 (10** μM).

D. BSA interaction studies

Fluorescence quenching study: A fluorescence quenching study was performed to investigate the better interaction among BSA and complexes **1, 2** and **3**. In this study, BSA (**6.06x10^{-5} M** in **0.05M** Tris-HCl buffer) was titrated by successive addition of the complexes. The mixture was allowed to equilibrate for 5 min after each addition. The fluorescence spectra were obtained from 300 nm to 470 nm using the excitation wavelength of **295** nm at room temperature.

Circular Dichroism (CD) Spectra: All CD spectra were recorded in the wavelength range 200 – 320 nm under continuous purging with nitrogen and a scan speed of 100 nm min–1. Here, a fixed concentration of BSA (0.75 µM) was titrated with the increasing concentration of complexes 1,2 and 3 from 0 µM to 4 µM in Tris-HCl buffer solution of pH 7.4 at 26 °C. Each CD spectrum was an average of three scans and the baseline correction was performed with Tris–HCl buffer signal.

Forster Resonance Energy Transfer (FRET) study: Energy transfer between the complexes and BSA can provide valuable information about BSA–complex binding. The fluorescence quenching of BSA upon its binding to metal complexes can be deduced from energy transfer between BSA and metal complexes. This energy transfer can be explained by fluorescence resonance energy transfer (FRET) theory [23] FRET "known as Förster's resonance energy transfer" is an interaction between the excited molecule and its adjacent molecule, upon it; energy absorbed by donor molecule is transferred to an acceptor [24]. According to this theory, energy transfer will observe if: (1) the donor acceptor is less than 8 nm [25]. The distance (r) and efficiency of energy transfer (E) between tryptophan residue of protein (BSA) and drug (complex) were calculated using this theory through the following equation:

$$E = 1 - \frac{F}{F_0} = \frac{R_0^6}{R_{0+r^6}^6}$$

where F_0 and F are fluorescence intensities of BSA in the absence and presence of complex, respectively. R_0 is the critical distance when the transfer efficiency is 50% and r is the distance between donor and acceptor. R_0 can be calculated by the following equation [26]:

$$R_0^6 = 8.79\times10^{-25}\,K^2\,N^{-4}\,J\Phi$$

In the above equation, the term K^2 is the orientation factor of the dipoles; N is the refractive index of medium, J is the overlap integral of the fluorescence spectrum of the donor with absorption spectrum of the acceptor, and Φ is the fluorescence quantum yield of the donor. In general, K^2 = 2/3, N = 1.336 and Φ = 0.15 for BSA.

The value of J can be calculated as follows

$$J = \frac{\sum F(\lambda)\varepsilon(\lambda)\lambda^4\Delta\lambda}{\sum F(\lambda)\Delta\lambda}$$

Here, $F(\lambda)$ is the fluorescence intensity of the donor in the absence of the acceptor at wavelength λ and ε is the molar absorption coefficient of the acceptor at λ. In general, K^2 = 2/3, N = 1.336 and Φ = 0.15 for BSA.

IV.3. RESULT AND DISCUSSION

Biological Activities

DNA interaction studies: DNA binding affinity of the complexes **1, 2** and **3** to CT-DNA was determined by using UV- Visible spectroscopy, fluorescence efficiency measurements and circular dichroism. The equilibrium binding constant (K_b) of the complexes to CT-DNA was calculated with the aid of UV-Vis titration experiments [27]**.** (Table **3** and Fig. **6**) The ligand to metal charge transfer transition bands were used to monitor the electronic absorption titration with the DNA. It is obvious that if there is any interaction between the complex and DNA then perturbation in the spectral transitions will occur. The addition of the CT-DNA to the complexes **1–3** exhibit hypochromic shift in the LMCT bands with a small change in the λ_{max} values. The hypochromic shift mainly occurs due to the interaction of the organic bases of DNA and chromophores attached with vanadium complexes via intercalation mode of binding. The binding ability of the complexes to the CT-DNA is reflected through the extent of hypochromism. Among all the complexes, complex **3** shows better hypochromism with a small red shift of λ_{max} value ~21nm. This bathochromic effect can be attributed to the strong π–π stacking interaction [28] between the phenanthroline moiety of complex **3** and the aromatic rings of DNA bases. The spectral change for complex **3** is depicted in Figure **1**. Binding constant (K_b) is a useful parameter to evaluate the binding capability of the complex to the DNA and can be determined from the variation in the electronic spectra before and after the addition of DNA

(20 µM) into the solution of complexes (0-100 µM) by applying Benesi–Hildebrand equation [29-30] given below:

$$\frac{A_0}{A - A_0} = \frac{\varepsilon_f}{\varepsilon_b - \varepsilon_f} + \frac{\varepsilon_f}{\varepsilon_b - \varepsilon_f} \frac{1}{K_b[DNA]}$$

where A_0 is the initial absorbance of free complex, A is the absorbance of the complex in the presence of DNA, ε_f corresponds to the extinction coefficient of the complex in its free form and ε_b refers to the extinction coefficient of the complex in the bound form. The plot of $A_0/(A - A_0)$ *versus* 1/[DNA] gives a straight line with an intercept of $\varepsilon_f/(\varepsilon_b - \varepsilon_f)$ and a slope of $\varepsilon_f/K_b(\varepsilon_b - \varepsilon_f)$. The value of K_b is calculated from the ratio of the intercept to the slope. **Table 1** shows the binding constant values of the DNA- complex interaction. Complex **3** shows strong interaction with DNA as the binding constant (K_b = **6.2 x 10^5**) is 100 to 1000 fold higher than other two complexes.

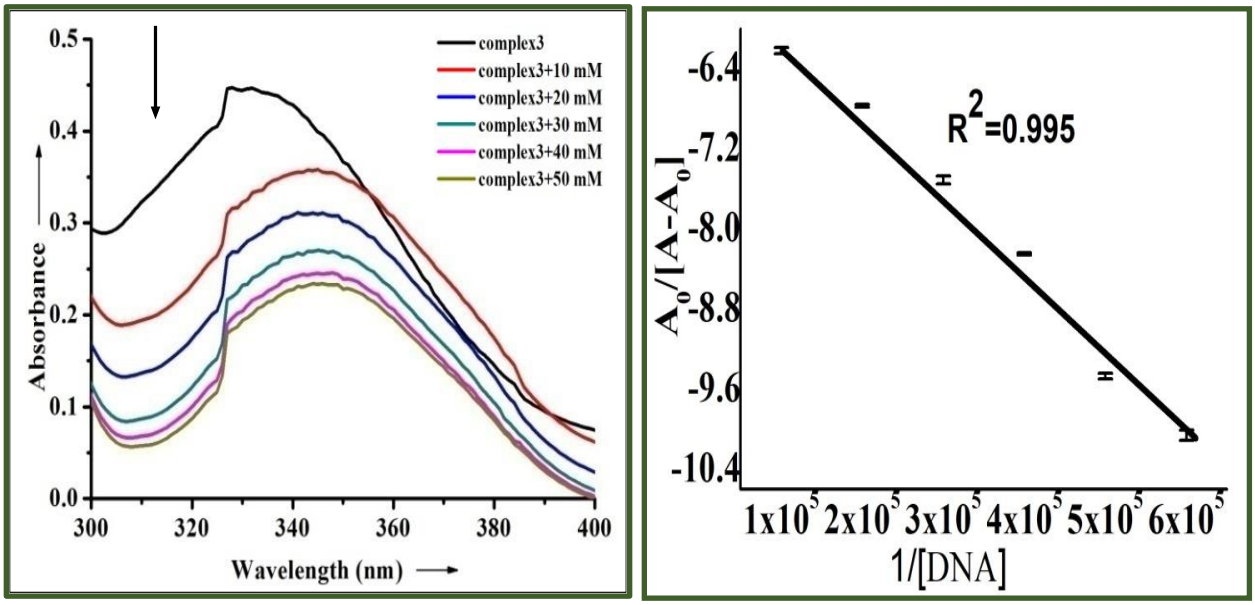

Figure 1: (Left) UV-Vis absorption spectral titration of complex 3 in presence of increasing concentration of CT-DNA. (Right) The plot of A_0/ [A-A_0] vs. 1/[DNA] for calculation of K_b, (Ratio of intercept to slope); plot for complex 3 is shown here.

Circular Dichroism study of DNA: CD spectral analysis is another significant method for studying the modes of binding of metal complexes. A complex can bind with CT DNA through major groove binding, minor groove binding, electrostatic interaction and intercalation. In the CD

spectra, the β form of the CT DNA shows characteristic positive cotton effect at 275 nm for base stacking and negative cotton effect at 245 nm for the helicity. In case of Intercalative mode of binding, changes in both the positive and negative cotton effect are observed. In case of minor groove binding and electrostatic interaction minor changes with either positive or negative cotton effect is observed. To study the conformational change of CT DNA associated with the interaction of a complex, CD spectral analysis was performed by incubation of oxidovanadium(V)/(IV) complexes with CT DNA taking same concentration each. A significant change in intensity of both positive and negative bands of CT DNA is observed which indicates the intercalative mode of binding of double helical conformation of CT DNA with complexes **1**, **2** and **3**. [31]Fig. **2** shows the positive and negative cotton effect of complexes with CT DNA.

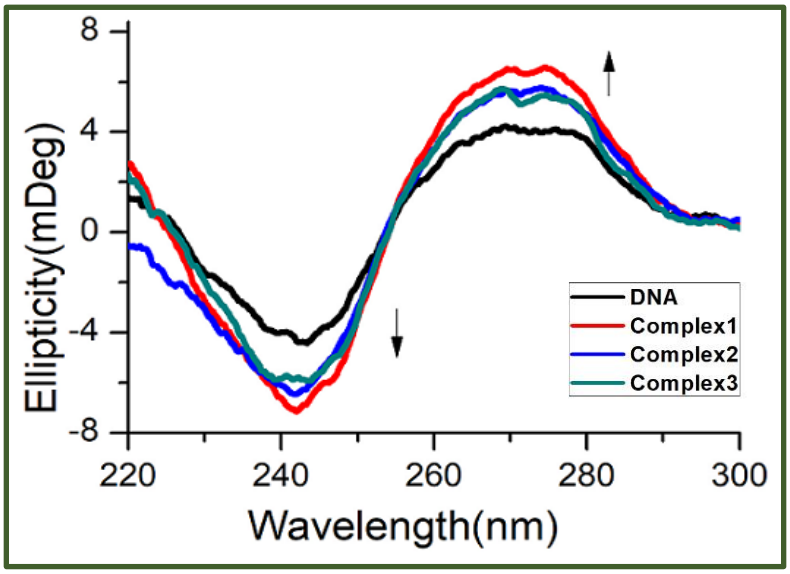

Figure 2. Circular dichroism spectra of a mixture of 10 μM complex 1, 2 and 3 separately containing CT-DNA 60 μM in 10 mM Tris-HCl buffer (pH 7.4).

Competitive binding experiments in the presence of Ethidium Bromide: Ethidium Bromide (EB) has well conjugated aromatic system which can be applied as a fluorescence probe in the study of competitive binding experiments of DNA with the synthesized Vanadium(V/IV) complexes. The fluorescence intensity of EB is usually very weak in aqueous solution but it increases to a significant extent when EB binds with DNA double helix through intercalation**.** So, the competitive DNA binding experiment is an efficient tool to understand the binding behaviour of the vanadium complexes with DNA. To prove whether the vanadium complex can displace EB from the DNA helix, we have examined the fluorescence spectra of EB-DNA adduct in the presence of

varying concentration of the complexes (0–100μM). The vanadium complexes under study are feebly emitter. Complex **3** shows greater extent of quenching of the fluorescence intensity upon addition of the complex into EB-DNA adduct whereas complexes **1** and **2** show a slight reduction of fluorescence intensity. This quenching ability of the complexes depicts that they can displace EB and binds with DNA double helix through intercalation mode of binding. Representing spectra of complex 3 is shown in **Fig.8** and Stern -Volmer constant and rate constant are calculated using linear Stern–Volmer equation:

$$\boldsymbol{F_0/F = 1 + K_{SV}[Q] = 1 + K_q\tau_0\,[Q]}$$

Here F_0 and F are the fluorescence intensities in the absence and presence of the quencher (Q) [Vanadium complex in this experiment] respectively. $\mathbf{K_q}$ is the bimolecular quenching constant and $\boldsymbol{\tau_0}$ is the lifetime of the fluorophore in the absence of the quencher (10^{-8} M^{-1} for EB). The results are included in Fig. **3** and Table **1**.

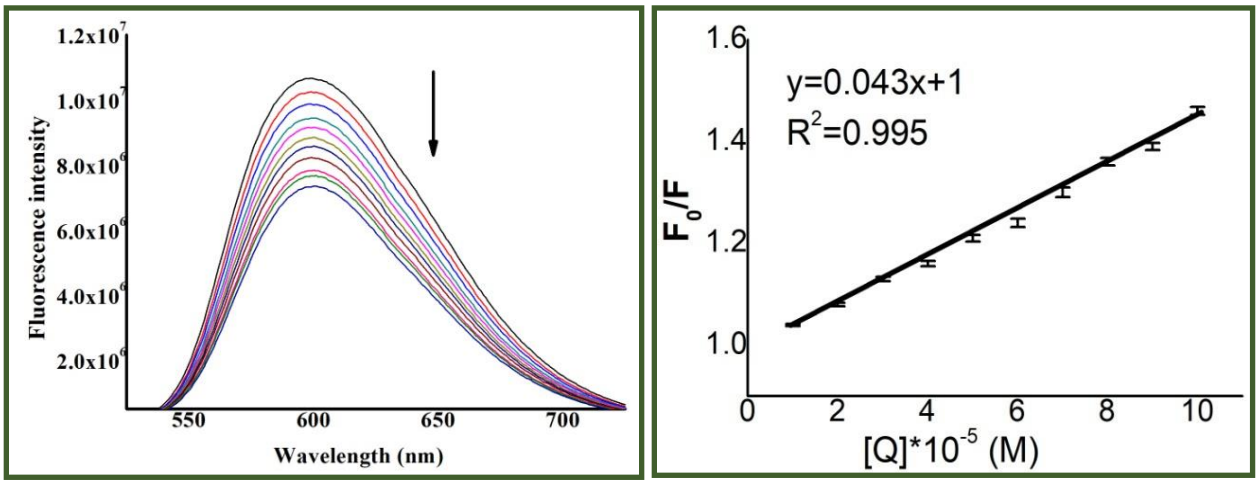

Figure 3: Ethidium bromide displacement assay of complex **3**

Table 1. K_b, K_{SV}, K_q values of complexes 1, 2 and 3 from complex-DNA interactions

Complex	Binding constant (K_b), M^{-1}	Correlation coefficient (R^2)	Stern- Volmer constant (K_{SV}), M^{-1}	Quencher rate constant (K_q)[a]	Correlation coefficient (R^2)
1	8.1×10^3	0.989	4.5×10^3	4.5×10^{11}	0.993
2	6.4×10^4	0.982	1.5×10^3	1.5×10^{11}	0.987
3	**6.2×10^5**	0.998	4.3×10^3	**4.3×10^{11}**	0.995

Viscosity Measurements of DNA: Viscosity measurements of DNA is another important tool to analyze the binding mode of compounds to DNA least ambiguous and effective way. Ethidium Bromide (EB) is considered as a classical intercalation probe. When EB intercalates with the two strands of DNA, a significant increase in viscosity of the DNA solution is observed due to an increase in separation of base pairs at the intercalation sites. This leads to an increase in overall DNA length. In contrast, partial, nonclassical intercalation of ligand could crook the DNA helix, resulting in shortening of DNA length and concomitantly reducing its viscosity. The thickness of CT-DNA increases with increase in the ratio of complexes to CT-DNA which is associated with the specific intercalation binding mode. **Fig.9**. depicts the plot of $(\eta/\ \eta_0)^{1/3}$ vs [complex]/[DNA] where those curves show the effective relative viscosity of all the complexes. In the plot, it is observed that EB-DNA curve exhibits high viscosity whereas complex-DNA curves reduce the viscosity in the order of complexes **3**>**2**>**1**. Thus, it can be assumed that the CT DNA length is shortened in a nonclassical way of intercalation mode of binding with the complexes.

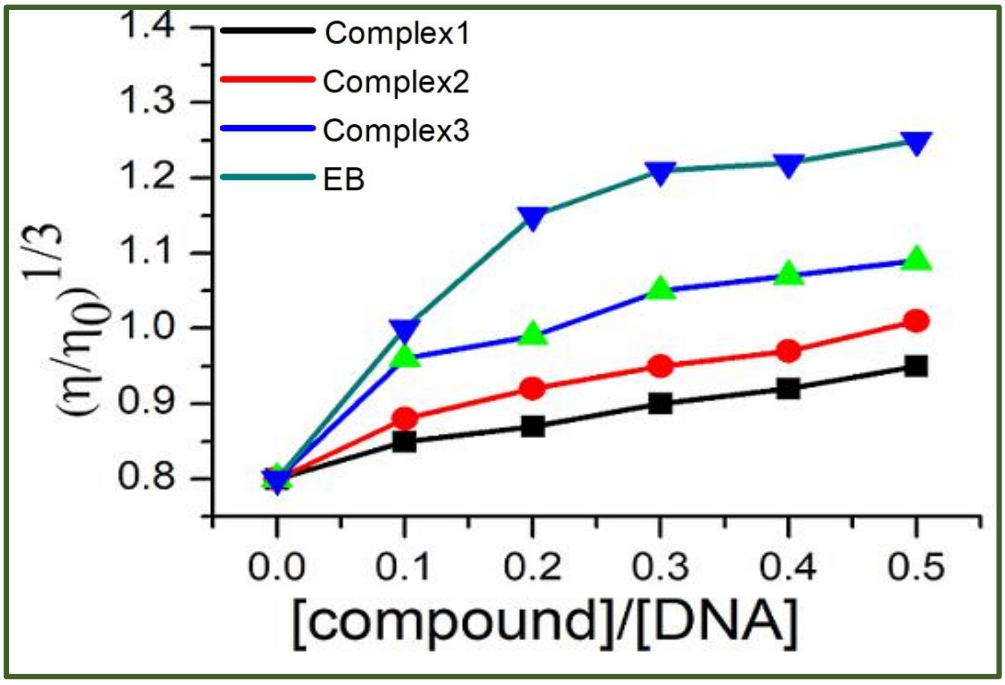

Figure 4. Effect on relative viscosity (±0.1) of CT-DNA under the influence of increasing amount of compounds at 26 ± 0.1°C in 5mM Tris-HCl bu.er (pH 7.4).

BSA interaction studies

Fluorescence quenching studies: The interaction between small molecules and serum protein is a significant characteristic of metal drug metabolism and can possibly effects the biotransformation and the mechanism of action of the chemotherapeutic agents. Due to its similarity with human serum albumin, BSA is often selected as a model protein to examine the interaction of the small molecules with serum albumins**.** Three amino acid residues i.e., tryptophan, tyrosine and phenylalanine are mainly responsible for the intrinsic fluorescence property of BSA. It exhibits tryptophan fluorescence at an excitation of 295 nm with an emission maximum at 344 nm. When a complex bind with BSA, certain conformational changes in the protein influences the fluorescence emission of the tryptophan residues of BSA. After gradual addition of complexes into the solution of BSA, fluorescence intensity decreases at 345 nm which indicates that the complexes interact with the BSA leading to some change in the tryptophan moiety of BSA. For complex **1** and **3**, the decrease in the emission intensity was drastic while for complex 2 it was observed a gradual decrease in fluorescence intensity. In order to quantify the mechanism of interaction of complexes with BSA, different binding parameters (Stern- Volmer Constant, Binding constant, k_{BSA} and number of binding sites, n) were calculated using Stern-Volmer equation and Scatchard equation [32] respectively.

$$\boldsymbol{F_0/F = 1 + K_{SV}[Q]} \qquad \text{Stern} - \text{Volmer equation}$$

$$\boldsymbol{log\left[\frac{F_0}{F} - 1\right] = \log k_{BSA} + nlog[Q]} \qquad \text{Scatchard equation}$$

Here F_0 and F are the fluorescence intensities of BSA in absence and presence of the complex (Q), respectively. $\mathbf{K_{BSA}}$ is the binding constant of the complex to BSA and **n** is the number of binding sites per albumin molecule. The following table shows the experimental results, which reveals that complex **2** gives better results in terms of binding efficiency with protein which is also reflected from the $\mathbf{K_{SV}}$ value as well as the value of binding stoichiometry with the BSA. Complex **2** is showing binding stoichiometry **1:1.41** which is much greater than the other two complexes (0.68 and 0.89 for complex **1** and **3** respectively). The results are depicted in Table **2** and Figure **5**.

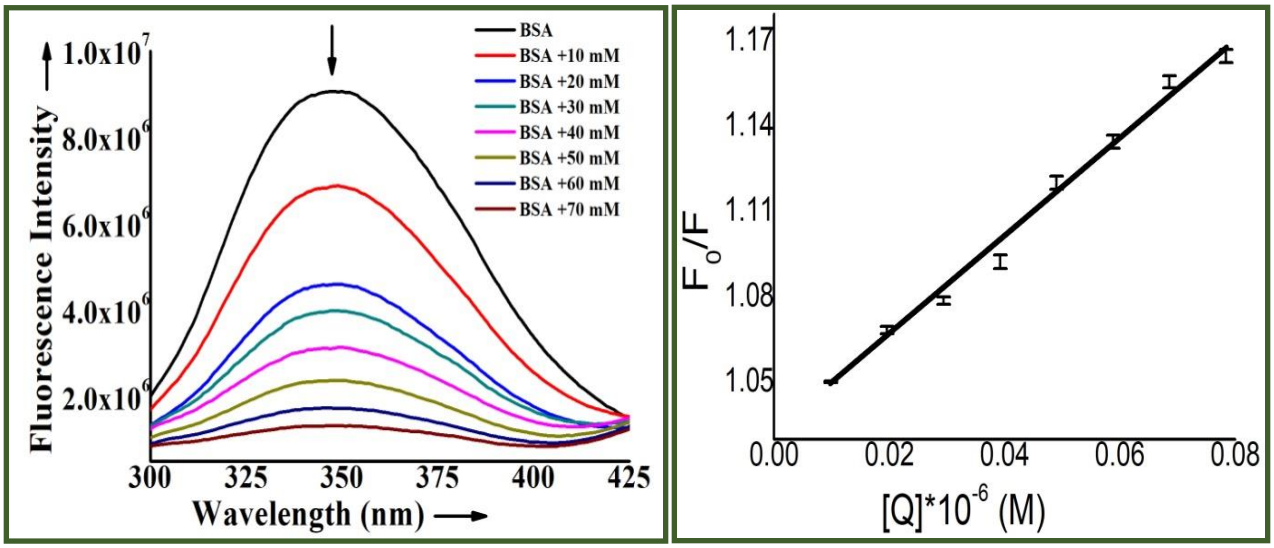

Figure 5. Fluorescence emission spectra of BSA in the absence and presence of increasing amounts of complex **2** at 298 K (left). Corresponding linear fit of F_0/F vs. [complex] and the K_{SV} value was calculated using Stern-Volmer Equation (right).

Table 2. Binding parameters of BSA using fluorescence quenching

Complex	Stern-Volmer constant, K_{SV}, (M^{-1})	Quenching constant, Kq, ($M^{-1}s^{-1}$)	Binding constant, K_{BSA}, (M^{-1})	Number of binding sites (n)
[VO(L_1)(OMe)] Complex 1	1.02×10^5	1.02×10^{13}	5×10^4	0.68
[VO(L_1)(8-Hq)] Complex 2	**1.6×10^6**	**1.6×10^{14}**	**3.7×10^6**	**1.45**
[VO(L_1)(1,10-phen)] Complex 3	1.2×10^5	1.2×10^{13}	4×10^5	0.89

Circular dichroism spectral studies of BSA: Circular dichroism (CD) spectroscopy is a sensitive technique to monitor the secondary structural change of protein upon interaction with small molecules. The CD spectra of BSA in the absence and presence of V(V)/(IV) complexes are shown in Fig. 12. BSA exhibits two negative bands at 208 and 222 nm in the UV region due to the $n \rightarrow \pi^*$ transition for the peptide bond of α- helix. Due to the interaction of BSA with complex 1 and 2 the intensity of the negative bands at 208 nm and 222 nm increases whereas for complex 3 the intensity of bands slightly decreases without any shift of wavelength. The results of CD spectra

obtained are analyzed in terms of mean residue ellipticity (MRE, deg cm^2 $dmol-1$) according to (Eq. (1)). The percentage of α-helical content is calculated using (Eq. (2)).

$$\mathbf{MRE(deg.cm^2.dmol^{-1})} = \frac{\boldsymbol{\theta obs}}{\boldsymbol{Cp \times n \times l \times 10}} \qquad \textbf{(Eq.1)}$$

where θ_{obs} is the observed ellipticity in milli-degrees at 208 nm, n is the number of amino acid residues, l is the path length of the cell, and C_p is the molar concentration of the protein. The values of n are taken as 583 for BSA [33]. The α-helical content is then calculated from the expression below:

$$\textbf{\% α-helix} = \frac{-(\boldsymbol{MRE222-2340})}{\mathbf{30300}} \times \mathbf{100} \qquad \textbf{(Eq.2)}$$

The estimated α-helix content in native BSA is found to be, which is in good accordance with the literature value. The decrease in the α-helix content is observed from ~60.5% in the native BSA to ~48.30% and ~51.00 % in presence of complexes 1 and 2 respectively, which indicates the destruction of α-helix structure of BSA. It is very interesting that, complex 3 shows increase in α-helix content to ~62.00 % which indicates that it binds with BSA amino acid residues. **Fig. 6** shows a complex-induced perturbation of the secondary structure of BSA.

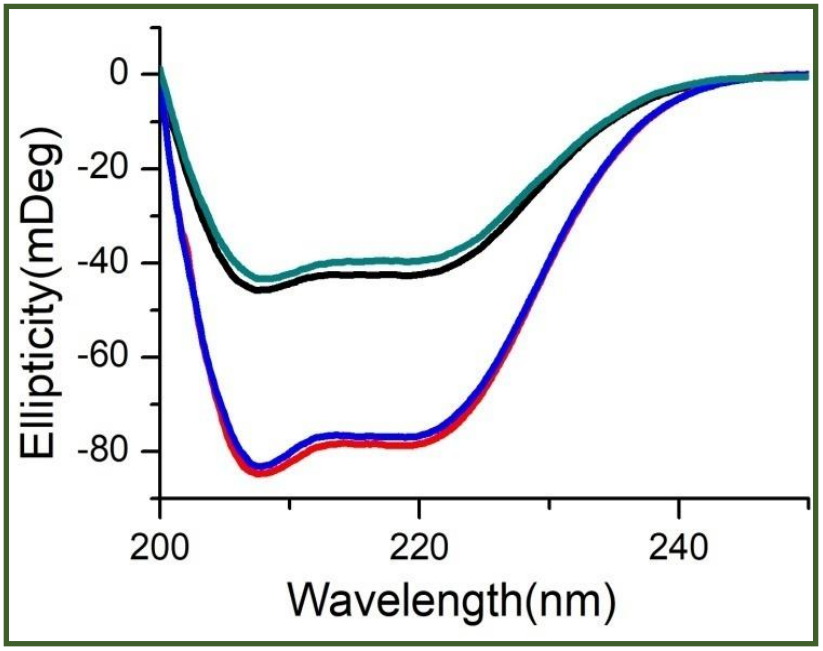

Figure 6: Circular dichroism spectra of a mixture of 10 µM complex 1, 2 and 3 separately containing BSA 60 µM in 10 mM Tris-HCl buffer (pH 7.4).

FRET study of the complexes with BSA:

The overlap integral of BSA fluorescence emission and electronic spectra of complexes **1-3** are shown in Fig. 7, where the concentrations of BSA and complex were kept same ($c = 2 \times 10^{-5}$ M). The values of all the energy transfer parameters are evaluated for the BSA-complex interaction and summarized in **Table 3**. According to the Forster resonance energy transfer theory, the binding sites r must be within the range of 2–8 nm in a state where $0.5R_0 < r < 1.5R_0$. The values of r (r = 3.35- 4.25) for all the complexes are less than 8 nm and suggesting that the energy transfer from BSA to the complexes occurs with high probability. The values obtained from the study also suggests the presence of static quenching interaction of BSA with complexes.

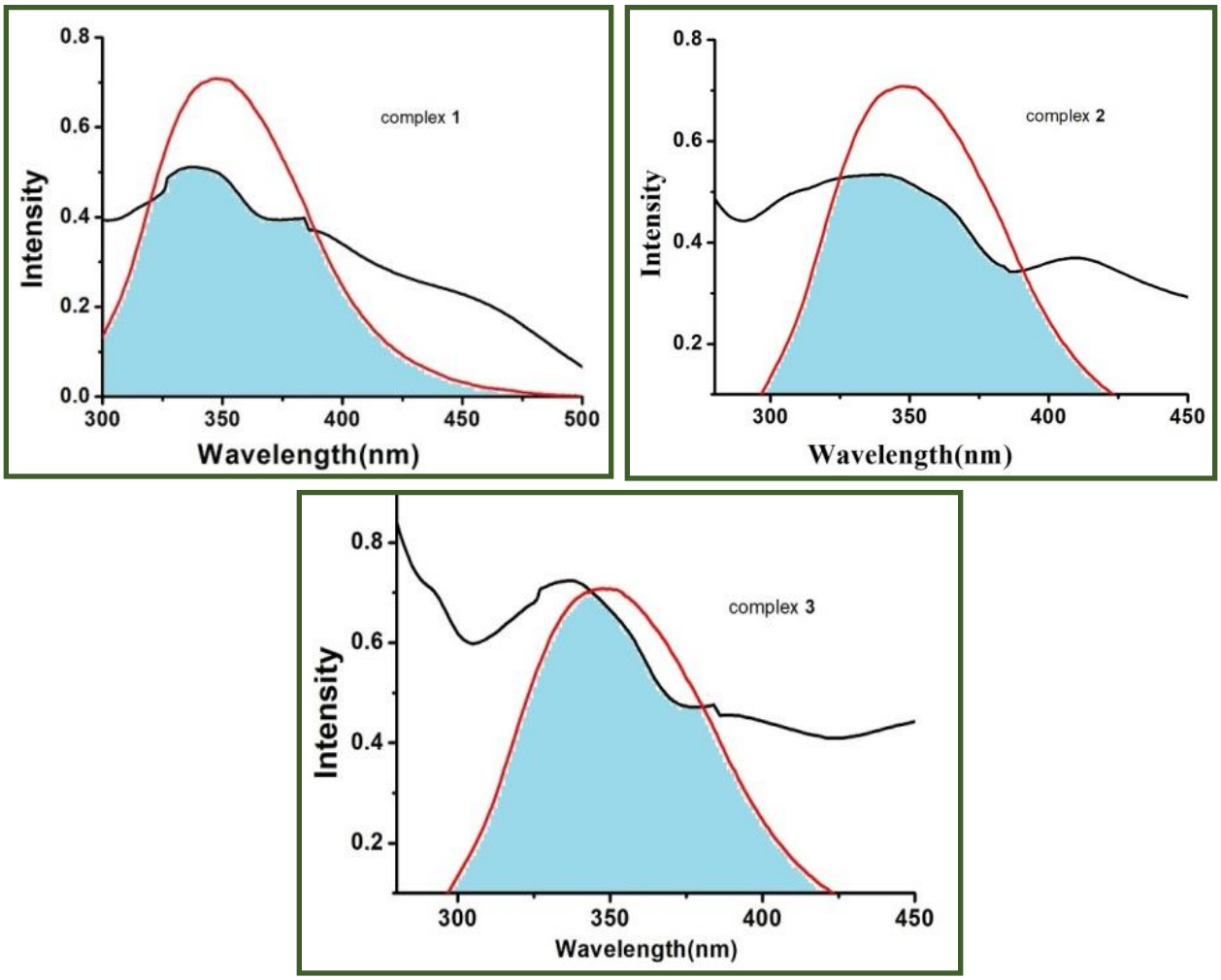

Figure 7. FRET between BSA and complexes **1**, **2** and **3**. The normalized donor emission spectra is shown in red, the acceptor molar extinction coefficient spectrum is shown in black, and the aqua blue shaded area represents the spectral overlap.

Table 3: FRET Parameters for the BSA−Complexes 1, 2 and 3 at 26 °C

Protein	Probe	J(cm^3.L.MOL^{-1})	R_0(nm)	E	r(nm)
BSA	**Complex 1**	6.55×10^{-14}	4.74	0.66	4.25
	Complex 2	7.80×10^{-14}	3.59	0.24	3.22
	Complex 3	9.90×10^{-14}	3.74	0.61	3.35

Docking Studies: Docking is a computational tool used for three purposes: 1) to find new pharmacophore [34] 2) to identify target bio-macromolecules [35], and 3) to understand the relation between small-molecule and macromolecules through different non-covalent interactions [36]. Here, the study was performed to find the behavior of complexes **1-3** with CT-DNA and BSA protein. All the results of binding energy are summarized in the **Table 4**. It was found that the complex **3** bind most strongly with DNA, where complex **2** showed highest binding affinity with the BSA protein and their binding energy are -7.08 and -7.59 kcal/mole, respectively. The order of the binding affinity of the complexes with CT-DNA and BSA protein are **3**>**2**>**1** and**2**>**3**>**1**, respectively. The results matches well with the experiment.

Table 4: Binding energy of complexes 1-3 with CT-DNA and BSA

Entry	Complex-CT-DNA	ΔG° (kcal/mol)		Entry	Complex-BSA	ΔG° (kcal/mol)
1	**Complex 1**	-6.05		1	**Complex 1**	-7.11
2	**Complex 2**	-6.55		2	**Complex 2**	-7.59
3	**Complex 3**	-7.08		3	**Complex 3**	-7.31

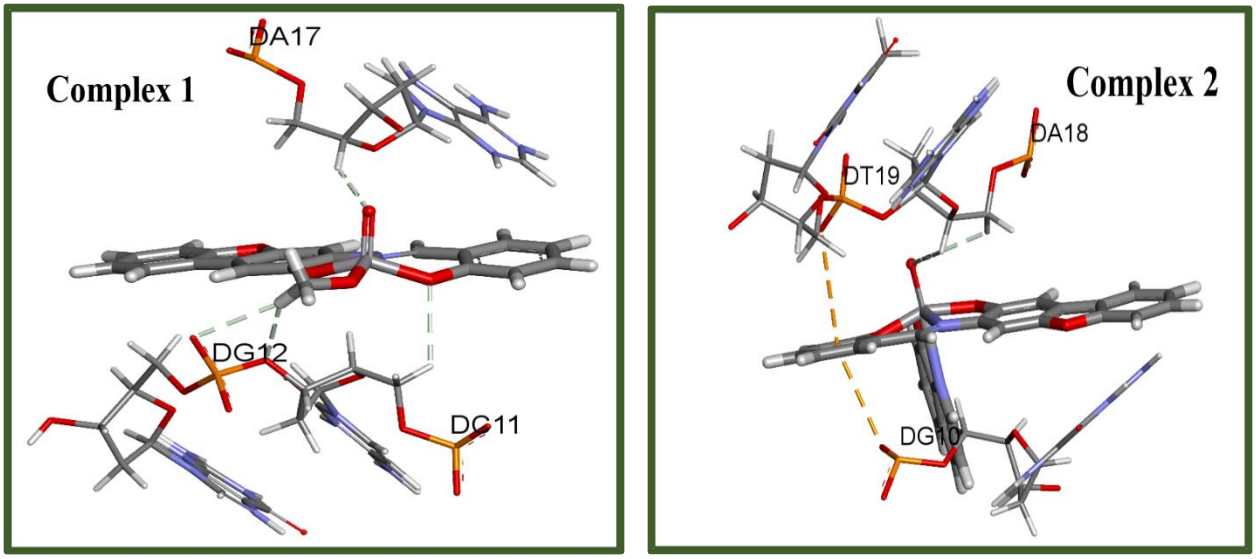

Figure 8: Docking pose of complex **1** and **2** with CT-DNA.

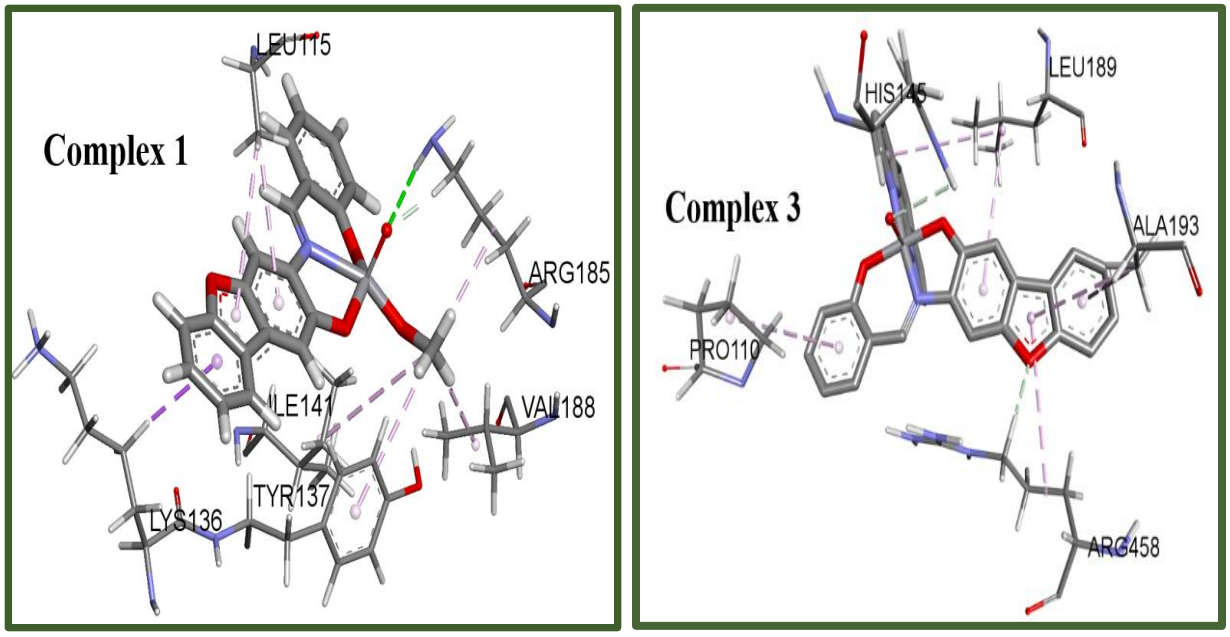

Figure 9: Docking pose of compound **1** and **3** with BSA.

The complex **3** was found to be minor groove binder to the CT-DNA. Here, the wide 3-aminodibenzo[*b*,*d*]furan-2-ol moiety is involved as key in the binding process(Figure **10**). The sugar CH_2 of DNA base C21 with V=O and aromatic CH with phosphate O interacted through non-conventional H-bond. The phosphate ion of T7, T8, and C21 interacted with the complex **3** through π…anion interactions.

In the case of BSA, dibenzo[*b*,*d*]furan moiety of **2** play a major role in the binding process. The compound bind at the hydrophobic pocket present at the surface of the protein (Figure Xb) with the help of dibenzo[*b*,*d*]furan moiety. The molecule use hydrogen bonding and different π-stacking interactions for binding process. The amino acid residues L115, D118 showed hydrogen bonding with V=O and O attached to dibenzo[*b*,*d*]furan. The π-stacking interaction by L115, L122, K136, and Y160 with long π-surface of dibenzo[*b*,*d*]furan unit was observed and CH…π and amide…π interactions was observed with K116.

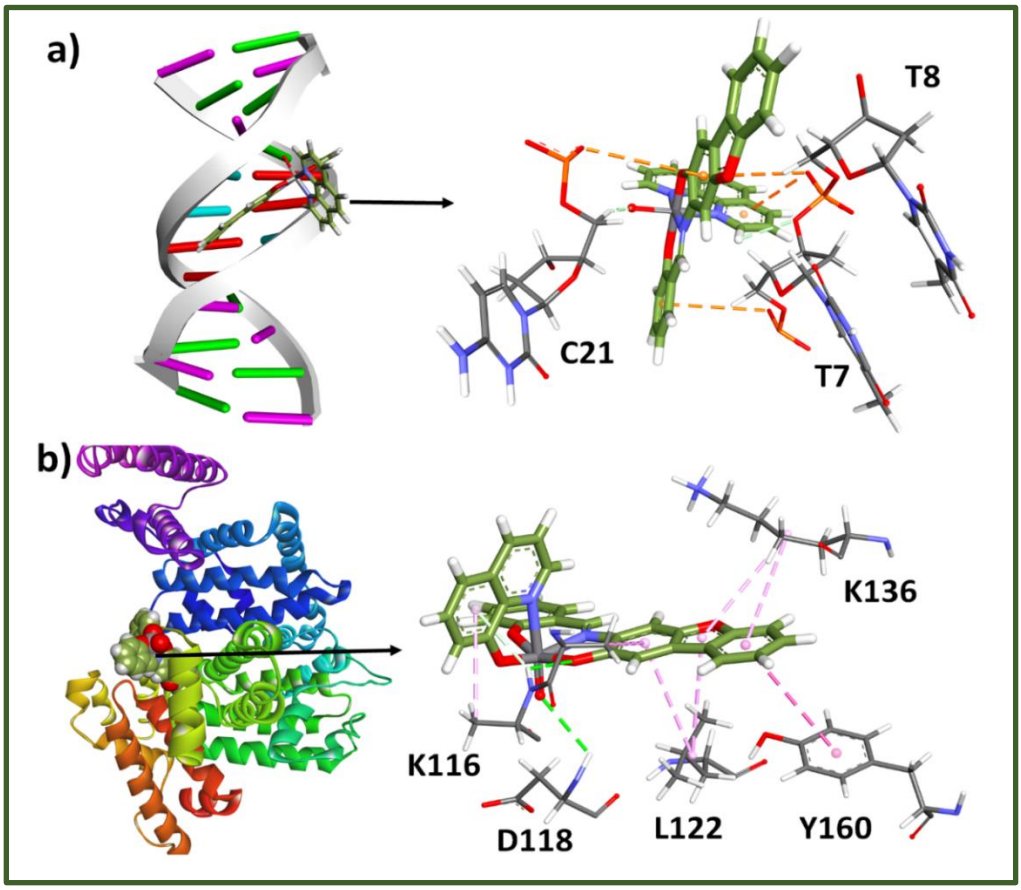

Figure 10: Docking pose of (a) compound **3** with CT-DNA and (b) compound **2** with BSA

Oxidative bromination of salicylaldehyde: Bromoperoxidase activities

Vanadium complexes are known to act as efficient model system for vanadium dependent halo-peroxidases. Vanadium is present as co-factor in naturally occuring haloperoxidase. It is quite logical to assume that the complexes may catalyse the bromination reactions of different organic molecules in presence of H_2O_2 and bromide anion.[37] In the present study oxidative bromination of salicylaldehyde is carried out in presence of synthesized vanadium complexes (15 mg) as catalysts in presence of H_2O_2 (120 mmol) and Water (40 mL) in each case. The catalytic oxidative bromination reaction produces three compounds viz. 5-Bromosalicylaldehyde, 3,5-dibromo salicylaldehyde and 2,4,6-tribromophenol as the end products. The addition of $HClO_4$ is done in four equal portions during the progress of the reaction, which is found to be necessary to prevent

the decomposition of the complex and to maximize the conversion of the substrate and to maintain optimum pH of the solution. Using similar reaction conditions, maximum 99 percent conversion is accomplished with complex **1** giving mono-bromo derivative as the main product. Selectivity order is as follows; 5-Bromosalicylaldehyde (77%)> 3,5-dibromosalicylaldehyde (23%)> 2,4,6-tribromophenol (1%). Complex **2** and **3** possess moderate conversion to dibromo derivative (56% and 67% respectively) as the main product. It is also observed that, if complex **2** was used in the bromination reaction; 2,4,6-tribromophenol was formed as bromination product with low yield (8%).Table **5** provides the percentage conversion of salicylaldehyde and selectivity of the products formed using equivalent reaction conditions for complexes **1, 2** and **3**. Interestingly, when the reaction is performed in the absence of catalyst, the reaction mixture gave very low conversion of salicylaldehyde with the selectivity order of the products as: 5-Bromosalicylaldehyde (86%)> 3,5-dibromosalicylaldehyde (28%)> 2,4,6- tribromophenol (13%).

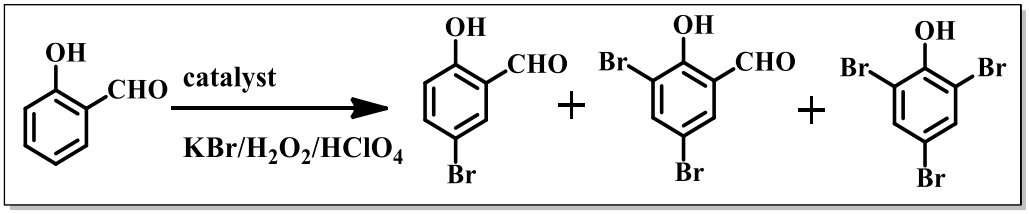

Scheme 1: Oxidative bromination of salicylaldehyde with vanadium complexes as catalyst.

Table 5: Different experimental findings of bromination reaction by vanadium complexes:

Complex	KBr (g,mmol)	H_2O_2 (g,mmol)	$HClO_4$ (g,mmol)	Complex as catalyst (g)	H_2O (mL)	% Conv.	TON	TOF (h^{-1})	% Selectivity		
									Mono bromo	**Di-bromo**	**Tri-bromo**
1	5.95, 50	15, 120	4.02, 80	0.015	40	**99**	2718	678	77	23	1
2	5.95, 50	15, 120	4.02, 80	0.015	40	**99**	**3135**	**783**	81	56	2
3	5.95, 50	15, 120	4.02, 80	0.015	40	**99**	**3142**	**786**	79	**67**	8
Blank Reaction				0.000		34			**86**	28	13

IV.4. CONCLUSION

To summarize, we have successfully synthesized a new dibenzofuran based tridentate O^N^O donor ligand to generate mononuclear oxovanadium (V and IV) complexes. The co-ordinating behaviour of the ligand was used to synthesize three complexes bearing oxovanadium moiety successfully with good yields and well characterized by single crystal X-ray diffraction studies and spectral techniques viz. UV-Vis, IR, NMR, ESI-Mass etc. To support experimental values DFT as well as TDDFT calculations were performed. The complexes under present work show significant interaction with DNA and BSA. Intercalative mode of strong binding affinity is dominated by complex 3 whereas strong interaction with BSA α-helix is observed by complex 2. UV-vis and fluorescence spectroscopy as well as fluorescence quenching experiments are performed to establish the intercalation of the title complexes with DNA and also BSA interaction activity. The presence of π–π stacking stacking interaction between the aromatic moeities of the complex and aromatic bases present in DNA is also proved my several experiments. Model catalytic bromination reaction of an aromatic aldehyde, salicylaldehyde was performed using the oxovanadium complexes to establish the halo-peroxidase mimicking activities of those. The experimental findings presented herein provide valuable insights into the planning of the preparation of strategically important complexes in the field of oxidovanadium chemistry. Further research aimed at the synthesis of polynuclear vanadium complexes using different polydentate ligands is currently under progress.

IV.5. REFERENCES

1. A. Mondal, S. Sarkar, D. Chopra, T.N. Guru Row, K. Pramanik, K.K. Rajak, Inorg. Chem., 44 (1999), 703-708.
2. R. Codd, T.W. Hambley, P.A. Lay, Inorg. Chem., 34 (1995), 877-882.
3. C. Leblanc, H. Vilter, J.B. Fournier, L. Delage, P. Potin, E. Rebuffet, G. Michel, P.L. Solari, M.C. Feiters, M. Czjzek, Coord. Chem. Reviews., 13 (2015), 4301-4302
4. D. C. Crans, J. J. Smee, E. Gaidamauskas, L. Yang, Chem. Rev.104 849-902.
5. (a) A. K. Goldfine, M. –E. Patti, L. Zuberi, B. J. Goldstein, R. LeBlanc, E. J. Landaker, Z. Y. Jiang, G. R. Willsky, C. R. Kahn, Metabolism49 400.

6. (a) D. C. Crans, L. Yang, T. Jakusch, T. Kiss,Aqueous, Inorg. Chem.39 4409-4416. (b) K. H. Thompson, V. G. Yuen, J. McNeill, C. Orvig, Chem. Rev.992561-2572. (c) K. H.Thompson, V. G. Yuen, J. McNeill, C.Orvig, Oxford University Press, New York, Ny, (1998) 329.
7. M. T. Sananes, G. J. Hutchings, J. C. Volta, Chem. Commun. 243-244.
8. J. Chen, J. Christiansen, R. C. Tittsworth, B. J. Hales, S. J. George, D. Coucouvanis, S. P. Cramer, J. Am. Chem. Soc.1155509-5515.
9. H. Vitter, H. Sigel, A. Sigel (Eds.), METAL IONS IN BIOLOGICAL SYSTEMS Marcel Dekker, New York (1995) 31, chapter 10.
10. J.N. Carter-Franklin, J.D. Parrish, R.A. Tschirret-Guth, R.D. Little, A. Butler, J. Am. Chem. Soc., 125 (2003), 3688.
11. (a) J. Littlechild, E. Garcia-Rodriguez, Coord. Chem. Rev., 237 (2003), 65-76. (b) D.E. Carpio, L. Hernándeza, C. Ciangherotti, V.V. Coa, L. Jiménez, V. Lubes, G. Lubes, Coord. Chem. Reviews., 372 (2018), pp. 117-140. (c) M. Debnath, M. Dolai, K. Pal, S. Bhunya, A. Paul, H.M. Lee, M. Ali, Dalton Trans, 47 (2018), 2799-2809.
12. Marcel Dekker, Inc., New York (1993), 425-445.
13. H. Michibata, T. Uyama, T. Ueki, K. Kanamori, Microsc. Res. Technol., 56 (2002), 421.
14. H. Michibata, N. Yamaguchi, T. Uyama, T. Ueki, Coord. Chem. Rev., 237 (2003), 41-51.
15. D. Rehder, Coord. Chem. Rev., 182 (1999), 297-322.
16. H. Michibata, H. Sakurai, Kulwer Academic Publishers, Boston (1990)
17. K. Kustin, G.C. McLeod, T.R. Gilbert, L.B.R.T. Briggs, Struct. Bonding., 53 (1983), 139.
18. U. Ndagi, N. Mhlongo, M.E. Soliman, Drug Des Devel Ther., 11 (2017), 599-616.
19. A. Rudbari, M. Sahihi, V. Mirkhani, M. Moghadam, S. Tangestanineojad, I.M. Baltor, K.S. Gharaghani Journal of Photochemistry and Photobiology B-Biology, 162 (2016), 448-462.
20. R.A. Rowe, M.M. Jones, Inorg Synth, 5 (1957), 113.
21. E. Runge, E.K.U. Gross, Phys. Rev. Lett., 52 (1984), 997-1000.
22. K. Savithri, H.D. Revanasiddappa, Bioinorganic Chemistry and Application (2018), Article 2452869.
23. Z. Bai, Y. Liu, J.Guo P.Zhang, Y. Ma, X. Yun, X. Zhao, R. Zhong, F. Zhang, Luminescence, 31 (3) (2021), 688-693.

24. Z.A. Boroujeni, S. Jahani, M.K. Motlagh, K. Kerman, N. Aramesh, S. Asadpour, M. Noroozifar, Journal of Biomolecular Structure and Dynamics (2020), 1538-0254.
25. P. Singla, V. Luxami, K. Paul, Eur J Med Chem, 19 (2016), 117 59-69.
26. Cathal O'Sullivan, Gillian Murphy, Brian Murphy, Brian Hathaway J. Chem. Soc Dalton Trans. (1999),1835-1844.
27. M. Mohamadi, S.Y. Ebrahimipour, M.T. –Mahani, S. Foro, A. Akbari, RSC Adv, 5 (2015), 101063-101075
28. U. Saha, K.K. Mukherjea, RSC Adv, 5 (2015), 94462-94473. C) D. Suh, J.B. Chaires, Biorg. Med. Chem. (1995), 3723-3728.
29. D. Yinhua, M.M Foroughi, Z.A. Boroujeni, S. Jahani, M. Peydayesh, F. Borhani, M. Khatami, M. Rohani, M. Dusek, V. Eigner, RSC Adv, 10 (2020), 22891.
30. I.D. Kuntz, F.P. Gasparro, M.D. Johnston, R.P. Taylor, Journal of the American Chemical Society, 90 (1968), 18.
31. G. Sahu, E.R.T. Tiekink, R. Dinda, Inorganics, 9 (9) (2021), 66.
32. Z.A. Boroujeni, S. Jahani, M.K. Motlagh, K. Kerman, N. Aramesh, S. Asadpour, M. Noroozifar, Journal of Biomolecular Structure and Dynamics (2020), 1538-025.
33. N. Sepay, P.C. Saha, Z Shahzadi, A. Chakraborty, U.C. Halder, Phys. Chem. Chem. Phys., 23 (12) (2021), 7261-7270.
34. A. Ali, S. Banerjee, S. Kamaal, M. Usman, N. Das, M. Afzal, A. Alarifi, N. Sepay, P. Roy, M. Ahmad, RSC Adv., 11 (24) (2021), 14362-14373.
35. N. Sepay, C. Guha, S. Maity, A.K. Mallik, European J. Org. Chem., 40 (2017), 6013-6022.
36. M. R. Maurya, S. Agarwal, C. Bader, M. Ebel, D. Rehder, Dalton Trans. 537-544.
37. M. Majumder, K.K. Rajak, Polyhedron, 176 (2020), Article 114241.

CHAPTER V

Synthesis of Novel Oxidovanadium Complexes containing Coumarin and Naphthalene moiety: Bromoperoxidase activity and DNA/BSA binding Study.

ABSTRACT

Two tridentate Schiff base ligands, $\mathbf{L_1}$ and $\mathbf{L_2}$ have been introduced in this current work towards the synthesis of mononuclear oxidovanadium complexes with a co-ligand 1,10-phenanthroline. Two mononuclear complexes [VO(L_1)(1,10-phen)], **1**; and [VO(L_2)(1,10-phen)], **2** have been effectively synthesized with high yields by reacting with [VO(acac)$_2$] in 1:1 ratio in methanol under refluxing condition. Where 1,10-phenanthroline was used as co-ligands in the synthesis of complex**1** and**2**. X-ray crystallographic studies unveil the structure of the complexes where ligands$\mathbf{L_1}$and $\mathbf{L_2}$bind with vanadium in O^N^O coordinating fashion. The synthesized complexes were well characterized by using UV-Vis, IR, NMR and Mass spectral techniques. The physiochemical properties have been well interpreted by density functional theory (DFT) and time dependent density functional theory (TDDFT) calculations.The mimicking of vanadium haloperoxidase was investigated by the bromination of the organic substrate phenol red by vanadium complexes in the presence of bromide and H_2O_2 and rate of the reaction is $\mathbf{2.68 \times 10^2}$ $(mol/L)^{-2}$ s^{-1} .The DNA and BSA protein binding interaction of vanadium complexes have been explored by UV–Vis and fluorescence spectral methods and viscosity measurements reveal that the complexes interact with CT-DNA through intercalation mode and follows the order [VO(L_1)(1,10-phen)](**$2.71x10^4$**)>[VO(L_2)(1,10-phen)](**$9.67x10^3$**) .The complexes exhibit binding interactions with BSA protein.

V.1. INTRODUCTION

The chemistry of vanadium has been a great deal of attention for several decades due to its rich presence in bio organisms as important enzymes like vanadium nitrogenase [1] and haloperoxidases [2-4]. Vanadium also acts as essential biometal and is known to have several anti-diabetes, anti-parasitic, anti-viral, anti-tuberculosis, and anti-cancer properties which assist in propagation of biomedical science [5-7]. Scientists have put an effort in mimicking the vanadium containing biomaterials which helped in understanding the mechanism behind oxidative transformations. Vanadium dependent enzymes like vanadium haloperoxidase (VHPO) which is often found in marine microorganisms are important due to their catalytic property [8-10] towards halogenation of organic compounds such as organic sulphides and alcohols. The peroxidative bromination is an important route for the biosynthesis of many natural brominated organic compounds [11-13]. Thus, the development of novel vanadium based complexes mimicking VHPO is worth of active research. Besides this, higher oxidation vanadium complexes show prodrug properties in various biological media.

Bio active compounds like coumarin [14] and hydroxy-naphthaldehyde are used in the ligand architecture in this study to create a bio friendly atmosphere around the metal center. Specially, coumarins are well known for their anti-inflammatory, anticoagulant, antibacterial, antifungal, antiviral, anticancer, antihypertensive, antituberculous, anticonvulsant, antiadipogenic, and antihyperglycemic pharmacological activities, as well as its antioxidant and neuroprotective actions. Coumarins are found in many medicinal plants and their derivatives are thermally stable.

On the other hand, DNA is assumed to be the primary target for cytotoxicity [15]. The vanadium metal complexes bind with DNA mainly through covalent and non-covalent interactions such as major and minor groove binding, intercalation and electrostatic interactions [16]. There is also a possibility that the interaction with various metal complexes leads to the destruction of DNA which in turn helps to terminate the cancerous cell. In biological fluids, there is a major contribution of serum albumin in circulatory system and has importance in physiological and pharmacological functions. As Bovine serum albumin (BSA) contains 76% sequence homology with Human serum albumin (HSA), [17] it can be taken as a model protein. So, BSA binding study with metal complexes is also important for the successful implementation of drug delivery.

The present study consists of successful synthesis of two mononuclear oxidovanadium complexes consisting of tridentate O^N^O schiff base ligands having dibenzofuran moeity. The crystal structures of the complexes are confirmed through X-ray crystallography. The binding ability and nature of interaction of these complexes with DNA/BSA has been evaluated by absorption titration, emission titration and viscosity measurements studies. Moreover, the complexes used here are able to show significant Bromoperoxidase activity with high yield in phenol red to bromophenol blue formation.

Here, we also present a full density functional theory (**DFT**) and time-dependent density functional theory **(TDDFT**) studies to get better understanding of the geometry, electronic structure and optical properties of these complex molecules, with good accuracy. Geometry optimizations of the singlet ground-state were carried out by means of DFT calculations. TDDFT calculations of several singlet states have been performed to gain a better insight on the electronic origin of the absorption spectra.The theoretically obtained results and experimental findings are found to be in good agreement.

V.2. EXPERIMENTAL SECTION

A. Materials

Vanadyl sulphate was obtained from S D Fine-Chem Limited, 4-Methylumbelliferone,2-hydroxynapthaldehyde and 1,10-Phenanthroline were bought from Sigma-Aldrich.β-napthol and potassium Bromide was purchased from Fischer scientific and Hydrogen peroxide (30% V/V) was obtained from Merck. Sodium salt of CT-DNA and ethidium bromide were purchased from Sigma-Aldrich. BSA was purchased from sigma. Tris-(hydroxymethyl)-aminomethane, 99.9% ultrapure grade was taken from Aldrich. HPLC water and phenol red indicator were purchased from Merck. The metal precursor [$V^{IV}O$- $(acac)_2$] was prepared as said by standard procedures described in the literature [18-19].1-aminomethylnapthalen-2-ol and 7-hydroxy-4-methyl-2-oxo-2H-chromene-8-carbaldehyde was prepared by literature reported methods [20-21]. Analytically pure solvents and chemicals are used throughout the study. All the reactions with metal salts are carried out under open air atmosphere.

B. Preparation of Compounds

Ligands (L_1 and L_2)

The aminomethylnapthalenol based Schiff base compounds, (**L_1** and **L_2**) were synthesized by the condensation of 1-aminomethylnapthalen-2-ol in methanol with their respective aldehydes (2-hydroxy-1-napthaldehyde for **L_1** and 7-Hydroxy-4-methyl coumarin for **L_2**) in equimolar proportions. The targeted light yellow Schiff base compounds (**L_1** and **L_2**) were filtered, washed with mother liquor, and dried over $CaCl_2$. Elemental analysis and ^1H NMR and IR data for both the compounds verified their composition. Characterization of **L_1** and **L_2** is listed below.

L_1. Yield: 2.61g (80%), ^1H NMR ($CDCl_3$, 400 MHz): δ 14.216 (s, 1H); 10.310 (s, 1H); 9.364 (s, 1H), 8.198-6.587(m, 12H), 5.284 (s, 2H, for $–CH_2$), Elemental anal. calcd. for $C_{22}H_{17}NO_2$: C, 80.71; H, 5.23; N, 4.28, O, 9.77. Found: C, 80.69; H, 5.25; N, 4.26, O, 9.79. IR (KBr, cm^{-1}): ***ν*** (O–H): 3047; ***ν*** (imine C=N): 1619, 2540 ($-CH_2$).

L_2. Yield: 2.5g (70%), ^1H NMR ($CDCl_3$, 400 MHz): δ 10.35 (s, 1H); 9.09 (s, 1H); 8.13 (s, 1H), 7.84-7.52 (m, 5H), 7.33 (s, 1H), 7.25 (d, 1H, J=8.8 Hz),6.68 (s, 1H)6.48 (d, 1H, J= 9.2Hz), 6.11 (s, 1H), 2.48 (s, 3H, for $–CH_3$), Elemental anal. calcd. for $C_{22}H_{17}NO_4$: C, 73.53; H, 4.77; N, 3.90, O, 17.81. Found: C, 73.48; H, 4.69; N, 3.95, O, 17.84. IR (KBr, cm^{-1}): ***ν*** (O–H): 3047; ***ν*** (imine C=N): 1634, 2506 ($-CH_2$).

Complexes

$[V^{IV}O(L_1)(1,10\text{-phen})]$, Complex 1: $[V^{IV}O(acac)_2]$ (1.33g, 5 mmol) was added to the hot solution of the ligand **L_1**(1.64g, 5 mmol) in methanol (10mL). The mixture was heated under refluxing condition for 2h. Then 1,10-phenanthroline (0.75g, 5 mmol) was added to the resulting clear light green coloured solution and stirred for 6h and the colour changed to deep red which was kept in air for slow evaporation. After a day red crystals suitable for X-ray diffraction analysis were generated. Yield: 1.23 g (79%). Elemental anal calcd for $C_{34}H_{23}N_3O_3V$: Theo: C, 71.33; H, 4.05; N, 7.34, O, 8.38. Found: C, 71.29; H, 4.02; N, 7.36; O, 8.39. IR (KBr, cm^{-1}): ν (O–H): 3034 (crystal associated MeOH moiety); ν (imine C=N): 1617, 956 (V=O stretch).

[$V^{IV}O(L_2)$(1,10-phen)]. Complex 2: [$V^{IV}O(acac)_2$] (1.33g, 5 mmol) was added to the hot methanolic solution of Ligand (**L_2**) (1.5g, 5 mmol) after that 1,10-phenanthroline (0.73g, 5 mmol) was added and heated under refluxing condition for 8h. The deep red coloured solution was appeared and kept for slow evaporation. Red coloured crystals suitable for single crystal X-ray diffraction analysis were obtained. Yield: 0.36g (75%) Elemental anal. calcd. for $C_{34}H_{23}N_3O_5V$: C, 67.55; H, 3.83; N, 6.95, O, 13.23, Found: C, 68.98; H, 3.95; N, 6.35; O, 12.12;.IR (cm-1): ν (imine C=N): 1622, 1599 (lactone), 963 (V=O stretch).

C. X-Ray Structure Determination

The single crystals suitable for X-ray crystallographic analysis were obtained by slow evaporation of methanolic solution of the complexes. A summary of crystal data and refinement details for complex 1 and 2 is provided in **Table 1**. The X-ray intensity data were collected on Bruker AXS SMART APEX CCD diffractometer (Mo K_α, $\lambda = 0.71073$ Å) at 293 K. The detector was placed at a distance 6.03 cm from the crystal. Total 606 frames were collected with a scan width of 0.3˚ in different settings of φ. The data were curtail in SAINTPLUS [22] and empirical absorption correction was applied using the SADABS package [23]. Metal atoms ware located by Direct Method and the rest of the non-hydrogen atoms were emerged from successive Fourier synthesis. The structures were refined by full matrix least-square procedure on F^2. All non-hydrogen atoms were refined anisotropically.

All the calculations were done using the SHELXTL V 6.14 program package [24]. Molecular structure plots were drawn using the Oak Ridge thermal ellipsoid plot (ORTEP) [25]. The CCDC numbers are **1944354** and **2129106** for the complex **1** and **2** respectively.

D. Physical Measurements

All physical measurements that included elemental analysis, IR, ^1H NMR, Absorption spectra, ESI mass spectra, emission spectra, were done as described in Chaptrer 1.

Table 1: Crystal data and structure refinement parameters of complexes 1 and 2:

	Complex 1	**Complex 2**
Formula	$C_{35}H_{26}N_4O_4V$	$C_{34}H_{23}N_3O_5V$
M_r	604.53	606.49
Crystal system	monoclinic	triclinic
Space group	C 1 2/c 1	P -1
a/ Å	27.642(2)	8.9472(11)
b/ Å	14.4783(11)	9.4068(11)
c/ Å	14.9790(11)	16.764(2)
α/°	90.00	93.790(3)
β/°	90.559(2)	99.542(3)
γ/°	90.00	92.294(4)
V/ $Å^3$	5994.5(8)	1386.5(3)
Z	8	2
D_{calcd} /g cm^{-3}	1.373	1.453
μ/mm^{-1}	0.379	0.409
θ/°	2.086- 27.127	2.173 – 27.494
T/K	273(2)	273 (2)
Reflns collected	6614	6354
R^1, wR^2 [I>2σ(I)]	0.0746, 0.1686	0.0685, 0.2019
GOF on F^2	0.998	0.996

$^{a}R1 = \Sigma \big| |F_o| - |F_c| \big| / \Sigma |F_o|$. ^{b} $wR2 = [\Sigma[w(F_o^2 - F_c^2)^2] / \Sigma[w(F_o^2)^2]]^{1/2}$

V.3. RESULT AND DISCUSSION

1. Synthesis

The ligand, L_1 and L_2 was synthesized in two steps. Initially, amino-methylation of naphthalene-2-ol was carried out to form 1-(aminomethyl)naphthalene-2-ol hydrochloride by using 2-chloro-N-hydroxymethylacetamide in dry ethanol solvent and concentrated HCl at refluxing condition. Finally, condensation reaction was performed between 1-(aminomethyl)naphthalene-2-ol hydrochloride and 2-hydroxynaphthalaldehyde forming ligand (L_1) and between 1-(aminomethyl)naphthalene-2-ol hydrochloride and 4-methyl-7-hydroxy coumarin forming ligand L_2.

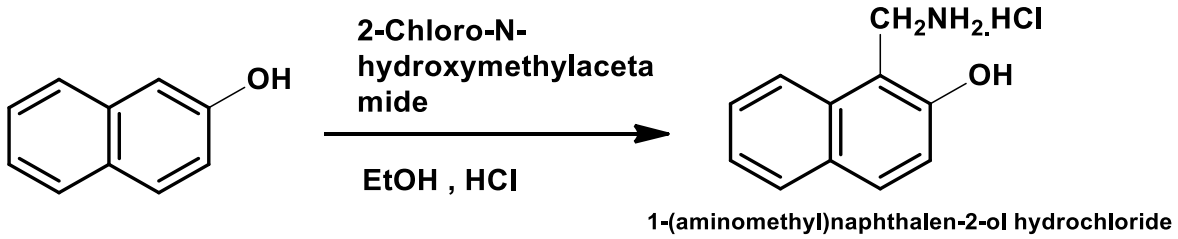

Scheme 1a: Synthesized method for 1-(aminomethyl) naphthalene-2-ol hydrochloride.

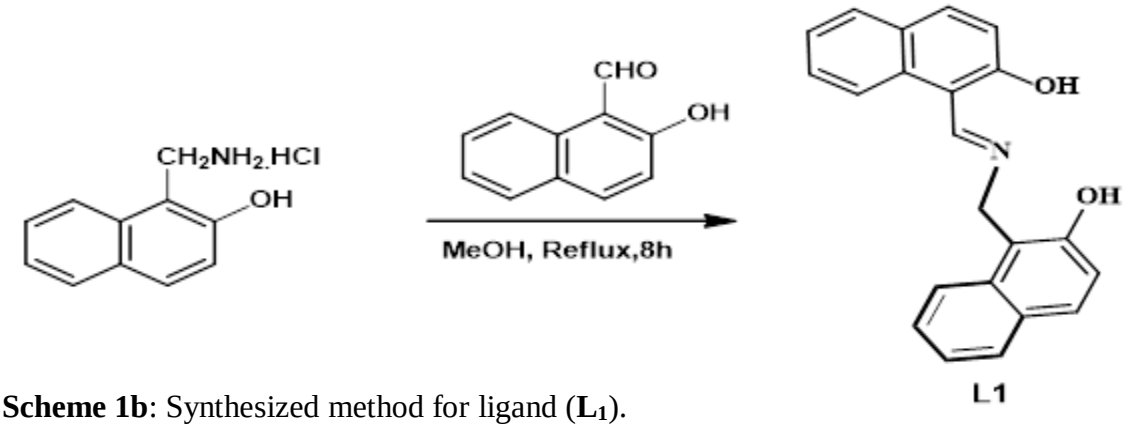

Scheme 1b: Synthesized method for ligand (L_1).

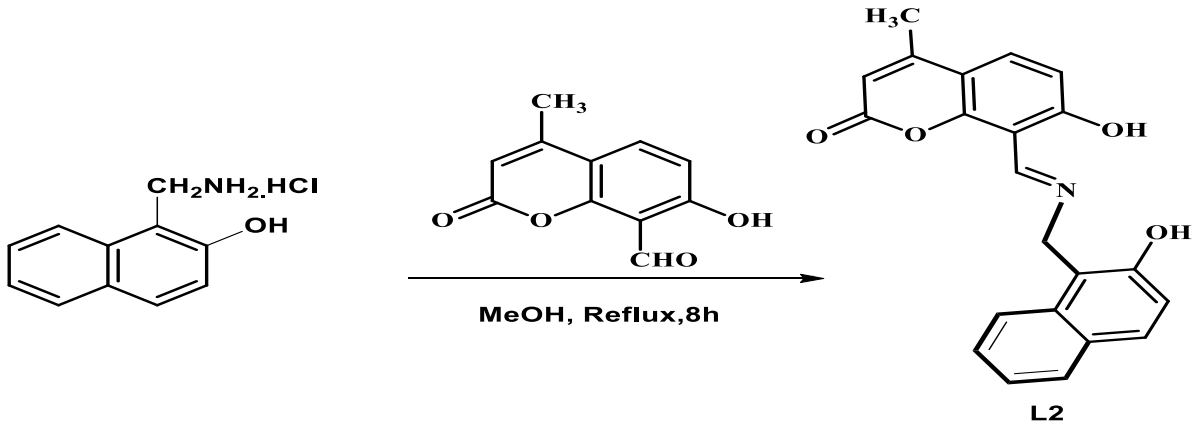

Scheme 1c: Synthesized method for ligand **(L_2)**.

The stoichiometric reaction of $\mathbf{L_1}$ and $\mathbf{L_2}$ with $[VO(acac)_2]$ and the co-ligand 1,10-phenanthroline in methanol produces compounds **1** and **2**. The synthesized ligand and complexes **1** and **2** (Scheme 2) were well characterized using different spectral techniques (UV, NMR, IR, Crystal Structure etc). In **1** and **2**, the altering binding sites produced V(IV) complexes.

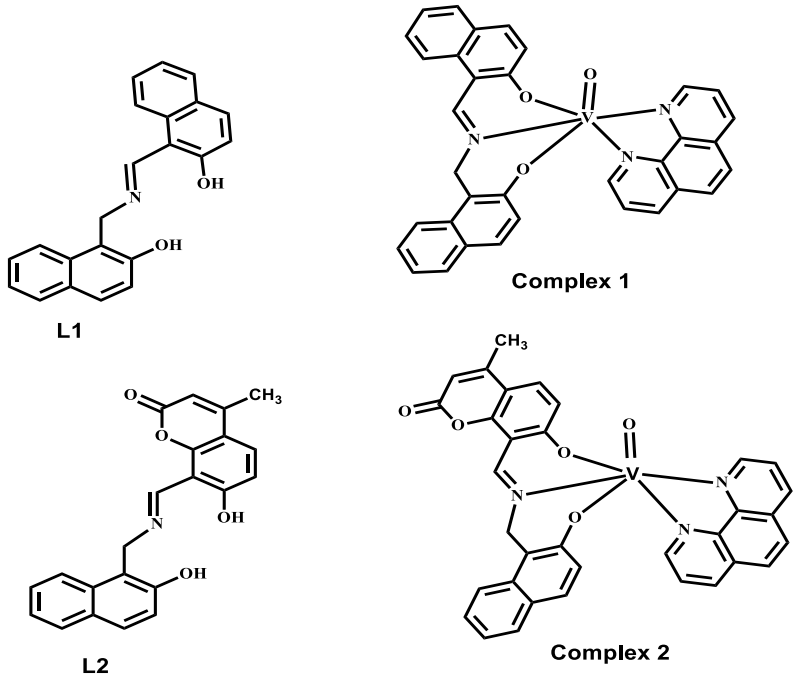

Scheme 2: The tridentate ligands and the synthesized complexes.

2. Characterization

Infra-red spectroscopy: The IR spectra of the ligand and its corresponding metal complexes were recorded in a KBr disk. The IR data of the ligand and the complexes were documented in the experimental section. In $\mathbf{L_1}$, sharp peaks appeared at 1619 cm^{-1} and at 3047 cm^{-1} which clearly proves the presence of imine (C=N) bond and free OH group and the peak at 2540 cm^{-1} indicates the $–CH_2$ group. In $\mathbf{L_2}$ peaks appeared at 1634 cm^{-1}, 3047 cm^{-1} and at 2506 cm^{-1} which aproves the presence of imine (C=N) bond, free OH group and the $–CH_2$ groups respectively. All the vanadium complexes exhibited spectral bands in the range of 1630-1620 cm^{-1} arising from the stretching vibrations of the imine moiety. The spectral bands in the range of 1000 cm^{-1}– 850 cm^{-1}indicates the presence of V=O bond in the Vanadium (IV) complexes.The relevant electronic spectra are depicted in **(Fig. 1)**.

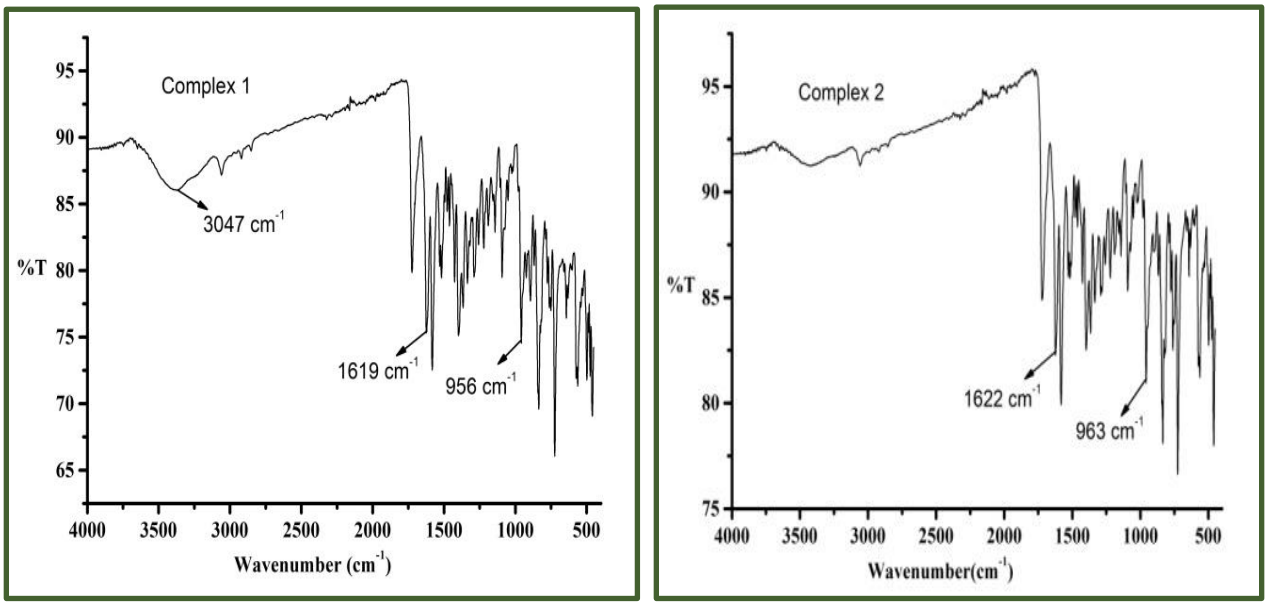

Figure 1: IR spectrum of complex **1** and **2**.

NMR Spectra of ligand: Both the ligands $\mathbf{L_1}$ and $\mathbf{L_2}$ are diamagnetic in nature and show well determined NMR spectra in $CDCl_3$ solution. The spectral data are given in the experimental section. The NMR peaks are assigned on the basis of the intensity and spin–spin splitting pattern. The appearance of singlet peaks at 14.216 and 10.310 ppm for $\mathbf{L_1}$ which disappears upon the addition of D_2O approves the presence of phenolic hydrogen. A singlet corresponding to the imine hydrogen atom was observed at 9.364 ppm and 5.284 ppm for the $–CH_2$ group in the ligand ($\mathbf{L_1}$).

In **L_2** also shows characteristics peak at 10.35, 9.09 and 8.13 ppm approves the phenolic –OH hydrogen and the imine hydrogen atom respectively. The singlet peak appeared at 2.48 ppm for the three hydrogen of coumarin moiety. Both the complexes are paramagnetic in nature for that reason EPR is done. The NMR data are shown in **SI (Fig. S5-S6)**.

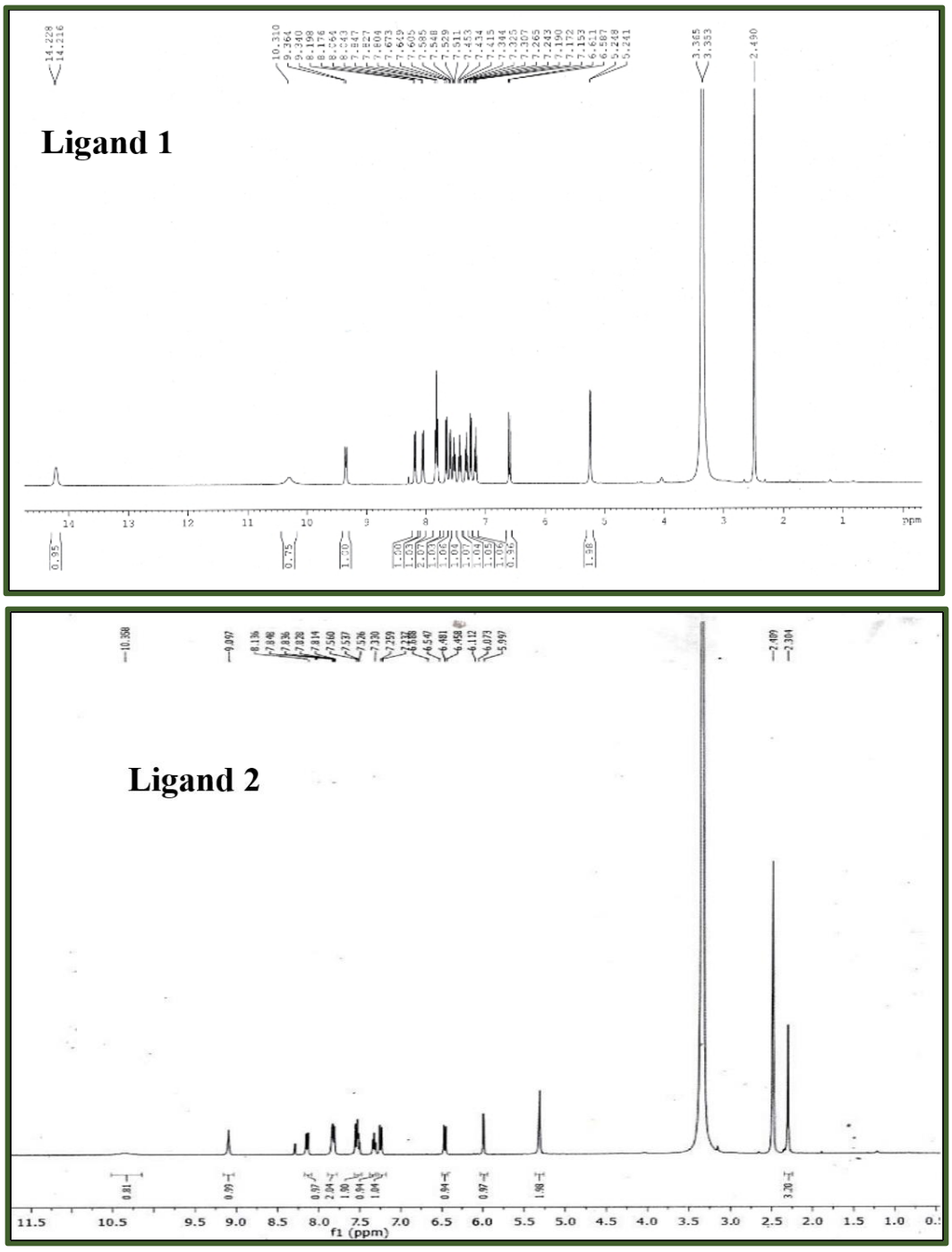

Figure 2: ^{1}H NMR spectra of ligand **1** and **2**.

EPR spectra of complexes: Both the complexes (**1** and **2**) exhibit one unpaired electron due to the presence of vanadium metal in it's **+IV** oxidation state. Generally, the paramagnetism corresponds to $\mathbf{3d_{xy}^{1}}$ configuration. Both the complexes are EPR active in CH_2Cl_2 solution at room temperature and the representative spectrum of the EPR study is given in Fig **3**. The average hyperfine splitting for complex **1** is 95.28 G and central field g-value is 1.9682 and for complex 2 is 95.37 G and central field g-value is 1.9882 with line width of 2.09 mT.

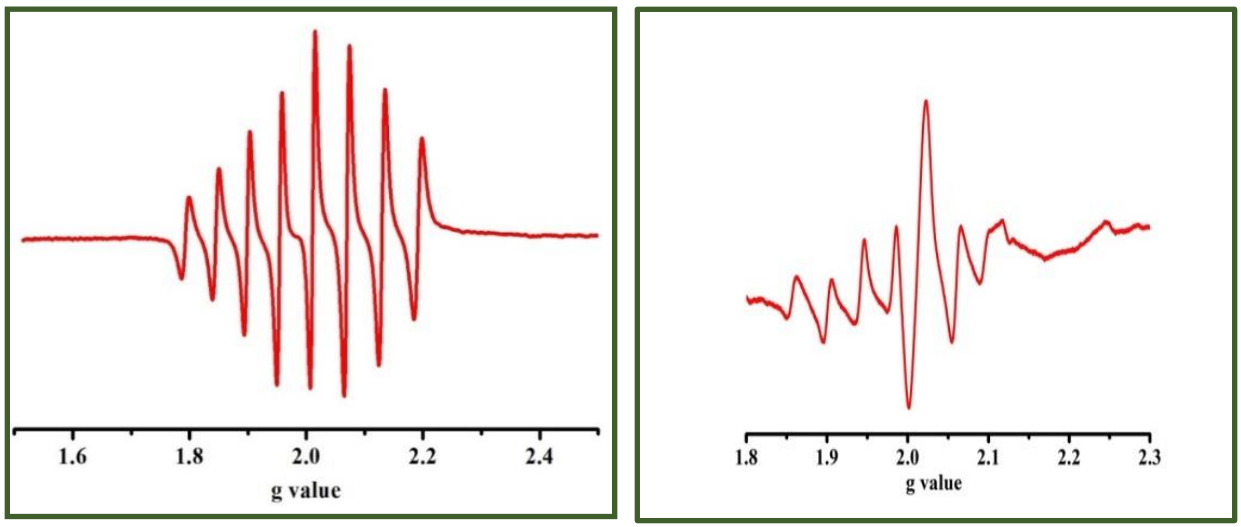

Figure 3: EPR spectrum of complex **1** and **2** in DCM/Toluene**.**

Crystal structure: The molecular structures of the complexes [VO(L_1)(1,10-phen)], **1** and [VO(L_2)(1,10-phen)], **2**, have been resolute by using single crystal X-ray diffractometer. The molecular structures of **1** and **2** are shown in Fig.**4**.

Complex **1** crystallizes in the monoclinic crystal system with C 2/cspace group. Here the ligand binds with the metal centre asan O^N^O coordinating dianionic ligand in tridentate mode. The ligand possesses two phenoxide groups and imine nitrogen, which are directly bound to the metal centre in a meridional fashion. The fourth coordination site of vanadium is occupied by oxo oxygen atom. The remaining two vacant coordination sites of vanadium are occupied by N,N-didentate 1,10-phenanthroline moiety owing to the formation of distorted octahedral geometry [26-27]. The V1-O1 bond length (1.587 Å) characterizes the presence of V=O moiety. Complex **2** also crystallizes in the triclinic crystal system with space group P -1. Here also the six coordination sites of the

metal were occupied in the similar fashion. The metal complex thus attains distorted octahedral geometry as in the previous case.

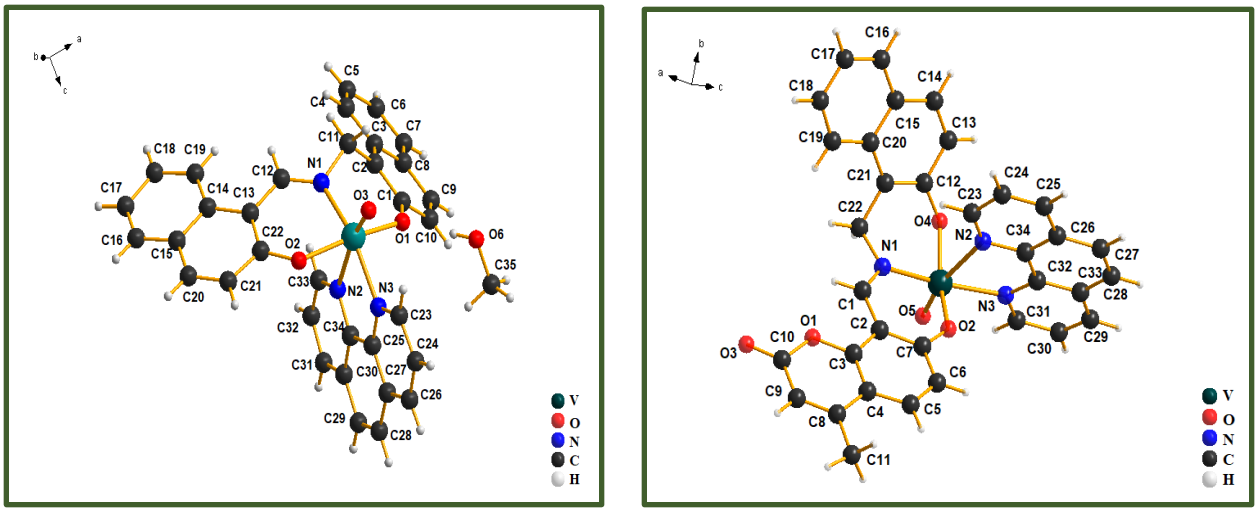

Figure 4: ORTEP plot of complex **1** & **2**, showing essential numbering; H atoms and solvent moiety are omitted for clarity.

Geometrical studies: Geometrical optimizations for complexes 1 and 2 are performed in presence of solvent. The main geometrical optimized parameters (Bond length and bond angle) of complexes 1, and 2 are given in the (**Table 2**). The optimized geometry reveals that the complexes have a distorted octahedral arrangement around the vanadium (V) metal centre. The optimized structures of these complexes are in good agreement with the experimentally observed structures and results, which were determined using single crystal XRD studies. A slight variation in structural parameters may occur due to crystal lattice distortion in real molecules [28].

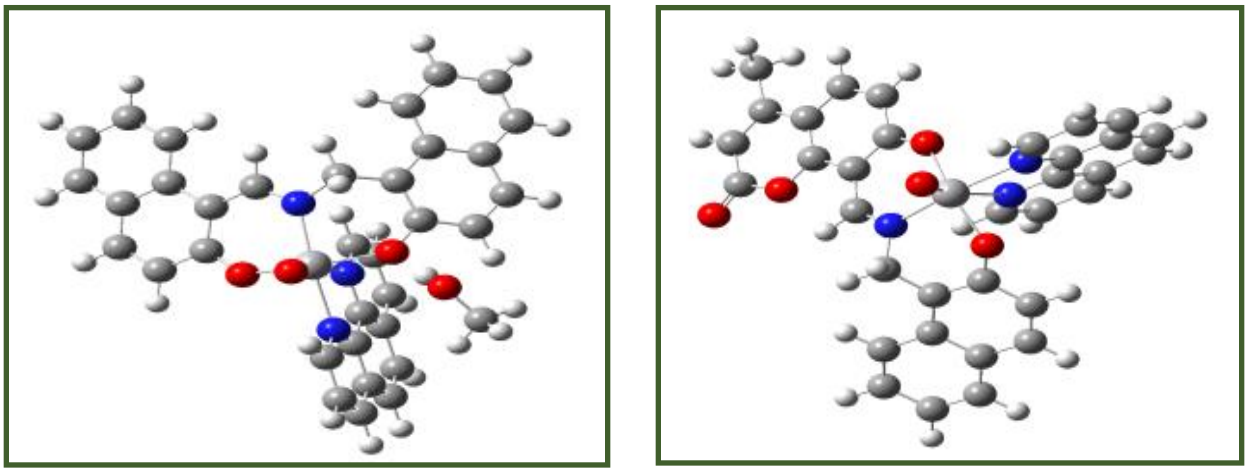

Complex 1 **Complex 2**

Table 2: Optimized and experimental geometrical parameters of complexes 1 and 2.

Bond Length (Å)					
Complex **1**			Complex **2**		
Bond type	Expt.	Theo.	Bond type	Expt.	Theo.
V1-O1	1.971(3)	1.971	V1-O2	1.983(2)	1.982
V1-O2	1.971(3)	1.971	V1-O4	1.950(2)	1.949
V1-O3	1.593(2)	1.593	V1-O5	1.593(2)	1.592
V1-N1	2.048(3)	2.047	V1-N1	2.072(2)	2.072
V1-N2	2.357(3)	2.357	V1-N2	2.359(3)	2.359
V1-N3	2.130(3)	2.129	V1-N3	2.143(3)	2.143
C12-N1	1.292(4)	1.271	C1-N2	1.286(4)	1.285
Bond angles (°)					
Complex **1**			Complex **2**		
Bond type	Expt.	Theo.	Bond type	Expt.	Theo.
O1-V1-O2	163.17(11)	163.175	O5-V1-O2	102.07(13)	101.992
O1-V1-O3	98.32(13)	98.329	O5-V1-O4	101.49(13)	101.555
O1-V1-N1	88.65(11)	88.702	O4-V1-O2	156.40(11)	156.420
O1-V1-N2	81.77(10)	81.755	O2-V1-N1	86.08(9)	86.108
O1-V1-N3	91.04(10)	91.014	O2-V1-N2	76.57(10)	76.570
O2-V1-N1	87.04(11)	86.990	O2-V1-N3	87.99(9)	87.956
O2-V1-N2	81.80(11)	81.815	O4-V1-N1	89.09(9)	89.105
O2-V1-N3	87.74(11)	87.764	O4-V1-N2	80.92(10)	55.897
O3-V1-O2	98.50(13)	98.492	O4-V1-N3	92.20(9)	92.198
O3-V1-N1	103.68(12)	103.649	O5-V1-N1	98.86(12)	98.770
O3-V1-N2	168.80(11)	168.833	O5-V1-N2	165.54(12)	165.560
O3-V1-N3	95.38(12)	95.419	O5-V1-N3	92.57(12)	92.657
N1-V1-N3	160.79(11)	160.770	N1-V1-N2	95.42(10)	95.477
N1-V1-N2	87.53(10)	87.518	N1-V1-N3	168.01(10)	168.001
N2-V1-N3	73.43(10)	73.423	N3- V1-N2	73.04(10)	72.979
C12-N1-V1	127.2(3)	127.237	C1-N1-V1	127.7(2)	127.826

The V–N and V–O bond lengths are in the range of 1.56–2.50 Å in both the theoretical calculation and experimental observation. A partial molecular orbital diagram with the HOMO and LUMO for all the three complexes is shown in Fig. **5**. In the ground state (S0), the HOMO of complexes 1 and 2 are quite similar in energy. But we can see the variation in the energies of LUMO for the complexes in their ground state. The LUMO of complex 1 is energetically much higher than complex 2. The HOMO - LUMO energy gaps in the complex 1 is 3.22 eV and for complex 2 is 3.14 eV. The corresponding orbital contribution for the two complexes is given in ESI (**Table 3**). The electron density in the HOMO of the

complex 1 mainly resides on the (iminomethyl)-napthalenenol moiety and a few electron densities on the napthalaldehyde moiety and in case of complex 2 the electron density resides equally on (iminomethyl)-napthalenenol and coumarin moiety. On the other hand, for the LUMO, the electron density mainly resides on the vanadium centre and the phenanthrolene moiety for both the complexes. This data depicts a very low density around the metal centre.

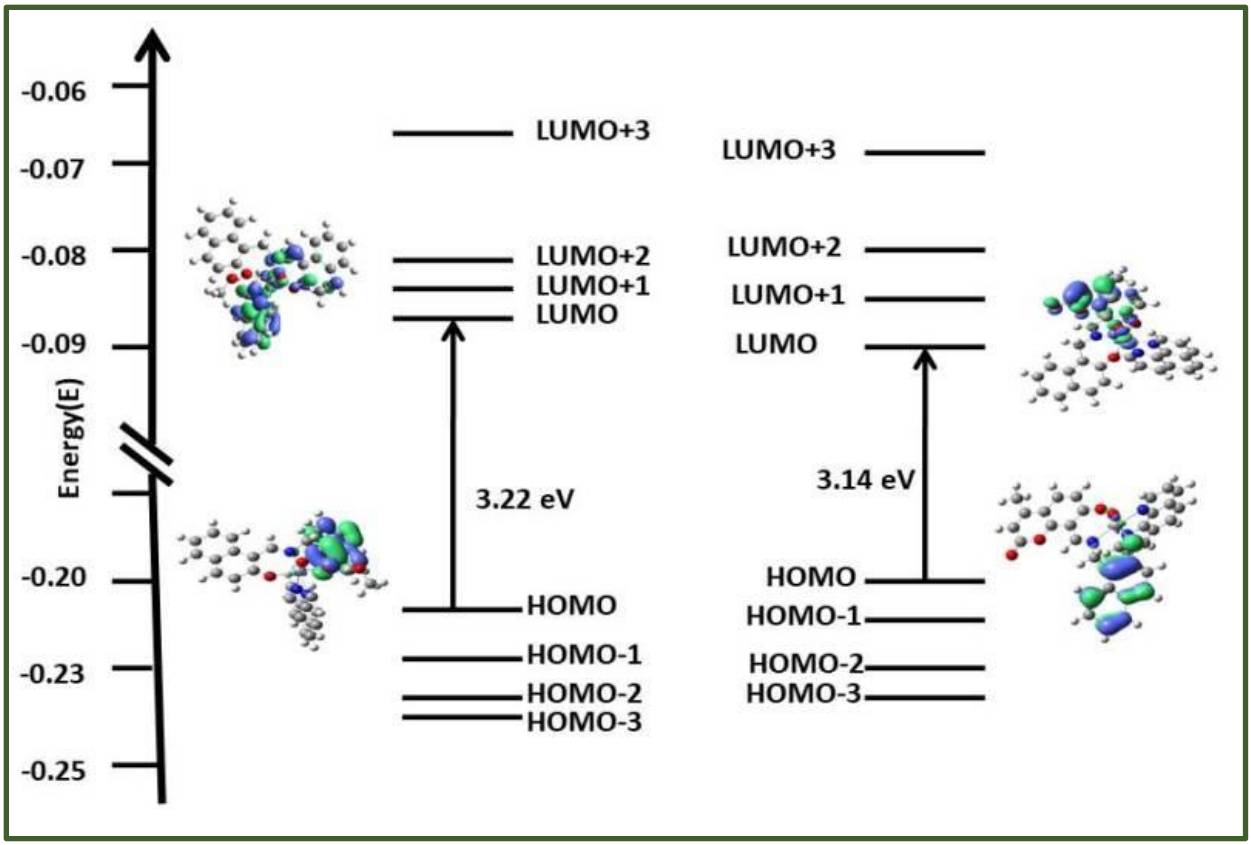

Figure 5: Partial molecular orbital diagram with the HOMO and LUMO for the complexes.

UV-Vis spectra and DFT studies: The UV- Visible spectral behavior of the ligands and its corresponding complexes were recorded in methanol. The spectral parameters with the experimental molar extinction coefficient (ε) value of all the compounds are listed in Table **2**The Ligand 1 and ligand 2 show characteristic peaks in the range of 300-420 nm. The peaks near 300 nm arise due to intramolecular π–π* transitions and peaks near 418 nm is responsible for n–π* transition. The complexes 1 and 2 display strong peaks at 406 nm and 325 nm respectively having molar extinction coefficient in the range of 35000 – 61000 $M^{-1}cm^{-1}$.

Table 3: Optimized geometries, HOMO-LUMO contour plots of metal complexes at the B3LYP/6-31G* level.

	Complex 1	Complex 2
Optimized geometries at the B3LYP/631G* level	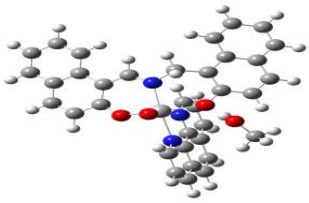	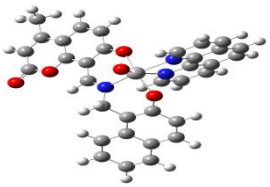
LUMO+2	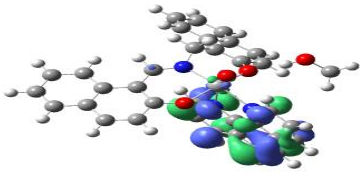	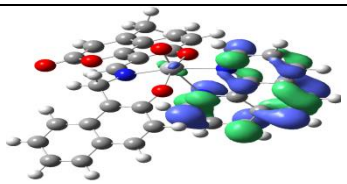
LUMO+1	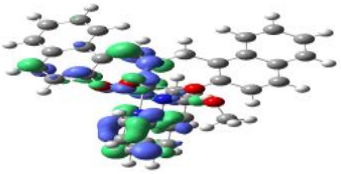	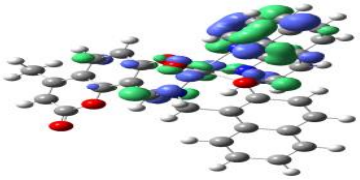
LUMO	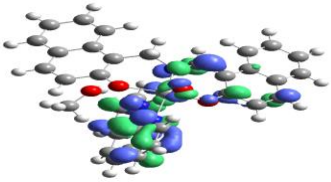	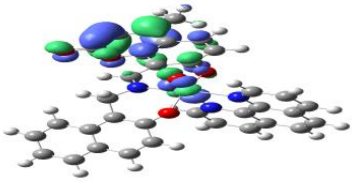
HOMO	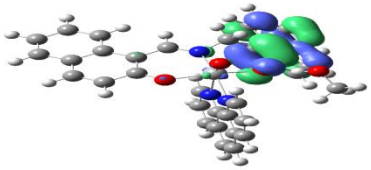	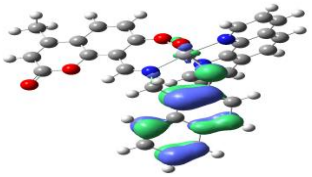
HOMO-1	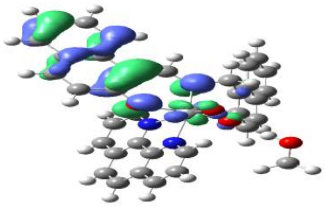	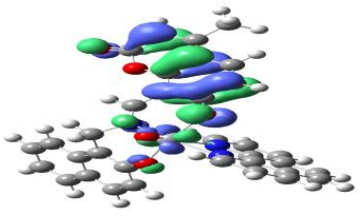
HOMO-2	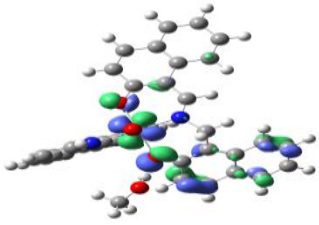	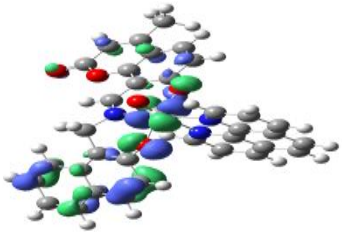

The bands in the longer wavelength region of these complexes can be attributed to the ligand to metal charge transfer [$H_2L_1 \rightarrow V(d\pi)$] transition. Only complex **2** shows low intense intra-ligand charge transfer transition. The corresponding spectra of the ligand and the complexes are shown in figure **6**.

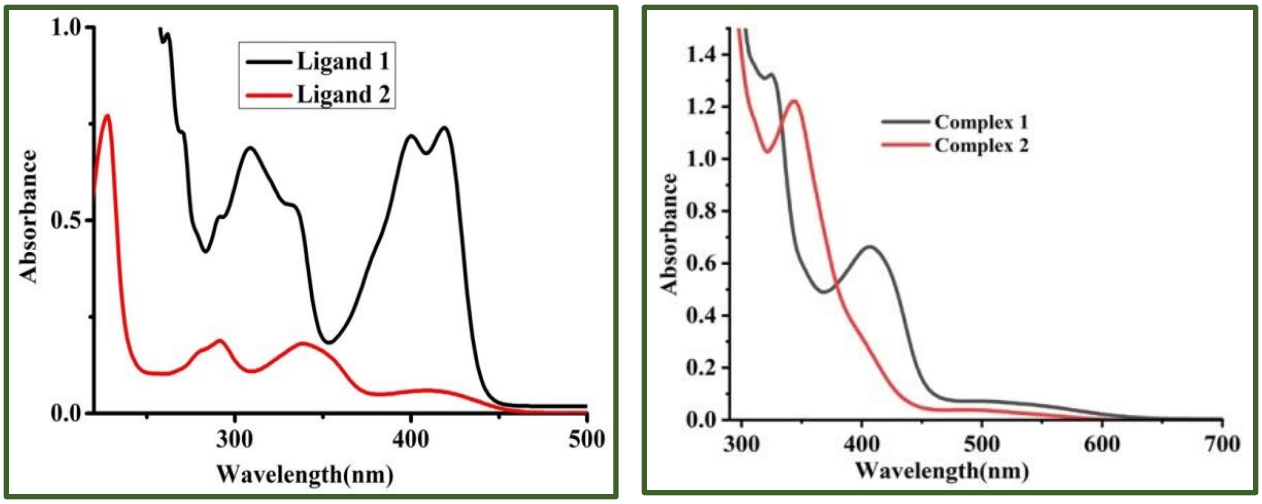

Figure 6: UV-Visible spectra of Ligands (**L_1** and **L_2**) and corresponding complexes (**1**and **2**) in methanol solution with a fixed concentration [2×10^{-5}].

To get a better insight in the UV-Visible spectrum of the metal complexes, detailed theoretical calculations were performed in presence of solvent (DFT studies) and the results are depicted in Table **3**.

Table 3: Calculated optical transitions for complexes 1-2

Complex	Electronic transition	composition	Excitation Energy(eV)	Oscillation Strength (f)	CI	Assign	λ_{exp} in nm (Ɛ in M^{-1} cm^{-1})
1	$S_0 \rightarrow S_{16}$	H-1→L+1	3.0574(405 nm)	0.0647	0.68232	LLCT	403(34950)
	$S_0 \rightarrow S_{32}$	H-4→L	3.6871(336 nm)	0.0560	0.69242	LMCT	332(66000)
2	$S_0 \rightarrow S_{30}$	H→L+4	3.5759(346 nm)	0.0151	0.61773	LLCT	343(61000)

3. Catalytic Activity

Bromination of alkenols using the complex as catalyst: To test the activity of the vanadium complexes as catalyst, the peroxidative bromination of phenolsulfonaphthalein (phenol red) to tetra-bromo-phenolsulfonaphthalein (bromophenol blue) was used. This is a facile method and easy to monitor by a UV–vis spectroscopic technique. [29] λmax values of pure phenol red and bromophenol blue were first determined from the UV–vis spectra of the substrates. The reaction was carried out in a mild acidic medium at a constant temperature of (30 ±0.5) ˚C in presence of H_2O_2 and KBr. An aliquot of 30% H_2O_2 (final concentration 2.0 mM) was added to a 4:1 H_2O–DMF solution of catalysts subsequently the addition of 4.0 mol L-1 of KBr maintaining PH at 5.8 after addition of NaH_2PO_4–Na_2HPO_4. By the addition of 0.1 mmol of phenol red the reactions were initiated. The increase in the absorbance at 580 nm for the bromination of phenol red was monitored at a specific time points The spectral data show the gradual disappearance of the peak at 443 nm due to the loss of phenol red and an increase in the absorbance of the peak at 580 nm due to the formation of bromophenol blue and spectral changes were recorded at 5 min intervals of time.From the spectral data (shown in **Figure 7**), it is evident that as the reaction proceeds, the peak at about $\lambda_{max} \approx 432$ nm corresponds to the phenol red decreases whereas the peak at about $\lambda_{max} \approx 592$ nm corresponds to the bromophenol blue increase, thus indicating the progress of the reaction. After ∼4 h, no further changes in the absorption peaks were observed, confirming the completion of the reaction. The spectra were recorded over 1hr as shown in fig **7**. The rate of this reaction is described by the rate equation: dc/dt = kc1xc2yc3z, from which the equation "log(dc/dt) = log k +x log c1+ y log c2 + z logc3" was obtained, corresponding to

"-log(dc/dt) = -x log c1 - b (b ¼=log k + y logc2+ z log c3)",

where k is the reaction rate constant; c1, c2, c3 are the concentrations of the oxidovanadium complex, KBr and phenol red respectively; while x, y, z are the corresponding reaction orders. The rate of the reaction for complex 1 was found to be 2.68 × 102 (mol/L)-2 s-1. The plots for the kinetic studies of the conversion of phenol red to bromophenol blue are shown in Fig. **8** and **9**. The same reaction was observed without addition of the oxidovanadium complex whereby no appreciable change could be observed. During the catalytic process, the catalyst (complex 1) might be converted to a bound peroxide intermediate in presence of peroxide in mild acidic medium. This intermediate in turn oxidizes the bromide (Br^-) ion to bromonium ion (Br+) which exists in

reaction medium as $Br3^-$, Br_2 or HOBr. Attack of a bromide ion at one of the peroxo atoms (IV) and the uptake of a proton from a surrounding water molecule leads to the generation of hypobromous acid (HOBr) followed by restoration of the native state. [29] The in situ generated bromonium ion reacts with the organic substrate (phenol red) to form corresponding brominated derivatives. In case of complex 2 the reaction is too fast to calculate the data.

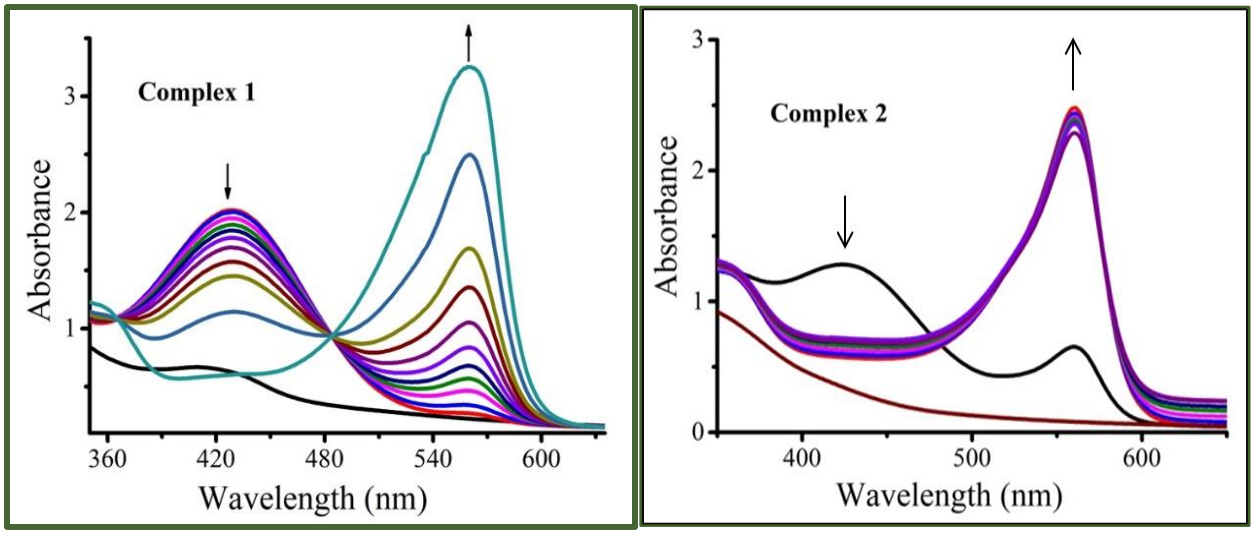

Figure 7: Oxidative bromination of phenol red catalysed by oxidovanadium complexes (0.04 mmol). Spectral changes at 5 min intervals. Spectral data taken of aliquots in pH = 5.8 aqueous phosphate buffer, $c_{(phosphate\ buffer)}$= 50 mmol L^{-1}, $c_{(KBr)}$= 0.4 mol L^{-1}, $c_{(phenol\ red)}$ = 10^{-4}mol L^{-1}.

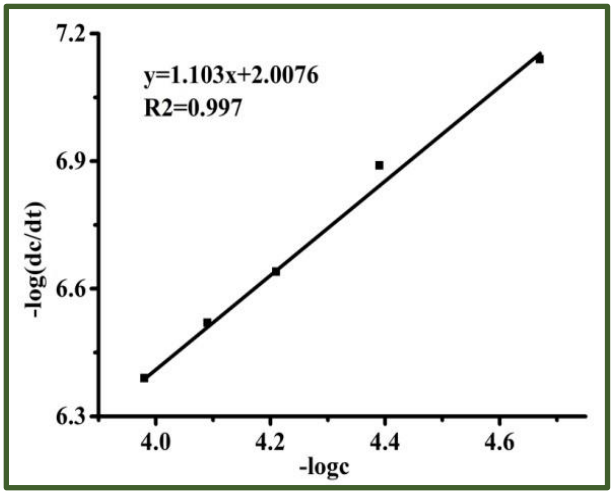

Figure 8: -log(dc/dt) dependence of -log c (c is the concentration of the oxidovanadium complex **1**); conditions used: c(phosphate buffer) = 50 mmol L^{-1}, pH = 5.8, c(KBr) = 0.4 mol L^{-1}, c(phenol red) = 10^{-4}mol L^{-1}.

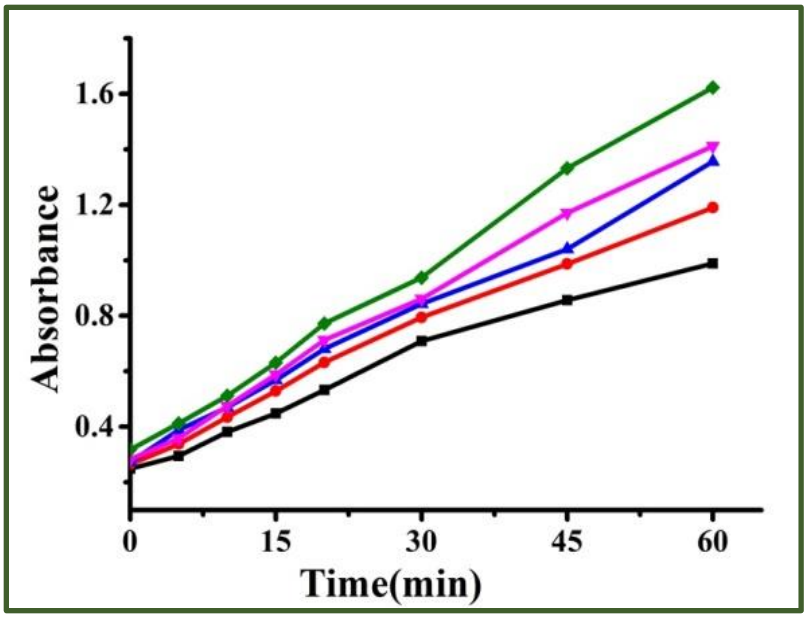

Figure 9: The measurable absorbance is depending on time for the oxidovanadium complex **1**. Conditions used: pH = 5.8, c(KBr) = 0.4 molL^{-1}, c(H_2O_2) = 2 mmol L^{-1}, c(phenol red) = 10^{-4}mol L^{-1}. c(complex/mmol L^{-1}) = a: 2 x10^{-2}; b: 4 x 10^{-2}; c: 6 x 10^{-2}; d: 8 x 10^{-2}; e: 1 x 10^{-1}.

4. Biological Activity

DNA interaction studies: As vanadium complexes are well-known for their interaction with DNA, various spectroscopic experiments were done to explore the DNA binding affinities of the synthesized complexes. The equilibrium binding constants (K_b) of complex 1-2 were evaluated by UV–vis titration experiments with CT-DNA. Generally, bathochromic and hypochromic shifts in the UV–vis absorption spectra indicate intercalating binding, while hyperchromic shifts in the titration curve indicate minor groove binding of the complexes with CT-DNA. The hypochromic shift mainly occurs due to the interaction of the organic bases of DNA and chromophores attached with vanadium complexes via intercalation mode of binding. On gradual addition of CT-DNA, a hypochromic shift was observed in the range 330 nm 403 nm and a hyperchromic shift was observed in the range 258 nm, having isobestic point at 300 nm for complex 1. For complex 2, hypochomic shift at 257nm and hyperchromic shift at 341 nm with isobestic point at 290 nm. The observed hypochromic and hyperchromic shifts may indicate that complex 1-2 interact with DNA through either intercalation or electrostatic groove binding. From the **fig. 10**, it is observed that complex 1-2 undergo both hypochromism and hyperchromism without much shift in λ_{max} value.

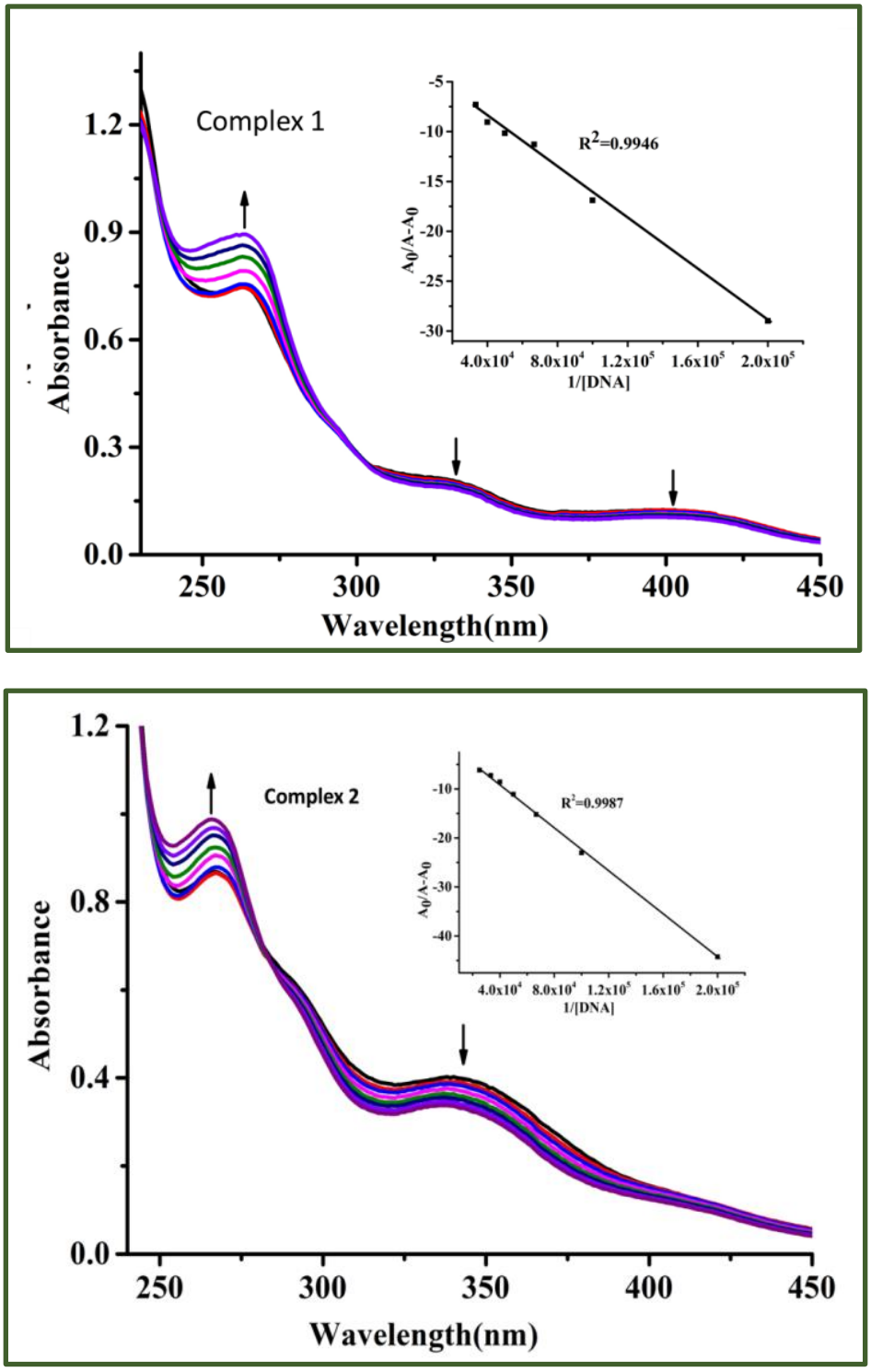

Figure 10: UV-Vis absorption spectral titration of complex **1** [25 μM] and complex **2**.in presence of increasing concentration of CT-DNA [0-50μM] in Tris-HCl buffer solution. The plot of A_0/ [A-A_0] vs. 1/[DNA] for calculation of K_b, (Ratio of intercept to slope); plot for complex **1** and **2** are shown here.

Binding constant (K_b) is a useful parameter to evaluate the binding capability of the complex to the DNA and can be determined from the variation in the electronic spectra before and after the addition of complex (25 μM) into the buffer solution with increasing concentration of DNA solution (0-50μM) by applying Benesi–Hildebrand equation [30,31] **(**equation 1) given below:

$$\frac{A_0}{A - A_0} = \frac{\varepsilon_f}{\varepsilon_b - \varepsilon_f} + \frac{\varepsilon_f}{\varepsilon_b - \varepsilon_f} \frac{1}{K_b[DNA]} \qquad Eq.\,1$$

where A_0 is the initial absorbance of free complex, A is the absorbance of the complex in the presence of DNA, ε_f corresponds to the extinction coefficient of the complex in its free form and ε_b refers to the extinction coefficient of the complex in the bound form. The plot of $A_0/(A - A_0)$ *versus* 1/[DNA] gives a straight line with an intercept of $\varepsilon_f/(\varepsilon_b - \varepsilon_f)$ and a slope of $\varepsilon_f/K_b(\varepsilon_b - \varepsilon_f)$. The value of K_b is calculated from the ratio of the intercept to the slope. The binding constant values of the DNA-complex interaction is in the order of 10^3-$10^4 M^{-1}$ (**Table 4**). This values suggests moderate interaction between complex and DNA.

Table 4: K_b, K_{SV}, K_q values of complexes 1 and 2 from complex-DNA interactions.

Complex	Binding constant (K_b), M^{-1}	Correlation coefficient (R^2)	Stern- Volmer constant (K_{SV}), M^{-1}	Quencher rate constant (K_q)[a]	Correlation coefficient (R^2)
1	$2.71x10^4$	0.9947	$1.1x10^4$	$1.1x10^{12}$	0.9932
2	$9.67x10^3$	0.9987	$1.5x10^4$	$1.5x10^{12}$	0.9869

Competitive binding experiments in the presence of Ethidium Bromide:

Competitive DNA binding is an efficient technique to investigate the interactions of small molecules with DNA. Ethidium Bromide (EB) can be applied as a fluorescence probe in the study of competitive binding experiments of DNA with the complexes as it has well conjugated aromatic system. The fluorescence intensity of EB is usually very weak in aqueous solution but it increases to a significant extent when EB binds with DNA double helix through intercalation**.** So, the competitive DNA binding experiment is an efficient tool to understand the binding behaviour of the vanadium complexes with DNA. The fluorescence intensity of the EB-bound DNA complex decreases with an increase in the concentration of the complexes (0–70 μM) because of the

displacement of EB from CT-DNA. This quenching ability of the complexes depicts their ability to displace EB and binding capability with DNA double helix through intercalation mode of binding. Representing spectra defining quenching effect of these complexes is shown in **Fig.11** and Stern -Volmer constant and rate constant are calculated using linear Stern–Volmer equation 2:

$$\boldsymbol{F_0/F = 1 + K_{SV}[Q] = 1 + K_q\tau_0\,[Q]} \qquad \text{Eq. } \mathbf{2}$$

Here F_0 and F are the fluorescence intensities in the absence and presence of the quencher (Q) [Vanadium complex in this experiment respectively. $\mathbf{K_q}$ is the bimolecular quenching constant and $\boldsymbol{\tau_0}$ is the lifetime of the fluorophore in the absence of the quencher (10^{-8} M^{-1} for EB). The results are included in Fig.**11** and Table **5**.

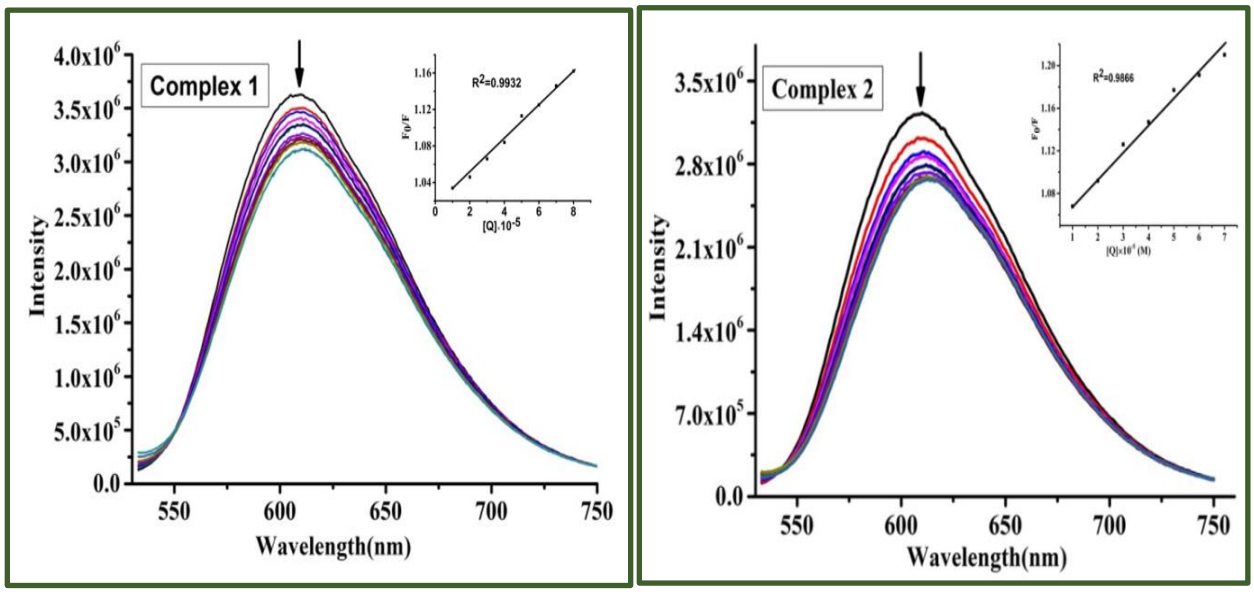

Figure 11: Ethidium bromide displacement assay of CT-DNA [50 μM] in Tris-HCl buffer with gradual increase (5 μM) in complex **1** and complex **2**.

Viscosity Measurements of DNA: Viscosity, which is very sensitive to molecular length increase, is considered as least ambiguous and most critical tests for discovering the binding mode of complexes with DNA. Viscosity measurements were used to further interpret the nature of the interactions between the complexes and DNA. Ethidium Bromide (EB) is a classical intercalation probe, causes a significant increase in the viscosity of DNA solution due to increased separation of the base pairs resulting in an increase in overall DNA length. In contrast, partial, non-classical

intercalation of ligand could crook the DNA helix, resulting in shortening of DNA length and concomitantly reducing its viscosity.

Viscosity experiments were allowed on the Ubbelohde viscometer at a fixed temperature (30±0.1°C). Complexes were added by a micropipette to the DNA solution (10 μmol·L^{-1}). With the increasing concentration of the compounds (0–10 μM) the flow time was recorded and data were graphically represented as $(\eta/\eta_o)^{1/3}$ versus the binding ratio of the concentration of compounds to DNA. Where η was the viscosity of the DNA in the presence of the complex and η_o was the viscosity of the DNA alone. The relative viscosity η was calculated using the following equation:

$$\eta = \frac{(t - t_0)}{t_0} \qquad Eq.3$$

Where, t and t_o shows the flow time of the buffer solution throughout the capillary and the observed flow time for the DNA in the presence and absence of complexes correspondingly. The mean of replicate measurements was used to evaluate the viscosity of the samples.

The thickness of CT-DNA increases with increase in the ratio of complexes to CT-DNA which is associated with the specific intercalation binding mode. Fig.**12.** depicts the plot of $(\eta/\eta_0)1/3$ vs [complex]/[DNA] where those curves show the effective relative viscosity of all the complexes. In the plot, it is observed that EB-DNA curve exhibits high viscosity whereas complex-DNA curves reduce the viscosity in the order of complexes1>2. So, the binding capacity of the complex 1 is relatively higher than complex 2. The intensity of complexes is lower than the EB-DNA interaction. This implies the groove binding with DNA molecules and it can be assumed that the CT DNA length is shortened in a non-classical way of intercalation mode of binding with the complexes.

BSA interaction studies: The BSA binding affinities of complex 1–2 were determined by fluorescence quenching experiments with 2 mL of (5x10-5 M) BSA (50 mM Tris-HCl buffer, pH 7.4) on a Horiba Fluoromax-4 spectrofluorometer. The mixture was allowed to equilibrate for 5 min after each addition. The fluorescence spectra were obtained from 280 nm to 450 nm using the excitation wavelength of **295** nm and with increasing complex concentrations (0–100 μM) at room temperature.

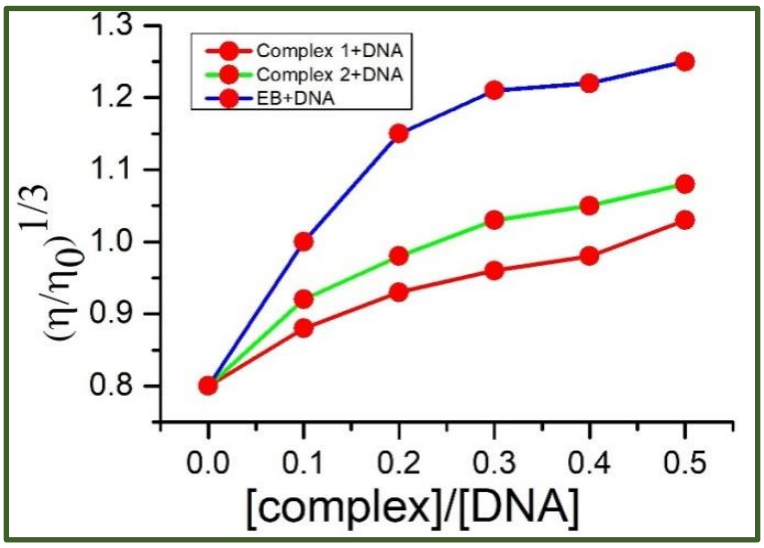

Figure 12: Effect on relative viscosity (±0.1) of CT-DNA under the influence of increasing amount of compounds at 26 ± 0.1°C in 5mM Tris-HCl bu.er (pH 7.4).

The absorption spectra of protein (BSA) with complex 1-2 were carried out to predict the type of quenching process. Addition of vanadium complexes to BSA protein, the absorption band is increased without any shift, which indicates the static quenching process. BSA is often selected as a model protein to examine the interaction of the amino acid residues i.e., tryptophan, tyrosine and phenylalanine which are mainly responsible for the intrinsic fluorescence property of BSA. It displays tryptophan fluorescence at an excitation of 295 nm with an emission maximum at 350 nm.

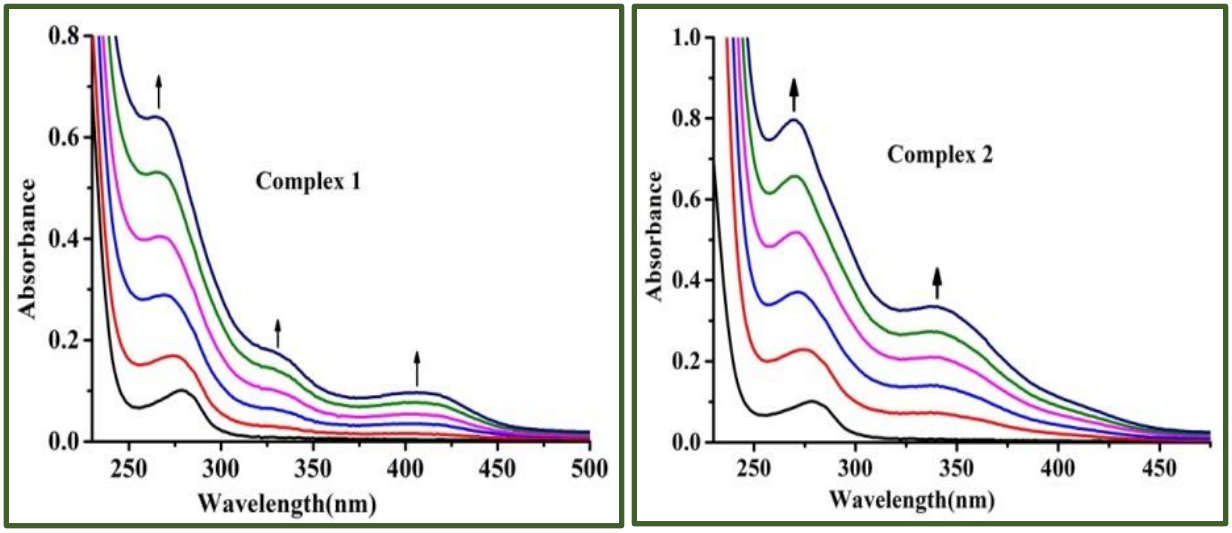

Figure 13: Electronic absorption spectra of BSA protein with complex **1-2**.

When complex binds with BSA, certain conformational changes in the protein influence the fluorescence emission of the tryptophan residues of BSA. After gradual addition of complexes into the solution of BSA, fluorescence intensity decreases at 350 nm showing a red shift which indicates that the complexes interact with the BSA leading to some change in the tryptophan moiety of BSA. For both the complexes the fluorescence intensity decreases depicting the interaction between BSA and complexes. In complex 2, the decrease in fluorescence intensity accompany with 30 nm red shift whereas complex 1 shows 10 nm.

In order to determine the mechanism of BSA-complex interaction, different binding parameters (Stern- Volmer Constant, Binding constant, k_{BSA} and number of binding sites,n) were calculated using Stern- Volmer equation and Scatchard equation[32] respectively.

$$\boldsymbol{F_0/F = 1 + K_{SV}[Q]} \quad \text{Eq. 4} \quad \text{Stern} - \text{Volmer equation}$$

$$\boldsymbol{log\left[\frac{F_0}{F} - 1\right] = \log k_{BSA} + nlog[Q]} \qquad \text{Eq. 5 Scatchard equation}$$

Here F_0 and F are the fluorescence intensities of BSA in absence and presence of the complex (Q), respectively. $\mathbf{K_{BSA}}$ is the binding constant of the complex to BSA and **n** is the number of binding sites per albumin molecule. The following table shows the experimental results, which reveals that complex **1** gives better results in terms of binding efficiency with protein which is also reflected from the $\mathbf{K_{SV}}$ value as well as the value of binding stoichiometry with the BSA. Complex **1** is showing binding stoichiometry **1:1.28** which is greater than the complex 2 (**1:1.12**). The results are depicted in Table **5** and Figure **13**.

Table 5: Binding parameters of BSA using fluorescence quenching of Complex **1** and **2**:

Complex	Stern-Volmer constant, K_{SV}, (M^{-1})	Quenching constant, Kq, ($M^{-1}s^{-1}$)	Binding constant, K_{BSA}, (M^{-1})	Number of binding sites (n)
1	$2.09x10^6$	$2.09x10^{14}$	$2.2x10^6$	1.28
2	$1.98x10^6$	$1.98x10^{14}$	$2.7x10^5$	1.12

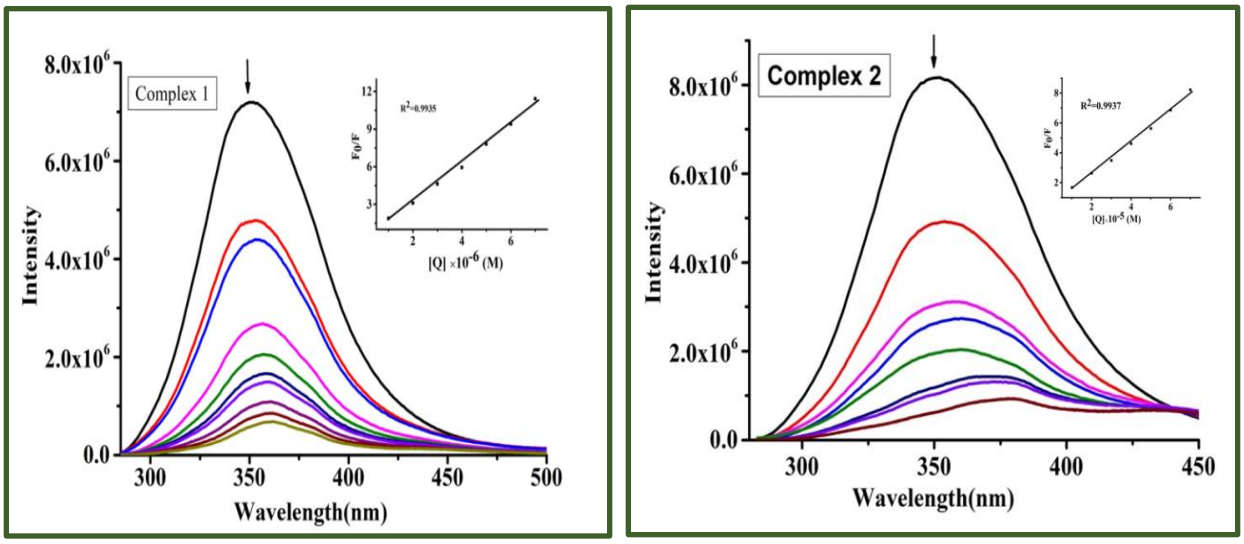

Figure 14: Fluorescence emission spectra of BSA [50**μM]** in the absence and presence of increasing amounts of complex **2 [0-70 μM]** at 298K (left). Corresponding linear fit of F_0/F vs. [complex] and the K_{SV} value was calculated using Stern-Volmer Equation (right).

Energy transfer from BSA to the complexes: FRET is a spectroscopic technique that can detect the energy transfer between fluorophores [33]. It is observed when the emission spectrum of donor molecule overlaps with the absorption spectrum of the acceptor molecule. Upon absorption of energy, the donor transfers the absorbed energy to the acceptor. [34] According to FRET, energy transfer will be observed when: (1) the donor acceptor is less than 8 nm [35]. The average distance r and energy transfer can be calculated according to Forster's theory

$$E = 1 - \frac{F}{F_0} = \frac{R_0^6}{R_0^6 + r^6} \qquad Eq.6$$

Where F_0 is the fluorescence intensity in absence of complex and F is the fluorescence intensity of BSA in presence of complex. R_0 is the critical distance when the transfer efficiency is 50% and r is the distance between donor and acceptor. R_0 can be calculated by the following equation [36]:

$$R_0^6 = 8.79\times10^{-25}\,K^2\,N^{-4}\,J\Phi \qquad Eq.7$$

In the above equation, the term K^2 is the orientation factor of the dipoles; N is the refractive index of medium, J is the extent of overlap between the emission of donor (BSA) and absorption of acceptor and Φ is the fluorescence quantum yield of the donor.

In general, K^2 = 2/3, N = 1.336 and Φ = 0.15 for BSA. The value of J can be calculated as follows

$$J = \frac{\sum F(\lambda)\varepsilon(\lambda)\lambda^4 \Delta\lambda}{\sum F(\lambda)\Delta\lambda} \qquad Eq.8$$

Here, $F(\lambda)$ is the fluorescence intensity of the donor in the absence of the acceptor at wavelength λ and ε is the molar absorption coefficient of the acceptor at λ.

The overlap integral of BSA fluorescence emission and electronic spectra of complexes 1–2 are shown in Fig. **15**, where the concentrations of BSA and complexes were kept same (c = 2 × 10^{-5} M). The values of all the energy transfer parameters are evaluated for the BSA-complex interaction and summarized in Table **6**. According to the Forster resonance energy transfer theory, the binding sites r must be within the range of 2–8 nm in a state where $0.5R_0 < r < 1.5R_0$. The values of r (r = 3.58 and 4.18) for the complexes are less than 8 nm and suggesting that the energy transfer from BSA to the complexes occurs with high probability. The values obtained from the study also suggest the presence of static quenching interaction of BSA with complexes.

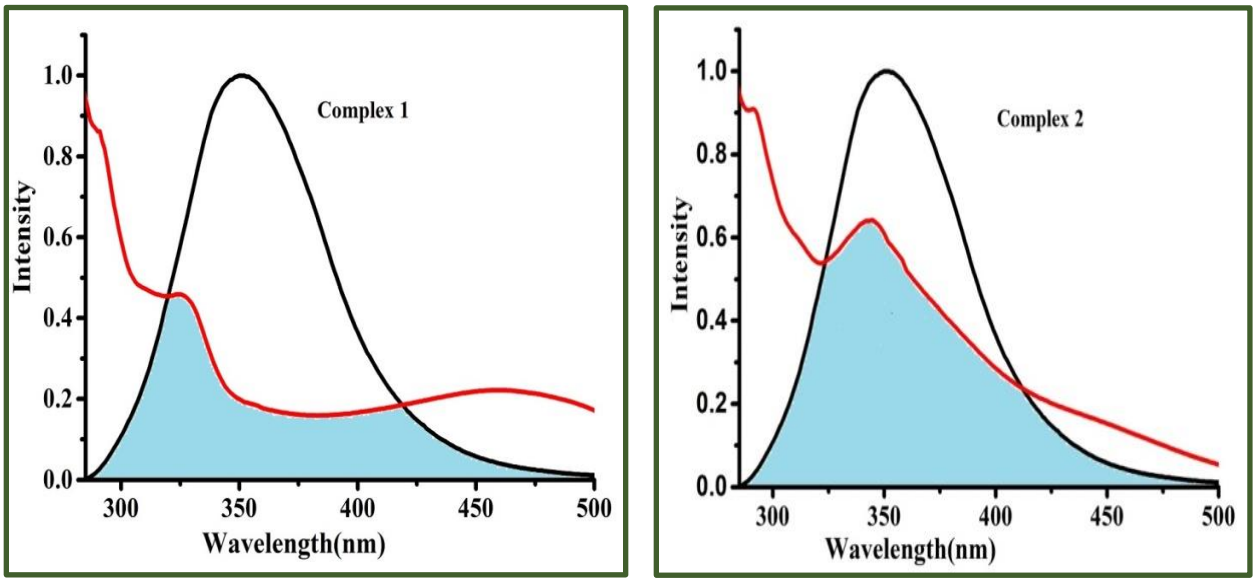

Figure 15: FRET between BSA and complexes **1** and **2**. The normalized donor emission spectra is shown in red, the acceptor molar extinction coefficient spectrum is shown in black, and the aqua blue shaded area represents the spectral overlap.

Table 6: FRET Parameters for the BSA−Complexes 1 and 2 at 26 °C

Protein	Probe	J(cm^3.L.MOL^{-1})	R_0(nm)	E	r(nm)
BSA	**Complex 1**	2.03×10^{-14}	2.88	0.46	3.58
	Complex 2	3.69×10^{-14}	3.17	0.40	4.18

V.4. CONCLUSION

To summarize, we have fruitfully synthesized two tridentate O^N^O donor ligand to produce mononuclear oxidovanadium (IV) complexes. The co-ordinating behaviour of the ligands were used to synthesize two complexes bearing oxidovanadium moiety successfully with high yields and well characterized by single crystal X-ray diffraction studies and spectral techniques viz. UV-Vis, IR, NMR, ESI-Mass etc. To attain a better insight on the electronic transition properties as well as to theoretically interpret the most stable structural features, detailed density functional theoretical (DFT) as well as time dependent density functional theoretical (TDDFT) calculations were performed. The results are in good agreement with the experimental observations.

Present work has been aimed to generate pentavalent mononuclear complexes bearing an oxidovanadium core which are known to have outstanding mimicking property of naturally occurring halo-peroxidases. They also efficiently interact with DNA through intercalation which occurs due to the presence of strong π–π stacking stacking between the aromatic moeities of the complex and aromatic bases present in DNA.UV-vis and fluorescence spectroscopy as well as fluorescence quenching experiments are performed to establish the intercalation of the title complexes with DNA and also BSA interaction activity. Model catalytic bromination reaction of an aromatic aldehyde, salicylaldehyde and alkenol, phenol red were performed using the oxidovanadium complexes to establish the halo-peroxidase mimicking activities of those. The experimental findings presented herein provide valuable insights into the planning of the preparation of strategically important complexes in the field of oxidovanadium chemistry. Further research aimed at the synthesis of polynuclear vanadium complexes using different polydentate ligands is currently under progress.

V.5. REFERENCES

[1] R. W. Miller, R. R. Eady. Biochem., 256, 429-432, (1988).

[2] M. Sandy, J. N. Carter-Franklin, J. D. Martin, A. Butlerb, Chem. Commun., 47, 12086–12088, (2011).

[3] N. Teshima, M. Kuno, M. Ueda, H. Ueda, S. Ohno, T. Sakai, Talanta., 79, 517-522, (2009).

[4] F. Natalio, R. Andre´, A. F. Hartog, B. Stoll, K. P. Jochun, R. Wever, W. Tremel, Nat. Nanotechnol., 7, 530-535, (2012).

[5] M. Maurya, Coord. Chem. Rev., 237, 163– 181, (2003).

[6] C. J. Ballhausen, H. B. Gray, Inorg. Chem., 1, 111– 122, (1962).

[7] B. Kaya, Z. K. Yılmaz, O. Şahin, B. Aslimb, B. Ülküseven, New J. Chem., 44, 9313-9320, (2020).

[8] M. Herberhod, G. Frohmader, T. Hofmann, W. Milius, J. Darkwa, Inorg. Chim. Acta., 267, 19-25, (1998).

[9] M. Etiennc, Coord. Chem. Rev., 156, 201-236, (1996).

[10] M. Kosugi, S. Hikichi, M. Akita, Y. Moro-oka, Inorg. Chem., 38, 2567-2578, (1999).

[11] Z. M. Dai, Z. Shi, G.H. Li, D. Zhang, W.S. Fu, H.Y. Jin, W. Xu, S.H. Feng, Inorg. Chem., 42, 7396-7402, (2003).

[12] S.H. Feng, R.R. Xu, Acc. Chem. Res., 34, 239-247, (2001).

[13] M. Schindler, F.C. Hawthorne, W.H. Baur, Chem. Mater., 12, 1248-1259, (2000).

[14] J. S. Rad, N. C. Martins, P. L. Jornet, E. P. F. Lopez, N. Harun, B. Yeskaliyeva, A. Beyatli, O. Sytar, S. Shaheen, F. Sharopov, Y. Taheri, A. O. Docea, Oxidative Medicine and Cellular Longevity. 6492346 (2021).

[15] A.Rebillard, D. L. Gossmann, M. T. D. Boitrel, Current Medicinal Chemistry., 15, 2656-2663, (2008).

[16] U. Ndagi, N. Mhlongo, M.E. Soliman, Drug Des Devel Ther., 11, 599-616, (2017).

[17] R.A. Rowe, M.M. Jones, Inorg Synth., 5, 113, (1957).

[18] N. Sharma, A. K. Sood, S. S. Bhatt, S. B. Kalia, S. C. Chaudhry, Catalysis letters., 23, 557-560, (2009).

[19] S. Salehzadeh, F. Hajibabaei, N.H. Moghadam, S. Sharifinia, S. Khazalpour, R. Golbedaghi, Journal of Fluorescence., 28, 195-206, (2017).

[20] A. A. Deana, G. E. Stokker, E. M. Schultz, R. L. Smith, E. J. Cragoe Jr, H. F. Russo, L. S. Watson, J. Med. Chem. 26, 580-585, (1983).

[21] C. F. Hu, P. L. Zhang, Y. F. Sui, J. S. Lv, M. F. Ansari, N. Battini, S. Li, C. H. Zhou, R. X. Geng, Bioorganic Chemistry. 94, 103434,2020.

[22] N. M. O'Boyle, A. L. Tenderholt, K. M. Langner, J. Comput. Chem., 29839–845.

[23] SMART, SAINT, SADABS, XPREP, SHELXTL, Bruker AXS Inc., Madison, WI, (1998).

[24] G. M. Sheldrick, SHELXTL, v. 6.14, Bruker AXS Inc., Madison, WI, (2003).

[25] C. K. Johnson, ORTEP Report ORNL-5138, Oak Ridge National Laboratory, Oak Ridge, TN, (1976).

[26] S. Mondal, S.P. Rath, K.K. Rajak, A. Chakravorty, Inorg. Chem., 37, 1713-1719, (1998).

[27] S.P. Rath, K.K. Rajak, S. Mondal, A. Chakravorty, J. Chem. Soc. Dalton Trans., 2097-2102, (1998).

[28] C.K. Johnson, ORTEP Report ORNL-5138, Oak Ridge National Laboratory, Oak Ridge, TN (1976).

[29] (a)U. saha and K. K. Mukherjea, RSC Adv., 5, 94462, (2015).

(b) M. Mohamadi, S.Y. Ebrahimipour, M.T. –Mahani, S. Foro, A. Akbari, RSC Adv., 5, 101063-101075, (2015).

[30] I.D. Kuntz, F.P. Gasparro, M.D. Johnston, R.P. Taylor, Journal of the American Chemical Society., 90,18, (1968).

[31] R.L. Scott, Recueil., 75, 787-789, (1956).

[32] Z.A. Boroujeni, S. Jahani, M.K. Motlagh, K. Kerman, N. Aramesh, S. Asadpour, M. Noroozifar, Journal of Biomolecular Structure and Dynamics., 1538-0254, (2020).
[33] Z. Bai, Y. Liu, J.Guo P.Zhang, Y. Ma, X. Yun, X. Zhao, R. Zhong, F. Zhang, Luminescence., 31, 688-693, (2021).
[34] Z.A. Boroujeni, S. Jahani, M.K. Motlagh, K. Kerman, N. Aramesh, S. Asadpour, M. Noroozifar, Journal of Biomolecular Structure and Dynamics., 1538-0254, (2020).
[35] P. Singla, V. Luxami, K. Paul, Eur J Med Chem., 19, 117 59-69, (2016).
[36] C. O'Sullivan, G. Murphy, B. Murphy, B. Hathaway, J. Chem. Soc., 1835-1844, (1999).